UV cured polysulfone based membranes for ultrafiltration

(Article begins on next page)

04 August 2020

Doctoral Dissertation
Doctoral Program in Chemical Engineering (30th Cycle)

UV cured polysulfone based membranes for ultrafiltration

By

Mian Farrukh Mehmood

Supervisor

Prof. Marco Sangermano

Doctoral Examination Committee:

Prof. Massimo Messori – Università degli Studi di Modena e Reggio Emilia, Italy

Prof. Roni Kasher – Ben–Gurion University of the Negev, Israel

Politecnico di Torino
2017

Declaration

I hereby declare that, the contents and organization of this dissertation constitute my own original work and does not compromise in any way the rights of third parties, including those relating to the security of personal data.

Mian Farrukh Mehmood

October 2017

I would like to dedicate this thesis to my late father Mian Mehmood Iqbal, my mother Nasreen Akhtar, my wife Ammara Masood, my daughter Zuha Farrukh and my siblings Ayesha Mehmood, Fatima Mehmood and Mian Daud Iqbal

Acknowledgment

During three years of my PhD I have been enjoying a unique research environment at Politecnico Di Torino that helps the researchers to come up with innovative ideas and work freely to accomplish their research targets. Furthermore the researchers are always encouraged to collaborate with other departments at Politecnico as well as universities and research centers all around the world. While pursuing my PhD I have received a lot of support and fortification from all sides which helped me to achieve my goals with full dedication. It is my great privilege for having opportunity of doing PhD at Politecnico Di Torino.

My first and sincere gratitude goes to Prof. Marco Sangermano, my PhD supervisor, for everything he taught me. I was so passionate on the day when Marco awarded me his kind supervision. Since then I have been enjoying his continuous support. He is very kind, inspiring and wonderful person. Marco always helped me in research activities and arranged the resources not only at Politecnico but also abroad through collaborations. I am so grateful to him.

I have been welcomed by my colleagues with open arms since I started working in Polymer Labs which always made me felt comfortable and motivated around them. Elena, Erika and Ignazio guided me about how to work on different lab instruments. Mauro Raimondo has been very supportive for SEM analysis and Luigi Capozzi had a good contribution for polydopamine coating of membranes. It is important to mention that Luigi contributed into this work when he was a reseach assistant and later he got to be a PhD student with quite different research

work. Among others, Mattia Giagnorio assisted me in filtration tests on the membranes and Prof. Alberto Tiraferri allowed me to use the dead–end filtration facility in his lab. I am thankful to all these helping hands at Politecnico.

For research activities abroad, I am highly thankful to Dr. Paula Bosch at CSIC Madrid Spain, Dr. Njabu and Prof. Peter Mallon at University of Stellenbosch South Africa and Prof. Marta Cerruti at McGill University Canada. Here again I am thankful to Prof. Marco Sangermano for arranging these research activities as fully funded within European Project MAT4TREAT. I am also very much thankful to Prof. Marco Vanni, the coordinator of PhD Chemical Engineering, for all his bureaucratic support in PhD related affairs.

My PhD at Politecnico DI Torino was funded by Higher Education Commission Pakistan, I am thankful to authorities over there for all the support they extended to me. Last but not least I want to thank all my family for their endless support and patience throughout the years of my studies. Their support always strengthened me in pursuing my PhD.

Mian Farrukh Mehmoood

Politecnico Di Torino

Abstract

Membrane technology has acquired significant importance in a variety of applications such as water treatment, health sector and food industry. Nevertheless there is a growing demand of more functional and stable membranes. This thesis is focused on improving solvent stability of polysulfone based membranes without compromising the flux properties.

Polysulfone (PSF) is a widely used membrane material for ultrafiltration process because PSF can be easily fabricated into highly porous structure via non–solvent induced phase separation (NIPS). Such a structure is imperative for ultrafiltration process as efficiency of filtration largely depends upon the size of pores and overall porosity of membrane. Generally membranes made of pristine PSF have good chemical and mechanical stability but get dissolved in many of organic solvents. Though previous attempts somehow attained solvent stability but membrane structure was deteriorated and so does the transport property.

In order to increase the solvent stability, an approach based on UV induced acrylic functionalization of PSF is described in this thesis. A two-steps method of membrane fabrication, involving NIPS and UV curing, was established. At first the acrylic functionality was introduced on the backbone of polysulfone chain through synthesis of methacrylated polysulfone (PSF–DM) macro-monomer. The thin films of PSF-DM containing phenylbis (2,4,6-trimethylbenzoyl) phosphine oxide (BAPO) photoinitiator cast on the glass plates were subjected to UV curing and NIPS processes to prepare the membranes. The reverse process i.e. NIPS followed by UV curing was also applied. The developed membranes were thoroughly characterized and the flux properties were evaluated in a dead–end filtration apparatus. The solvent stability was good in DMSO and acetone. Regardless of sequence of operations the average flux values were in the range of tight ultrafiltration. The sequence UV–NIPS resulted into more uniform and structurally stable membranes.

The next approach was based on incorporating acrylic functionality in a way that a diacrylate monomer was added into pristine PSF solution in DMF and the membranes were fabricated following the previously established method i.e. UV curing followed by NIPS. For this purpose two structurally different di-acrylates, Bisphenol A ethoxylate diacrylate (BEDA) and Poly (ethylene glycol) diacrylate (PEGDA) were incorporated and in order to study the effect of concentration, different amounts of acrylic resins were investigated. The acrylic double bond conversions were studied through FTIR and ATR–FTIR. The viscoelastic properties were analyzed via dynamic mechanical thermal analysis (DMTA) and morphological properties were studied through field emission scanning electron microscopy (FESEM). The solvent stability was analyzed by immersing the membranes cutouts in a number of solvents for 120 hrs at room temperature. The flux properties were evaluated in a pressurized stirred cell apparatus and the rejection of 27 nm polystyrene particles was also collected. Almost all the formulations came up with excellent solvent stability in DMF, DMSO, THF, Acetone, Toluene and Ethyl Acetate. The 10 % BEDA functionalized PSF membrane exhibited the best flux properties, i.e. very close to that of pristine PSF, along with good rejection (>90 %) of 27 nm polystyrene particles.

The UV cured acrylic functionalized PSF membranes were further applied to specific contaminant removal. The previously developed best UF membranes were coated with polydopamine (PDA) in order to combine the rejection of ultrafiltration membrane with the adsorption of contaminant by PDA layer. As BEDA cross-linked membranes were developed through UV curing followed by NIPS so the strategy of PDA coating was coupled with NIPS either as a separate action next to NIPS or in a more facile and advantageous one–step method where NIPS and PDA coating occurred at the same time. In order to study the increased adsorptive behavior of PDA coated membranes, methylene blue (MB) was taken as a model contaminant. The removal of MB was investigated both in batch and continuous filtration. The Zwitterionic behavior of PDA was effectively exploited and the coated membranes released MB in acidic condition thus regenerated for next adsorption. The cyclic stability of several adsorption and desorption cycles was studied.

Above stated all three works discussed the development of UV cured membranes through NIPS. In recent years, electrospun nano-fibrous membranes (ENMs') have been employed as successful replacement of phase separation membranes because of high porosity thus much lower mass transfer resistance. We designed a reactive electrospinning setup where electrospinning was

coupled with online UV irradiation. The same BEDA functionalized PSF formulation was taken as feed solution. All the parameters of electospinning and UV curing were thoroughly investigated, optimized and correlated so the optimum curing of acrylic monomer and production of nano fibers take place simultaneously. The electrospun mats were also prepared via offline curing method and compared with the counterparts. All the UV cured mats were fully characterized and solvent stability was assessed in the same way as reported before.

Contents

List of Figures

No.	Title	Page

List of Tables

Abbreviations / Nomenclature

ASTM   American standard test method

ATR–FTIR   Attenuated total reflectance – Fourier transform infrared

BAPO   Phenylbis (2,4,6-trimethyl benzoyl) phosphine oxide

BEDA   Bisphenol A ethoxylate diacrylate

BP   Benzophenone

CA   Cellulose Acetate

DG   Degree of grafting

DMAc   Dimethyl acetamide

DMF   Dimethyl formamide

DMSO   Dimethyl sulfoxide

DMTA   Dynamic mechanical thermal analysis

DSC   Differential scanning calorimetry

EIPS   Evaporation induced phase separation

ENM   Electrospun nanofibrous membrane

FESEM   Field emission scanning electron microscopy

FO   Forward osmosis

FTIR   Fourier transform infrared

GDP   Gross Domestic Production

GPC   Gel permeation chromatography

GS   Gas separation

HPLC   High-performance liquid chromatography

MB   Methylene blue

MBR   Membrane bioreactor

MET   Membrane extraction technology

MF   Microfiltration

MWCO   Molecular weight cut–off

NF   Nanofiltration

NIPS	Non–solvent induced phase separation
NMP	N-methyl pyrrolidone
NVP	N-vinyl pyrrolidone
PAEK	Poly aryl ether ketone
PAN	Polyacrylonitrile
PC	Polycarbonate
PDA	Polydopamine
PDI	Polydispersity index
PEGDA	Poly (ethylene glycol) diacrylate
PEO	Poly (ethylene oxide)
PEPP	Poly (4-ethylphenoxyle)(phenoxy) phosphazenel
PES	Polyethersulfone
PI	Polyimide
PP	Polypropylene
PSF	Polysulfone
PTFE	Polytetrafluoroethylene
PV	Pervaporation
PVDF	Polyvinylidene fluoride
Ret	Retention
RO	Reverse osmosis
TEM	Transmission electron microscopy
TFC	Thin film composite
TGA	Thermal gravimetric analysis
TIPS	Thermal induced phase separation
THF	Tetrahydrofuran
UF	Ultrafiltration
UV	Ultraviolet
VIPS	Vapor induced phase separation
VOCs	Volatile organic compounds

Chapter 1

Introduction

Water is the most valuable resource of the earth but it is becoming perilously scarce and befouled [1, 2]. The water scarcity is one of the serious global emerging challenges what humanity is facing today. At present more than one-third of the world's population is living in the water–stressed countries and by 2025 this figure is anticipated to rise to almost two–third [3]. The vast majority of earth's water is saltwater (97%) in the oceans; the fresh water constitutes only 2.5% and the remainder (0.5%) is found in underground aquifers and surface estuaries [4]. Out of available freshwater, 70% goes to irrigation, 20% is used in industry and just 10% finds domestic use [5] so human beings consume less than 1% of water on the earth. These stats are enough to describe the real threat since 1.2 billion people across the globe lack the safe drinking water and some 2.6 billion are deprived of adequate sanitation [2]. The diarrheal diseases alone result in 1.8 million deaths every year and 88% of which are attributed to unsafe drinking water and inadequate sanitation [6]. Over the last century the water usage increased twice of the growth of the population and the improvement in these circumstances remains unsatisfactory. It's predicted that there will be an increase of three billion in the world population by the year 2050 and 2.7 billion will be in the developing countries where the economic impacts of unsafe water and pathetic sanitation facilities are likely to devastate the society. The shortage of safe water resources has impact beyond human health for example the annual loss in Africa, because of lack of drinking water and sanitation is estimated $28 billion (5% of GDP) and in Asian countries like Philippines, Cambodia, Indonesia and Vietnam this figure is $9 billion (2% of GDP) [7]. These are notable negative economic impacts resulting from water scarcity and poor sanitation.

Another related study is recently carried out by Mekonnen and fellows [8]; they reported that every year worldwide four billion people suffer from water scarcity for more than one month. Further they found that groundwater consumption is twice of the water reintegrated in the system by the rains. Almost half a billion people in this world suffer from severe water scarcity all year round. There is an emerging demand to escalate water-use and water-treat efficiencies, to put cap to water consumption by river basin and better management of limited fresh water resources so the threat posed by water scarcity on human welfare and biodiversity could be reduced.
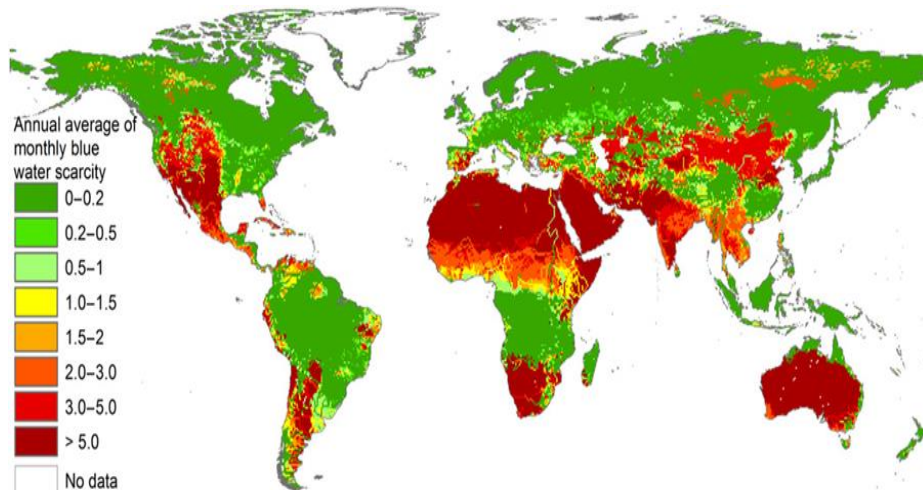
Figure 1.1: Global annual average monthly blue water scarcity

The World Economic Forum has also mentioned in its Global Risk Report 2016 that water crisis is the biggest problem world is likely to face in next ten years [9].
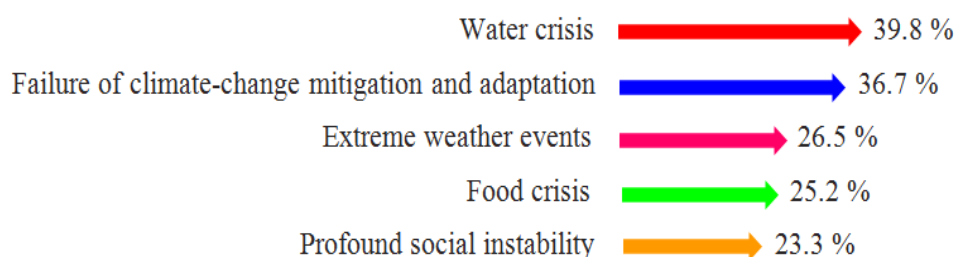
Figure 1.2: Top five global risks by World Economic Forum 2016

The climate change, the rapid growth of population and the excessive industrialization are the factors intensifying the global water scarcity. Besides the problem of water scarcity; the available drinking water sources, such as lakes and rivers are being contaminated with the pollutants that instigate from agriculture, municipal and industrial waste waters [10]. In order to address this challenge there is an indispensable need of the energy efficient and sustainable treatment technologies to tap the unconventional sources of water so the water supply is augmented beyond what is obtained from the hydrological cycle [2].

The traditional methods to remove contaminants from water and wastewater are sand filtration, sedimentation, coagulation, flocculation, extraction, ion exchange, electro-deposition, precipitation and biological degradation [11, 12] but most of these operations require lengthy operating period and large area thus not so efficient in terms of cost as well as time of operation [12, 13]. Furthermore the increased complexity of industrial waste water, such as those from oil and gas industries and coal fired plants, has become a major challenge in the recent years [14–16]. These wastewaters are characterized by very high level of dissolved solids i.e. approximately six times that of seawater thus carries high fouling potential [16]. These wastewaters are very difficult to treat with the conventional technologies. Besides these challenges, there is a growing interest in recovering

valuable resources from municipal and industrial waste water [17, 18]. The municipal wastewaters could be taken as renewable resources from which we can have not only water but also nutrients (like phosphorous and nitrogen), energy and bio plastics [19, 20]. In years ahead the resources recovery would be integral part of waste water treatment. These evolving features of wastewaters necessitate the development of low cost, energy efficient and sustainable water treatment technologies [21, 22]. In recent years it has been established that membranes-based treatment of water and wastewater has potential and diversity to fulfill the majority of the aforementioned requirements [23–40].

1.1. The membrane technology

A membrane is often described as a selective-permeable interface between two adjacent phases. A membrane is generally characterized by two performance indicators; one is permittivity that is allowing a substance to move across the membrane this is also called flux while the other parameter is selectivity that is rejection of a contaminant by the membrane and quantitatively it's termed as rejection. Thus a membrane acts as a selective barrier that controls the exchange of substances between two compartments and this exchange is influenced by the physical and chemical interaction between the substance and membrane. A schematics representation of a membrane is given in Figure 1.3. The membranes based process of purification has become indispensable in the production of safe drinking water, dialysis, pharmaceutical purification, desalination and controlled release of drugs. In contrast to conventional water treatment technologies; the membranes are less sensitive to the feed quality fluctuations and have much smaller footprints. Moreover membrane-based desalination have been proved more energy efficient than thermal operations. For example the energy required for seawater desalination by the modern reverse osmosis (RO) membranes is five times less than thermal desalination [41].
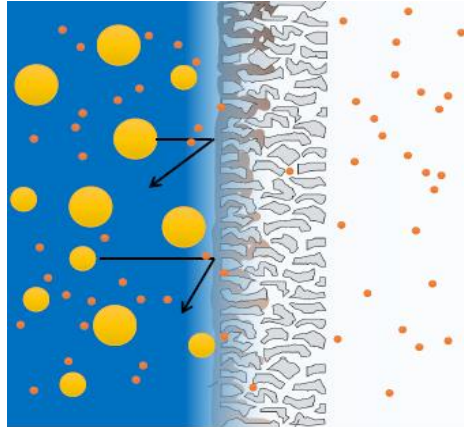
Figure 1.3: Schematic representation of a membrane

The membranes can be classified with respect to different aspects associated;

i)   The material of the membranes (natural or synthetic)

ii)   The structure of the membranes (porous or nonporous)

iii)   Symmetry of the membranes (symmetric or asymmetric)

iv)   Different phases to separate (gas–gas / gas–liquid / Liquid–liquid / Liquid-solid)

v)   Separation mechanism (diffusive, absorbance, ionic-exchange, osmotic)

Some functional membranes such as reactive membranes (ion-exchange membranes) have been developed in order to modify the physical or chemical condition of the permeable species and modulate the permeated amount in control release.

A wide range of membrane material, both inorganic and organic, have been already worked on and more fascinating membranes are continuously being developed with the availability of new materials and technologies such as new polymers, new synthetic routes for inorganic materials and recently developed promising nano-technologies. Moreover the development of block copolymer and self-assembly opens a new concept of preparing iso-porous membranes. New low-temperature synthesis of inorganic materials allows growth of inorganic or ceramic layers directly into porous structures. The integration of smart and responsive polymers into or onto membranes leads to enhanced functionalities. The mixed matrix membranes came up with improved performance being robust and stronger than pure membrane materials. The molecular dynamics simulation is providing new insights of both material and design of membranes [42]

Based on the structure, a membrane can be classified as symmetrical or asymmetrical. The symmetrical membranes are isotropic in nature i.e. uniform pores structure across the membrane. The majority of microfiltration and ultrafiltration membranes have isotropic porous structure. On the other hand the asymmetrical membranes have pores of changing size from one surface to other in a way that bulk of membrane has macro voids and top layer is almost dense. The asymmetrical membranes are also characterized by thin selective layer "active layer" on a support that is made of highly porous structure. This distinguished structure of anisotropic membranes ensures the separation on the active layer. The majority of modern nano-filtration and reverse osmosis membranes make use of this thin film asymmetric structure.

A membrane-based separation process carries three distinguished types of flow. The feed flow is split by the membrane into permeate (or product) flow and concentrate (or retenate) flow. The concentration of contaminants in feed flow is

higher than permeate flow and lower than concentrate flow. The flow across a membrane doesn't occur automatically. In fact membrane itself is a resistance to flow while the dissolved solids in the aqueous feed solutions generate an osmotic pressure "π" that has to be overcome for transportation across the membrane. Thermodynamically the osmotic pressure is defined in terms of the activity of solvent (water),

$$\pi = -\frac{RT}{\nabla_w} \ln a_w \qquad (1.1)$$

Where ∇_W is the partial molar volume of the solvent, R is the gas constant, T is the absolute temperature and a_w is the activity of the solvent [43]. For sufficient dilute solutions the equation 1.1 simplifies to the well known Van't hoff equation

$$\pi \cong CsRT \qquad (1.2)$$

Where Cs is the molar concentration of the solute

In order to achieve the separation through semipermeable membrane, the applied trans–membranes pressure (the pressure difference across the membrane) should be greater than the osmotic pressure difference between the feed and permeate solutions. The flux of water across the membrane can be positive (in the direction of the solution of lower solution concentration) or negative (in the direction of solution of higher concentration) depending upon the applied pressure difference as illustrated in Figure 1.4.
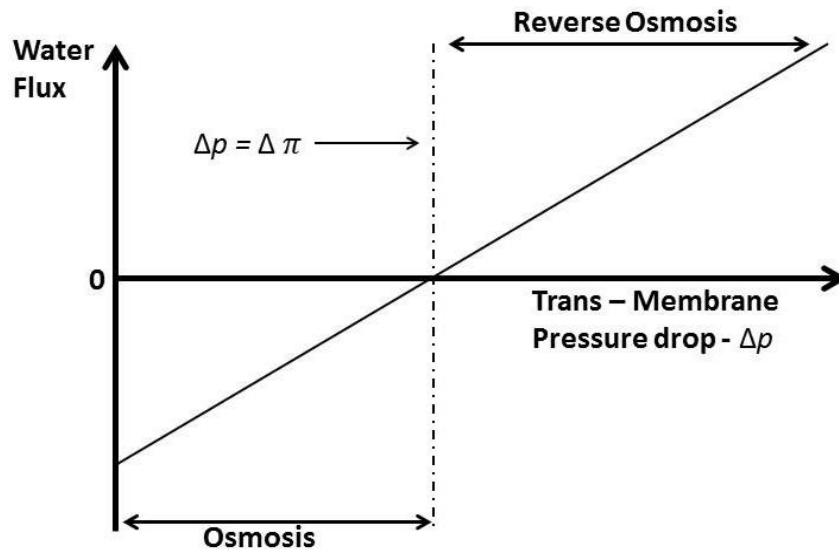
Figure 1.4: Membrane flux versus trans–membrane pressure difference

The data, collected in table 1.1, represents the range of osmotic pressures of different feed solutions. It is important to note that osmotic pressure is highly dependent on the salinity and composition of the solution. Moreover that osmotic pressure is sensitive to the total concentration of the species (ions and molecules) in the solution. [44].

Table 1.1: Osmotic pressure of different feed solutions at 25 ^{o}C [44]

Solute or Solution	Total dissolved solids (mg / L)	Molar concentrations (mmol / L)	Osmotic Pressure (psi)	Osmotic Pressure (bar)
Brackrish Water	2,000 – 5,000	-	15 – 40	1.0 – 2.7
Seawater	32,000	-	340	23.4
NaCl	2,000	34.2	22.8	1.7
NaCl	35,000	598.9	398	27.4
NaHCO$_3$	1,000	11.9	12.8	0.883
Na$_2$SO$_4$	1,000	7.1	6.0	0.41
MgSO$_4$	1,000	8.3	3.6	0.25
MgCl$_2$	1,000	10.5	9.7	0.67
CaCl$_2$	1,000	9.0	8.3	0.57
Sucrose	1,000	2.9	1.05	0.0724
Dextrose	1,000	5.5	2.0	0.14

In order to have flow across the membranes the osmotic pressure of feed solution must be overcome through application of a driving force. This driving force normally originates from potential gradient across the membrane in terms of concentration, pressure, electric potential or temperature.

The flux through the membrane is proportional to the driving force as described in equation 1.3

$$J_i = -Lp \frac{\Delta F_i}{l} \qquad (1.3)$$

The proportionality coefficient Lp / l is called permeance of the membrane and it relates flux to the driving force where Lp is permeability of species in the solutions that is purely an intrinsic material property while l is the thickness of the membrane. The phenomenological equations of different driving forces, originating from different sources, are given in table 1.2.

Table 1.2: Phenomenological equations of forces to drive the flux [45]

Mass flux	$J_m = -D\dfrac{\Delta c}{l}$	Fick	Diffusion coefficient
Volume flux	$J_v = -L_p\dfrac{\Delta P}{l}$	Darcy	Permeability coefficient
Heat flux	$J_h = -\lambda\dfrac{\Delta T}{l}$	Fourier	Thermal diffusivity
Momentum flux	$J_n = -v\dfrac{\Delta v}{l}$	Newton	Kinematic viscosity
Electrical flux	$J_i = -IR\dfrac{\Delta E}{l}$	Ohm	Electrical conductivity

Besides flux, the selectivity is equally important performance indicator in membranes based separation processes. The selectivity could be described as ability of the membrane to separate the components of a solution. The selectivity of a contaminant present in the solution is expressed as retention (Ret). For a dilute solution the retention (Ret) of a specific component is given by the equation

$$Ret = \frac{C_f - C_p}{C_f} = 1 - \frac{C_p}{C_f} \qquad\qquad (1.4)$$

Where C_p is concentration of solute in permeate and C_f is the concentration of solute in the feed.

1.2. Transport mechanisms

The mechanism of permeation across the membrane can be described by two models [30, 34, 46]

1. Pore Flow

2. Solution diffusion

Pore flow is a simplest filtration model that takes into account porous membranes. It is mainly used in microfiltration and ultrafiltration processes. The barrier structure is porous thus separation is predominantly accomplished by size–sieving mechanism. The flow through the active layer of the porous membrane, shown in figure 1.5, is modeled as laminar flow through an array of cylindrical pores.
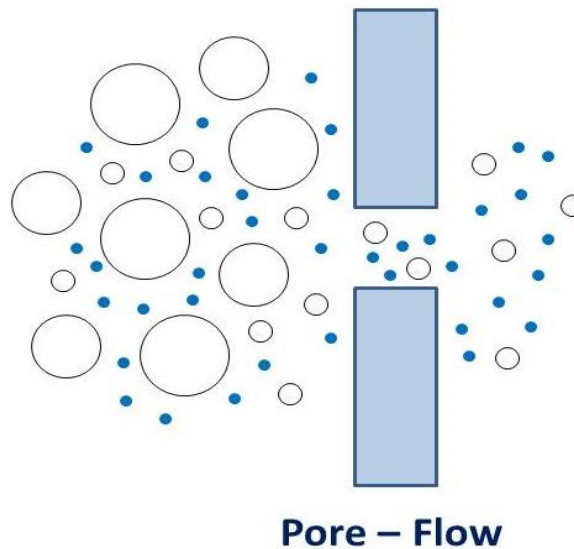
Pore – Flow

Figure 1.5: Pore–Flow transport mechanism

The water permeability is described by Hagen–Poisuille equation (1-5) that relates permeability (A) with the solution viscosity (μ) and morphological characteristics of the active layer namely the pore radius (r_p), surface porosity (ε) and active layer thickness (δ_m) [30]

$$A = \frac{\varepsilon \, rp^2}{8\mu\delta_m} \tag{1.5}$$

This simplified relationship describes an ideal membrane, with uniformly sized cylindrical pores, known as iso-porous membrane. In reality, membranes developed through phase inversion have tortuous and non–cylindrical pores that substantially vary in size. In addition to affecting the water permeability, the pore size distribution also influences the rejection of the salute particles present in the solution whereas the rejection is determined by the equation 1.4.

For non–porous dense membranes, water and solute transport is described through solution–diffusion model. Water and solute molecules partition in the active layer of the membrane, diffuse through the polymer matrix down their chemical potential gradients and desorb into the permeate solution. A schematic representation of solution diffusion model is given in Figure 1.6

Solution Diffusion
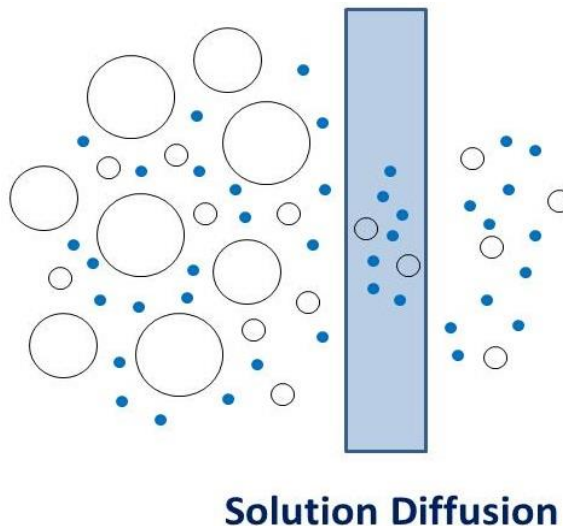
Figure 1.6: Solution–Diffusion transport mechanism

The solubility and diffusivity combine to determine the diffusive water permeability and diffusive solute permeability both of which are intrinsic material properties thus independent of thickness of membrane. The water permeability coefficient of active layer is related to the diffusive water permeability and layer thickness by the equation 1-6

$$A = \frac{P_w \cdot V_w}{\delta_m \, R \, T} \qquad (1.6)$$

Where

A	=	Water permeability coefficient
P_w	=	Diffusive water permeability
V_w	=	Molar volume of water
R	=	Gas constant
T	=	Absolute Temperature
δ_m	=	Active layer thickness

Similarly solute transport is modeled by Fick's law given here in equation 1.7

$$J_w = \frac{P_s}{\delta_m} \, \Delta C_m = B \Delta C_m \qquad (1.7)$$

Where B is the solute permeability coefficient and ΔC_m is the solute concentration difference across the active layer. Together the coefficients A and B largely define the selective layer performance of non–porous membranes. The working principle of reverse osmosis membranes is exclusively based on

solution–diffusion model but the performance of nano-filtration membranes display a combination of pore–flow and solution diffusion.

The aforementioned two models cover almost all the filtration processes. An overview of the most relevant membranes and their transport mechanisms is given in table 1.3 [49]

Table1.3: Important membranes processes and transport mechanisms [48]

Membrane Process	Membrane Structure	Two Phases	Driving Force	Transport Mechanism
Micro filtration	Porous (d > 100 nm)	L / L	ΔP	Pore Flow
Ultra filtration	Porous (d ≅ 2 – 100 nm)	L / L	ΔP	Pore Flow
Nano Filtration	Porous & micro-porous	L / L	ΔP	Pore Flow & Solution Diffusion
Reverse Osmosis	Nonporous	L / L	ΔP	Solution Diffusion
Gas Separation	Nonporous	G / G	ΔP	Solution Diffusion
Pervaporation	Nonporous	L / G	ΔC	Solution Diffusion
Electrodialysis	Nonporous	L / L	ΔE	Solution Diffusion Pore Flow
Diaylsis	Porous (d ≅ 2 – 100 nm)	L / L	ΔC	Solution Diffusion Pore Flow
Membrane distillation	Porous (d ≅ 2 – 100 nm)	L / G	ΔT	Vapor Diffusion

The current thesis is about ultrafiltration membranes that follows the pore flow transport mechanism. An ideal membrane is supposed to have both high permeability and high selectivity – a combination that is difficult to achieve. Almost all the recent studies proposed that porous and nonporous membranes, used in water separation, exhibit a permittivity–selectivity trade–off similar to

Robenson plot which has been extensively used in the area of polymeric gas separation membranes [49]. All observed trade–offs have a common implication i.e. an increase in the permeability of a highly permeating specie (say water) also increases the permeability of relatively less permeable species (say contaminants).

1.3. Selectivity mechanisms

The selectivity of a membrane could be explained through one of the following three mechanisms. These selectivity mechanisms originate from the physical and chemical interaction between membrane and the solute in the feed solution.

1. Physical sieving

2. Donnan effect

3. Adsorption

Physical sieving or size exclusion is the mechanism of separating the individual components on the behalf of difference in their sizes. The separation by a porous membrane predominantly makes use of physical sieving mechanism for instance commercially available porous polymeric membranes cover the range of pores' sizes from 0.004 to 10 µm. Thus solute particles smaller than the membrane's pores can permeate and the larger in size are rejected. Some conventional separation processes involving physical sieving are virus filtration [49–53], protein purification [54–56], sterilization and drinking water production [57–66] and particle filtration [58, 67]. A review on mathematical modeling of physical sieving has been reported by Bungay [68]. In a porous membrane if '*Ao*' is the effective cross sectional area of pore having radius 'r' then the available area '*A*' for separation of a solvent and solute of molecular radius 'a' is given by the equation 1.8 [69]

$$A = Ao \left(1 - \frac{a}{r}\right)^2 \qquad\qquad \textbf{(1.8)}$$

This mathematical approach doesn't consider any kind of physical or chemical interaction like diffusion or electrical interaction between the membrane and the solute. For this reason, the estimation of rejection based on this model is not applicable to all kinds of membranes and restricted mainly to the field of ultrafiltration. The sieving effect can also occur in a depth filtration mechanism which means that solute particle is captured in the interior of membrane because of size exclusion.

The donnan exclusion theory is profusely used to explain the salt separation by nanofiltration charged membranes. The introduction of charged species on the surface of membrane is a well-established method to create good selectivity of membranes. In this mechanism, the selectivity could be acheived in two opposite ways i.e. electrostatic attraction or repulsion. When the electric field is applied, the purported ion exchange membranes are capable of repelling ions of the same charge whereas the oppositely charged ions can pass through [70–72]. The charge on the surface of these membranes could be either positive or negative. A positively charged membrane is named "anion exchange membrane" and a negatively charged membrane is termed as "cation exchange membrane". The electrically charged surface ensures selectivity by adsorbing the opposite charged species for example a polymer membrane with positively charged surface can adsorb viruses [73]. The negatively charged protein shell of the virus (capsid) could be electrically attracted to the positively charged membranes surface whereas the uncharged species can travel unhindered through the membranes under the applied pressure [74–79].

Adsorption is a complex process that can involve different selectivity mechanisms at one time. It could include;

1. Specific adsorption by affinity membranes

2. Inertial capture

3. Brownian diffusion

4. Electrostatic adsorption

The electrostatic adsorption could be obtained using either charged membranes or affinity membranes. The affinity membranes are found to perform specific selectivity. These membranes were mainly developed to overcome the problem that arise from the use of membranes operating purely on the size exclusion principle in which broad pore sizes distribution leads to lack of optimum selectivity. The chemical modification and radiation grafting are commonly used methods to introduce functional groups on the surface of affinity membranes [80–83]. These functional groups can bind specific molecules thus creating selectivity of the membrane. Though extensive research is done in this field but few affinity membranes could reach the market because up-scaling of membrane modification technologies is still a big challenge [80].

In an ideal case, ignoring the physical sieving and Donnan effect, the particles follow the liquid flow. If the particle size is big enough to touch the collector wall the inertial effect following the rule described in equation 1.9 occurs.

$$Inertial\ effect: \eta I = \frac{2ap2}{9ac2} \qquad \textbf{(1.9)}$$

Where a_p is particle area and a_c is collector area.

An increased tortuosity can also contribute to the inertial capture especially in case of small particles having low momentum [34]. The Brownian diffusion (equation 1.10) tackles the movements of the particle into the membrane's wall quite differently from the inertial effect and influences particularly smaller particles. Smaller particles have a high tendency to follow the fluid flow but are more affected by the diffusive transport rate.

$$Brownian\ diffusion: \eta D = 4.04\ Pe\ 2/3 \qquad \textbf{(1.10)}$$

Where

$$Pe: Peclet\ number = \frac{advective\ transport\ rate}{diffusive\ transport\ rate}$$

In case of charged membranes, the electrostatic adsorption mechanism is mainly attributed to the interaction between particle and charge present on the membrane surface. These charged groups present on membrane surface provide adsorption sites for the particles having opposite charge. If the electrostatic adsorption is the primary mechanism to play, the rejection slightly falls during the time because of the progressive saturation of the charged groups. Figure 1.7 displays how multiple mechanisms can endanger the adsorption of particle [34]. A combination of aforementioned methods is always desirable to achieve highest possible rejection. For example a commercial product "3M zeta plusTM filter" uses a combination of size exclusion and electric attraction to achieve high value of virus retention [84].
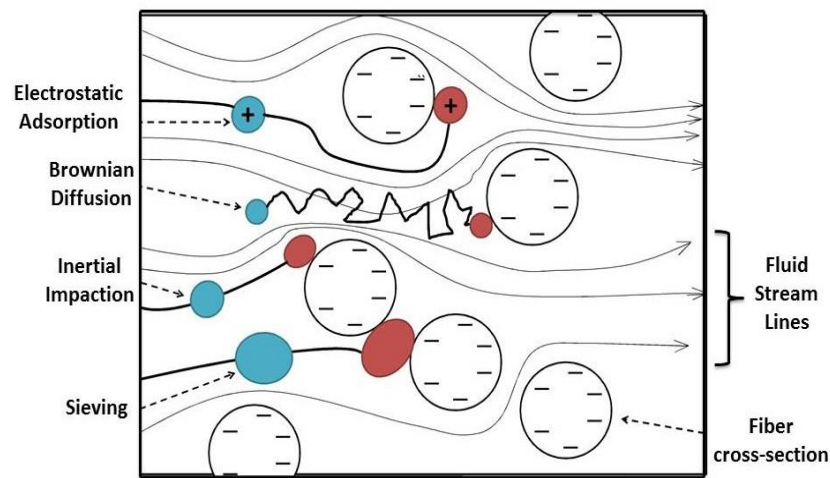
Figure 1.7: Multiple transport mechanisms

1.4. Filtration modes

Depending upon direction of flow on the membrane surface, the filtration modes can be divided into two categories

- Cross–flow filtration
- Dead–end filtration

In cross flow mode, the feed solution moves parallel to the membrane surface thus a shear stress is generated that scours the surface. A schematic representation of cross–flow filtration is shown in Figure 1.8. This filtration mode is principally effective when feed water is contaminated with high level of foulants like macromolecules and suspended solids. Though a bit higher energy is required in this mode but thickness of cake layer could be controlled. All membrane bio reactors (MBR) and most of waste water filtrations are based on cross–flow mode.

Cross–flow Filtration
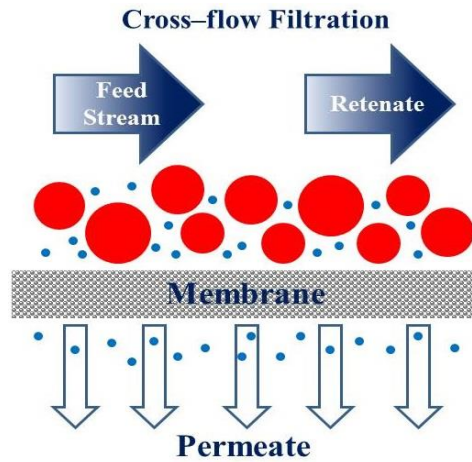
Figure 1.8: Cross–flow filtration mode

In dead–end filtration mode, the feed solution moves towards the membrane surface. Since no cross–flow exists, so process is not sustainable forever and after certain time of operation it becomes imperative to remove accumulated solids and perform backwashing. A schematic representation of dead–end filtration mode is shown in Figure 1.9. This filtration mode is suitable only if feed water has low level of foulants. The dead–end filtration mode is mainly used in pretreatment of sea water reverse osmosis process, tertiary filtration and surface water filtration.
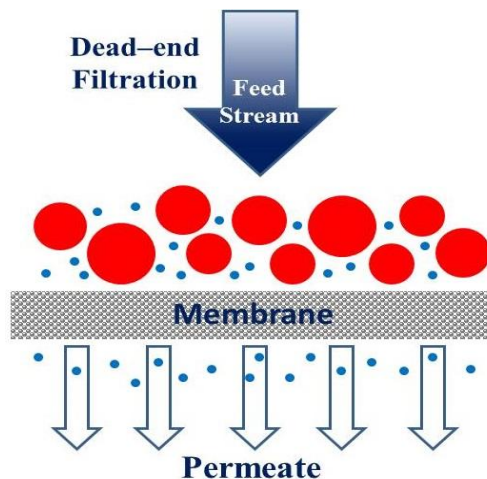
Figure 1.9: Dead–end filtration mode

Chapter 2

Polymeric Membranes

The membrane processes are currently employed in several ways to purify water such as microfiltration (MF), ultrafiltration (UF), nano filtration (NF), reverse osmosis (RO) and recently developed forward osmosis (FO). These methods have been recognized as new generation of water purification and reclamation technologies. The inherent attributes include promising sought–after outcomes, continuous and automatic operations, easy scale up, chemical–free or little need of chemicals and low energy consumption [37–40]. This combined with the rapidly growing need to purify more and more water represents a way long growth opportunity for membrane technology. The demand for better membranes is already fostering so a technological push is there. Though a broad range of inorganic and polymeric materials is used to manufacture the membranes but the polymeric membranes acquire by far major market share because of high process-ability and low cost. The current thesis is focused on polysulfone as a membrane material so a state of the art on polymeric membranes and their corresponding fabrication techniques are discussed in this chapter.

2.1. Preparation of Polymeric membranes

2.1.1. Phase separation polymeric membranes

The most common and oldest technique to fabricate porous polymeric membranes is phase separation. Besides many emerging fabrication techniques, the phase separation (also known as phase inversion) is still the predominant membrane

production technique [85, 86]. There are several ways to induce phase separation in the polymeric solutions [87–96]. The four major phase separation technologies are given as;

i. Evaporation induced phase separation – EIPS

In this process, the polymer is dissolved in a mixture of nonvolatile non–solvent and a volatile solvent. The phase separation takes place by the evaporation of solvent as polymer solubility decreases in non–solvent [97, 98].

ii. Vapor induced phase separation – VIPS

This method produces phase separation in polymer solution via adsorption of non–solvent from the vapor phase [99–101]

iii. Non solvent induced phase separation – NIPS

This is oldest and most common method of fabricating porous membranes [102–111]. The process of phase separation takes place when a polymer is dissolved in a good solvent and thereafter homogenous polymer solution is put into a non–solvent (typically water) with which solvent is miscible and the polymer is not. The exchange of good solvent with the non–solvent introduces phase separation of polymer solution i.e. polymer rich and polymer poor phases are distinguished. These two phases ultimately form pores (from the polymer-poor phase) and the solid membrane matrix (from the polymer-rich phase). This process is also called emulsion precipitation. A micrograph image of cross-section of UV–crosslinked methacrylated polysulfone membrane developed through NIPS, reported by Marco Sangermano et. al. [102], is shown in Figure 2.1
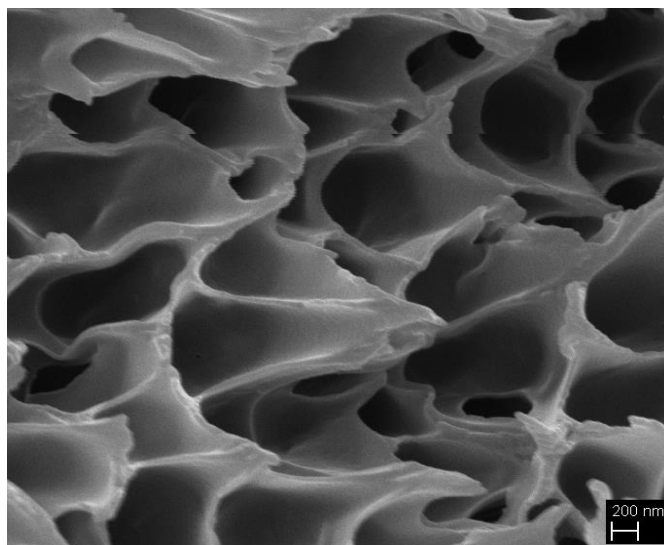
Figure 2.1: Cross sectional morphology of methacrylate PSF membrane from NIPS [102]

The emulsion precipitation takes place as a three steps procedure. At the first step, polymer is dissolved in an adequate solvent. This solution is then cast on a support structure (typically polymeric nonwoven) via doctor blade coating or continuous roll coating. On industrial scale this coating speed is usually 1–50 meter per minute. The third and last step is consisted of immersing the cast solution into coagulation bath so the polymer precipitates. The bath usually contains a non–solvent which is miscible with the solvent. Since most of the immersion precipitations involve water as non–solvent so NIPS, somehow, is restricted to water miscible solvents. The typical polymers employed for immersion precipitation and their solvents are given in the table 2.1

Table 2.1: Polymers and relevant solvents suitable for NIPS

Polymer	Solvent
Polysulfone (PSF)	Dimethylformamide (DMF)
	N-methylpyrrolidone (NMP)
Polyethersulfone (PES)	Dimethyacetamide (DMAc)
	N-methylpyrrolidone (NMP)
Cellulose (C) Cellulose Acetate (CA)	Dimethyl sulfoxide (DMSO)
	Dimethyacetamide (DMAc)
	N-methylpyrrolidone (NMP)
Polyvinylidene fluoride (PVDF)	Dimethyacetamide (DMAc)
	N-methylpyrrolidone (NMP)
	Dimethyl sulfoxide (DMSO)
	Dimethylformamide (DMF)
Polyacrylonitrile (PAN)	Dimethyacetamide (DMAc)
	N-methylpyrrolidone (NMP)
	Dimethylformamide (DMF)

The membrane morphology out of NIPS is governed by several important parameters such as polymer type, nature of solvent and non–solvent, polymer concentration and fabrication technique. The exchange of solvent with non–solvent dictates the size of pores, distribution of pores and the physical structure of solid membrane [112]. Due to stochastic nature, NIPS results into poly disperse pore-size distribution that adversely affects the selectivity. Nevertheless at present an extensive knowledge exists on how to "tailor" the membrane's pore structure including its cross–section morphology by the selection of adequate non–solvent and solvent for polymer, additives, residence times and other parameters involved in NIPS [113, 114]. For instance an important structure obtained through NIPS is thin "Skin" nano-porous top selective layer (which is often called an active layer) with underlying micro-porous structure that ensures good selectivity and high permeability. This kind of asymmetric membrane is prepared in a way that top surface of the cast film comes in contact with the non–solvent at first thus creating a finely porous selective skin layer. The precipitated skin layer slows the penetration of non–solvent thus causing the polymer below the skin layer to

precipitate slowly i.e. a delayed demixing and subsequently the sub structure is resulted into macro voids.

These asymmetric membranes are generally used in ultrafiltration. An analogous method is wet spinning to make the fibers [115–118] where the solidification step is called "Coagulation". Till today there is a reasonable quantity of literature dedicated to the analysis of NIPS or coagulation processes [119–129] nevertheless this practice, in large, is still an empirical art. The NIPS is particular suitable for the manufacturing of ultrafiltration membranes while microfiltration membranes are mainly produced through thermal induced phase separation (TIPS).

iv. Thermal induced phase separation – TIPS

This method is based on the phenomenon that quality of solvent decreases with the decrease of temperature. A polymer is dissolved in a low molecular weight compound that acts as solvent at higher temperature and non–solvent at low temperature. After the solution is cooled down, the phase separation occurs through crystallization or glass transition and the low molecular weight compound is extracted [130]. The TIPS is suitable for the polymers which are difficult to dissolve for example polypropylene.

2.1.2. Membranes preparation through stretching

Though phase inversion is predominant technique in the industrial production of microfiltration and ultrafiltration membranes. Nevertheless the pores size and distribution of pores sizes are difficult to control thus the number of polymers to be applied for phase inversion ultrafiltration membranes is restricted by the solvent–nonsolvent miscibility. In order to overcome these challenges associated with the phase inversion process, some other membrane manufacturing techniques were developed. Stretching is a solvent–free technique to develop pore flow membranes. This method involves stretching of melt-cast polymer films in order to create the micro–pores in crystalline and semi–crystalline polymers which are not workable with the phase inversion. The process was thoroughly investigated by Celanese to develop the product Celgard® from polypropylene (PP) and described in many patents [131, 132]. These patents covered many polymers and were used mostly in the battery separators and medical dressings.

Gore also applied the stretching technique for the production of well-known Gore-Tex® - a porous fabric made of poly teterafluoro-ethlyene [133]. The process begins with a precursor film that exhibits row-nucleated lamellar morphology. The precursor film is typically annealed to eliminate any inconsistencies lying in the crystal structure. The stretching is then carried out first at low temperature to create voids and subsequently at high temperature to widen these voids [134]. The morphology of precursor film plays an important role in stretching. The crystals formation takes place as a result of stress and elongation induced during extrusion process. The formation of crystals depends on different processing parameters and most importantly on the molecular weight of polymer [135]. A critical molecular weight is believed to exist in a way that it depends upon shear rate and temperature up to certain degree of shear rate and after that it is no more dependent on process conditions [136]. In polypropylene membranes, the high molecular weights were found to contribute an increase in size and uniformity of pores thus high water vapor transmission [134]. Moreover it has been observed that in case of poly (vinylidene fluoride) membranes, a specific crystalline structure is readily formed in the precursor film when a blend of low molecular weight and high molecular weight polymers was used [137].

2.1.3. Track–etch membranes

The track–etch is another industrial technique to fabricate micro-porous membranes [86]. Track etching consists of two steps: 1) partial degradation – a polymer film is bombarded with charged particles to create "track" through the film 2) chemical etching – the film is immersed in a chemical etchant to generate circular pores. The etching removes free bonds created by bombardment and almost perfectly straight capillaries are developed in the polymer film [138]. In contrast to other approaches, track-etched membranes have uniform pore size and thickness. Mostly polycarbonate (PC) and polypropylene (PP) films have been employed to produce track-etched membranes [139]. The main drawback of track-etched membranes is low void volume within the body of membrane which is normally kept lower than 5 % to avoid pores overlapping. The low porosity leads to low water permeability thus restricting track-etched membranes for analytical and scientific applications [140–143].

2.1.4. Block copolymer membranes

Selective removal of one component from self–assembled block copolymers displays a very remarkable and emerging technique to prepare porous polymeric membranes of high uniformity [144]. The covalently bonded two di-block or higher blocks (say tri-block) of immiscible polymers (e.g. polystyrene and poly-isoprene) form a block copolymer. This immiscibility favors the formation of structure that minimize the contact between the unlike polymers. The solution of these block copolymers can be cast on substrates and annealing leads to the formation of highly oriented structures. Depending on the volume fraction of the components and the composition of the copolymers, the following structures can occur [145–148].

- Lamellae (di-block copolymer)

- Cubic gyroid (di-block copolymer)

- Cylinders (di-block copolymer)

- Spheres (di-block copolymer)

- Cylinders between lamellae (tri-block copolymer)

- Rings around cylinder (tri-block copolymer)

- Tri-continuous diamond network (tri-block copolymer)

2.1.5. Template removal membranes

In order to fabricate a highly structured porous membrane, hard template removal from polymer matrix is an approach similar to block copolymer membranes. In this technique mostly an inorganic template in infiltrated by a monomer. Subsequent polymerization and template removal lead to an interconnected porous structure [149–153]. Only highly precise template replicates one structure into another so the main focus lies on the application of ordered mesoporous silica nanoparticles or generally speaking colloidal crystals as templates [154–157].

2.2. Areas of application

In porous polymeric membranes, the size of pores and percentage porosity determine the possible application of membranes. The porous polymeric membranes cover the pore size from 10^{-4} to 10 µm. The decision on the pore size is crucial for an optimum selectivity and permeability in a membrane operation. Generally a filtration process is supposed to ensure the rejection of at least 90% of the contaminant. Nevertheless high rejection rates are achieved at the expense of fast separation processes. Most often the membranes supplier companies mark the specification of a membrane as a molecular weight cut-off (MWCO) limit. This precautionary measure could be attributed to the broad pore size distribution – a predominant aspect of phase inversion membranes. The four most common membrane based separation processes are microfiltration (MF), ultrafiltration (UF), nano-filtration (NF) and reverse osmosis (RO). In all these operations the driving force is the hydraulic pressure. The applied pressure increases with the decrease of pore size. The filtration levels, the corresponding pore sizes and the applied pressures are given in Figure 2.2.

Pressure (Bar)

| < 1 | 1 – 10 | 20 – 40 | 30 – 60 |

| **Micro Filtration** | **Ultra Filtration** | **Nano Filtration** | **Reverse Osmosis** |

| $10^{1} - 10^{-1}$ | $10^{-1} - 10^{-2}$ | $10^{-2} - 10^{-3}$ | $10^{-3} - 10^{-4}$ |

Pore size (µm)
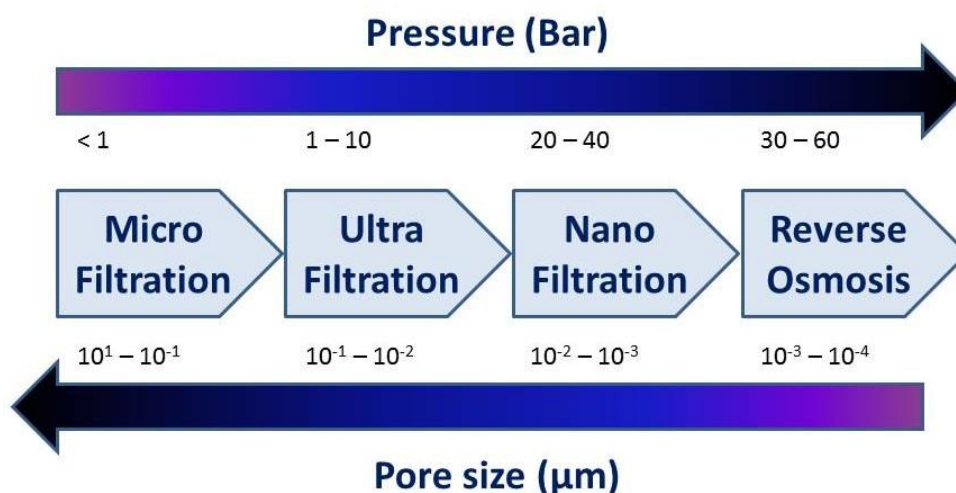
Figure 2.2: Different filtration levels where driving force is hydraulic pressure

Besides above stated filtration processes another recently developed and remarkable technology is forward osmosis (FO) process. The forward osmosis process rejects minerals, solids and other contaminants almost at the same level as that of RO. However this technique is quite energy efficient because in order to drive the flux it makes use of "Draw solution" on permeate side instead of hydraulic pressure on the feed side. The driving force is based on the natural equilibrium process i.e. "Osmosis". Being energy efficient the FO process is also

termed as "Green technology" [158]. Figure 2.3 shows different filtration levels in terms of size of contaminant removed as well as the selectivity mechanism involved at each level.
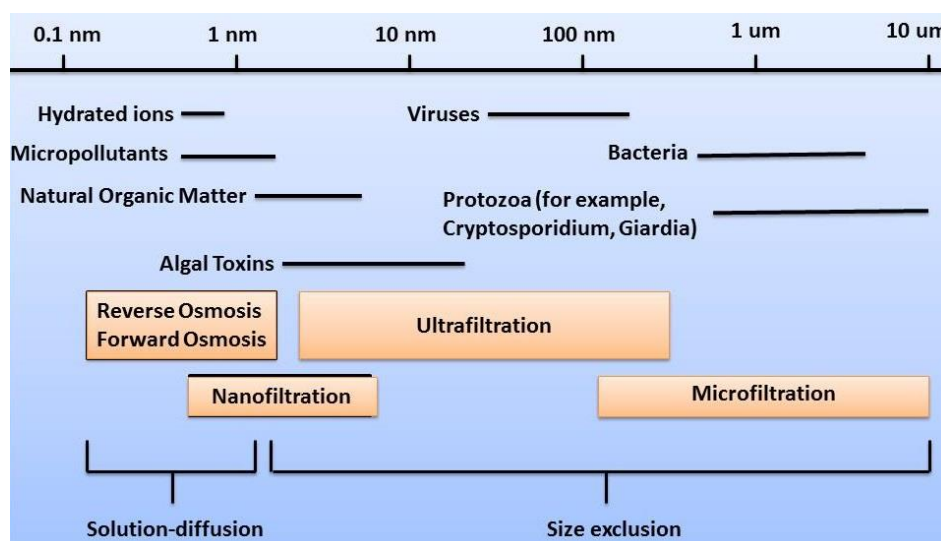
Figure 2.3: Filtration levels in terms of size of contaminant to be removed

2.2.1. Microfiltration

Among polymeric membranes, microfiltration membranes have the largest pore size range. The pore size ranges from 0.1 to 5 μm. The rejection process is purely based on size–exclusion sieving mechanism. Many suspended micro particles such as bacteria and colloids are rejected by microfiltration. This filtration level offers high water flux at reasonably low pressure (<1 bar). However there is no effective removal of germs and viruses. Thus microfiltration membranes are generally used for the disinfection steps of biotechnology and drinking water production [49, 53, 159]. These membranes are mainly developed through phase separation technique more precisely thermal induced phase separation – TIPS [138, 160–165]. The microfiltration membranes have been also produced through stretching of semi–crystalline polymer [139, 141, 166–167] and track–etching [148]. The most common polymers for hydrophobic microfiltration membranes are PVDF, Polyporpylene (PP), Polytetrafouroethylene (PTFE), Polyethylene

(PE) and Polysulfone (PSF) while hydrophilic microfiltration membranes could be manufactured from cellulose acetate (CA) and polycarbonate (PC) [65].

The hydrophobic microfiltration membranes developed via stretching method are very well known in the market under different registered brand names. Gore-Tex® is prepared from the chemically stable PTFE. Due to its hydrophobic nature, this membrane exhibits excellent properties as functional textile membrane. The membrane doesn't wet even upon contact with water but the pores are large enough to let the water vapors (perspiration) to pass through easily. Another well-known hydrophobic microfiltration brand is Celgard®. This stretched film from PP has been successfully employed as lithium ion separator with excellent resistance to bases, acids and oxidation. The membranes used in batteries separate the electrodes to prevent a short circuit while ions can travel through unrestrictedly. Besides application in the purification of drinking water the hydrophilic micro-porous membranes, produced via TIPS, have also become indispensable components in the production of beverages. Micro-organisms such as fungi, virus, bacteria, algae and protozoa pose a serious health risk and should have been removed in the production of beverages [168, 169]. Typical microfiltration membranes act as pre-filters to remove bacterial contamination [66, 170]. ASTM F838 confirms a microfiltration membrane as a sterile filter only if 99.99 % of *brevomundis diminuta* of 10^7 cell ml^{-1} is removed through filtration [171, 172]. Coupled together, microfiltration and ultrafiltration membranes are found to be effective in complete removal of biologically hazardous components [65, 173–174]. This combination is also suitable to meet the demand of purifying water for pharmaceutical sectors as well as electronics industries.

2.2.2. Ultrafiltration

The ultrafiltration (UF) membranes are generally used to separate colloids and macromolecules from solutions. The average pore size in UF membranes ranges from 1 to 100 nm. The UF membranes, in large, are produced by phase separation method more precisely non–solvent induced phase separation (NIPS). The commonly used polymers to prepare UF membranes include Polysulfone (PSF), Poly(ethersulfone) (PES), cellulose acetate (CA), Poly (ether imides), aromatic polyamides, Poly (vinylidence fluoride) (PVDF) and Poly (vinyl pyrrolidone) [34, 95, 175–176]. The asymmetric UF membranes are conventionally prepared through the Loeb – Sourirajan process [177, 178]. These asymmetric membranes

have dense top layer (lower surface porosity and smaller pore size) while the core of membranes consists of macro voids. These membranes are fabricated on the top of very open micro–sized substrate. Such a fine porous surface presents higher hydrodynamic resistance and ensures optimum separation. The micro-porous support provides sufficient mechanical strength.

An ultrafiltration membrane operates through size or shape sieving mechanism that is working principle of typical porous membranes. The cut-off of UF membranes is normally specified by the molecular weight of solute being rejected. However the shape of the molecules to be rejected also influences the overall rejection by an UF membrane [34]. Normally the rejection of linear and flexible macromolecules is much lower than what recorded for globular and rigid proteins of same molecular weight. The low rejection could be attributed to the easy sneak of linear molecules through the membrane pores under an agitated state triggered by external driving forces. The protein molecules, of same molecular weight, exist in the solution as a tightly wound globular coils which are held together by hydrogen bonds. These globular structured molecules are rejected primarily because of the shape. The properties of solution such as ionic strength and pH can also affect the permeation and rejection of ultrafiltration membranes.

Nowadays the ultrafiltration membranes are being used in a variety of separation processes carried out in pharmaceutical, dairy, food, biotechnology, textile and different chemical industries [49–50, 52–53, 179–180]. The first successful commercial application of UF membranes was the recovery of electro-coat automotive paint [34]. Thereafter several applications in the food and diary industries were developed such as production of cheese and juices [181–184].

Furthermore this class of membranes is very suitable for concentration and purification of proteins, biomolecules and antibodies [54–55, 185]. The asymmetric UF membranes display very small surface pores thus the smallest parvoviruses (of size approximately 20 nm) can be removed by ultrafiltration. This characteristic of asymmetric UF membranes holds great significance for the pharmaceutical industry and production of drinking water [49–50, 52–53, 179–180]. A flow chart of structural and performance related parameters of asymmetric porous UF membranes is given in Figure 2.4
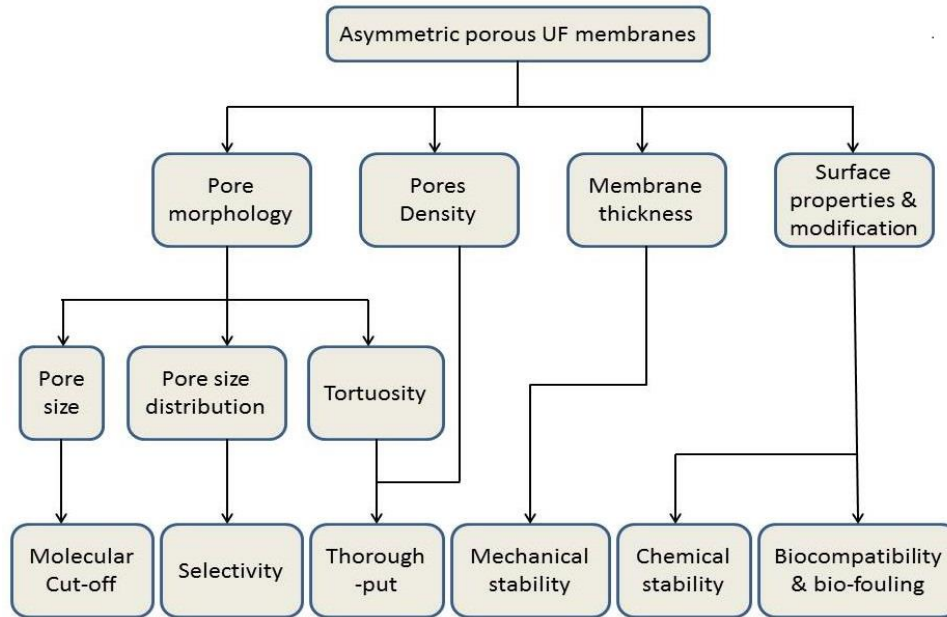
Figure 2.4: Parametric analysis on structure of asymmetric UF membranes

The majority of commercially available ultrafiltration membranes are made of polysulfone. This material can be easily fabricated into high porous structure via NIPS. Besides highly porous structure, the material also exhibits excellent temperature and pH stability. The glass transition temperature of polysulfone is reported around 185 ^{o}C [102]. Nevertheless the hydrophobic properties of polysulfone account for certain disadvantages of ultrafiltration membranes made of this material. The hydrophobic nature of polysulfone promotes the binding of micro-organisms to the surface of membranes causing the blockage of surface pores thus reducing the water flux [186–190]. The retained macromolecules continue to accumulate on the membrane surface thus causing a concentration build up that leads to concentration polarization on the feed side of UF membranes. In a continuous operation, at one stage the concentration of the accumulated macromolecules may become so high that a gel layer could be formed on the surface of membranes and this is known as "fouling" i.e. deposition of retained macromolecules and colloids on the surface of membrane. The fouling and concentration polarization could reduce the flux drastically and shorten the membrane life. Hence, in addition to principal parameters i.e. flux and the selectivity, the ability to overcome fouling has also become an important consideration in the selection of an UF membrane. Several modifications have

been proposed to control the fouling of polysulfone based ultrafiltration membranes such as blending with hydrophilic polymers [65, 191], use of a wetting agent [192] and some novel surface functionalization [193]. As a general understanding when UF membrane is employed to treat an aqueous solution the fouling could be minimized only if the top layer of membrane is hydrophilic. Once the hydrophilicity is rendered, the membranes could be useful for prolonged operations in water treatment, sterile filtration, buffer filtration and tissue culture media filtration [194–196].

Besides fouling, another important shortcoming of polysulfone based membranes is related to stability in organic solvents. The membranes made of pristine polysulfone are not resistant to majority of organic solvents [102, 103]. There have been several attempts to increase the solvent stability of polysulfone based membranes. Though specific solvent stability is somehow achieved but almost all those approaches resulted into severe flux decline. In order to improve solvent stability, this thesis is focused on UV–induced acrylic functionalization of polysulfone aiming solvent stable polysulfone membranes in a way that flux could be retained at much higher level in contrast to previous works.

PVDF is another polymeric material used to prepare UF membranes. It has glass transition temperature equal to $-40 \, ^{\circ}C$ and exhibits better resistance to organic solvents. The semi crystalline PVDF poses certain elasticity and feels soft. Being soluble in NMP it can be fabricated into porous membranes through NIPS. Naturally PVDF is enormously hydrophobic and displays good binding of protein and nucleic acid. Therefore an unmodified PVDF membrane with pore size 0.2 to 0.4 μm is ideally suitable to function as a transfer membrane in blotting applications [197–199]. In order to make hydrophilic PVDF membranes, almost similar approaches could be used what has been reported for polysulfone membranes. A hydrophilic PVDF membrane could be a valid alternate to PSF membranes for applications like protein purification and sterile filtration [200–202]. Despite conferring hydrophilicity to the hydrophobic polymers, an alternate approach to overcome the fouling of membranes is use of cellulose based naturally hydrophilic membranes [86]. Most common products of this class are cellulose acetate, cellulose ester and cellulose nitrate. The self-wetting properties of these membranes make them useful in dialysis applications [55]. The membrane cartridges or tubes made of cellulose ester are filled with the solutions of proteins, biomolecules or antibodies and thereafter immersed in deionized water thus contaminants and molecules diffuse through membrane following the concentration gradient. Small particles tend to diffuse much faster than small

molecules while the size of membrane surface pores ensures size exclusion. All these steps involved in dialysis process efficiently remove residuals from biomolecule synthesis and can be applied for buffer exchange as well.

Unfortunately the dialysis processes are very slow and could take days to complete but dialysate has to be replaced at least once a day to maintain a high concentration gradient. A Californian-based company, Spectrum Labs, has developed so-called dynamic membranes to reduce the change-over of membranes. A constant counter-flow, of dialysate and solution, guarantees a steady and highest concentration gradient thus increases diffusion rate and efficiency [194–196].

Among all reported techniques to prepare UF membranes, the phase separation is dominating method due to ease of fabrication and simplicity of the process. On the other hand the process of phase separation is very quick and a good control on this process is not possible thus resultant morphology has broad distribution of pores sizes. The poly-dispersion of pores sizes leads to insufficient membrane selectivity consequently broader molecular weight cut-off limits the applicability of UF membranes to many applications [91].

The advance polymer synthesis and polymer processing techniques are being explored to optimize the performance of UF membrane for example fabrication of track–etched polycarbonate (PC) based UF membranes shown in Figure 2.5 [203]. This kind of membrane has uniform and narrow pore size distributions thus exhibit a sharper molecular weight cut-off. Nevertheless the low pore density of track–etched UF membranes displays a very low flux.
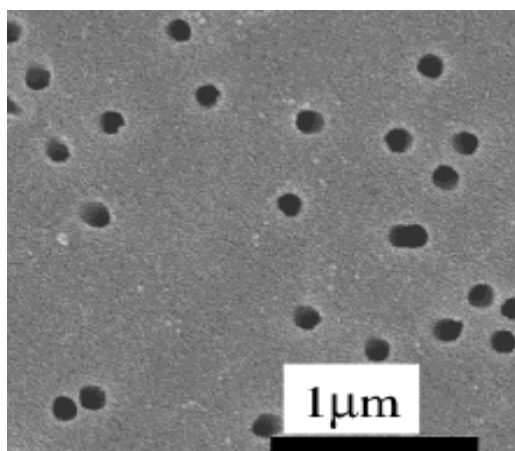
Figure 2.5: A track–etched polycarbonate based UF membrane [203]

2.2.3. Nano-filtration and Reverse Osmosis membranes

Both nano–filtration and reverse osmosis (RO) membranes were initially produced by the Loeb-Souirajan process from cellulose acetate through phase inversion process but currently these membranes are largely developed as thin film composite (TFC) structure where a thin non-porous skin layer is deposited on the top of a conventional porous UF membrane. Unlike Loeb–Sourirajan integrally skinned membranes, the two components of TFC membrane almost always have different chemical compositions and therefore need to be optimized for optimum separation. Soon after Loeb–Sourirajan published their phase inversion method; Francis developed composite membranes [148] and Peterson provided an extensive review of composite nano-filtration and reverse osmosis membranes [31]. Initially cellulose acetate phase separation membranes were used as support material but nowadays polysulfone (PSF) and polyethersulfone (PES) pull off major share.

The composite structure of TFC membranes could be formed in different ways including laminating together separately formed support and top layers but as of today the vast majority of nano-filtration membranes are produced by interfacial polymerization of a set of monomers on the support. Linear aromatic polyamides are one of the polymers taken as selective layer [31] in TFC membranes.

The TFC membranes are non–porous in nature. The application of NF and RO membranes, in water desalination and treatment of organic solvents, has been

tremendously augmented in last twenty years. As the name reveals, RO means the inverse of Osmotic pressure. If the applied pressure is raised to a level > 30 bar, the dissolved components tend to travel against the osmotic pressure [204]. Today RO membranes find application mainly in the field of desalination of seawater as proposed by Reid and Breton back in 1959 [205].

The dense skin layer of these membranes, when comes in contact with water, swells and thereafter tinny channels are formed which allow only water molecule to pass through whereas monovalent and divalent ions are rejected. Nano-filtration is relatively new terminology and from literature we come to know different definitions of this class of membranes [86, 206]. RO membranes are mostly being used in the treatment of aqueous solutions while nano-filtration membranes are focused on the treatment of organic solvents [207–209].

The selectively of RO membranes exclusively follows solution–diffusion mechanism and for NF membranes it is reported as combination of pore–flow and solution–diffusion [42]. Regarding application of NF membranes in the treatment of organic solvents, first major advancement was the work by the group of Prof. Livingston from Imperial College London. The chemically cross–linked polyimide (PI) nano-filtration membranes were found to withstand antagonistic organic solvents such as NMP, THF and DMF [210]. An asymmetric PI membrane, prepared by the phase inversion method, was immersed in a bath of cross-linker and methanol for 24 hrs. This kind of NF membrane was developed as an integral asymmetric membrane rather than predominant TFC nano-filtration membrane. These NF membranes exhibited superior solvent stability in comparison to membranes made of ordinary PI whereas MWCO was collected between 250 to 400 Da. This innovative work led to the foundation of membrane extraction technology [MET] Ltd. which was acquired by Evonik in 2010.

2.2.4. Forward osmosis

Forward Osmosis (FO) is a new and energy efficient technique to remove pollutants from water. Like reverse osmosis (RO) the FO also involves solution–diffusion mechanism to reject the contaminants but avoids typical fouling problem associated with RO. The fouling is produced by the application of high hydraulic pressure on the feed side while in FO operation the flux driving force is not hydraulic pressure but a "draw" solution on the permeate side. The high osmotic

potential of "draw" solution provides the "power" to FO operation thus flux is driven by the fundamental principal of natural equilibrium process i.e. Osmosis.

FO has certain advantages [158] over hydraulic driven RO technique such as;

- FO overcomes fouling – an inherent shortcoming in pressure driven membrane
- FO can process feed streams which have normally high level of contaminants
- As osmosis is naturally driven process so FO requires either little or no energy

Chapter No. 3

Photo-irradiation of polymeric membranes

3.1. State of the art

Over last three decades the use of polymeric membranes in separation technologies has attained an exponential growth so does the modification to improve the performance. One of the most fascinating technologies, to couple with fabrication of membranes, is the use of photo-irradiation to tailor the membrane structure thus broadening the spectrum of membrane functionality for different applications. The current thesis is focused on the use of UV irradiation in the development of novel Polysulfone based membranes so recent works on the use of photo-irradiation in membrane technologies are discussed in this chapter.

The photo-initiated reactions, applied in membrane technologies, have a tendency to influence the structure of membranes and subsequently the performance in many different ways. The observed effects on the ultimate properties of polymeric membranes mainly depend on the membrane material, membrane structure (porous or non-porous) and affinity of the membrane (charge or uncharged) [48]. The photo-irradiation technique could be applied to membrane technologies in two main pathways one right from the beginning of membrane manufacturing and other as a post modification.

The role in the preparation of polymeric membranes is mainly consisted of either photo-initiated polymerization [211–214] or photo–crosslinking [215]. While the post modification, also known as membrane functionalization, is employed to escalate the functionality of already prepared membrane. The new functionalization on the membranes could be obtained through photo–crosslinking [216, 217] or photo–grafting [218, 219]. Another application of photo–irradiation is partial degradation of membrane material for the sake of development of pores but such a photo–degradation is rarely applied [220].

The photo–irradiation based membrane functionalization has conferred an evidently increased sustainability of the membranes in prolonged operations. For instance, in order to maintain the selectivity of the non–porous membranes used in NF, RO and PV, the unwanted swelling of barrier layer should be prevented [221]. The swelling of the barrier layer is dominant when applied to the liquids while the magnitude of the effect is larger in PV and NF and smaller in RO. The photo-crosslinking of barrier layer has been proved an effective modification to avoid the swelling. A schematic representation of UV cross-linked barrier layer is shown in Figure 3.1a

The membranes dealing with aqueous based complex solutions often face the problem of fouling thus cleaning intervals increase the cost of operation and reduce the overall efficiency of system. In most of the cases the fouling occurs because of undesired interactions between the contaminant and active surface of membrane. The surface bound UV technologies, developing grafted layers or thin coatings, can potentially serve the purpose of anti-fouling [218, 219].

Another important implication of photo–irradiation is realized in the enhanced functionality of porous MF membranes where the separation of substances is obtained through reversible binding of the functionalized pores. A schematic representation of UV functionalized pores is shown in Figure 3.1b. The UV–induced functionalization of suitable porous membranes, mostly macro-porous filters or MF membranes via "grafting-to" [222] or 'grafting-from" [223] could be efficient approaches.
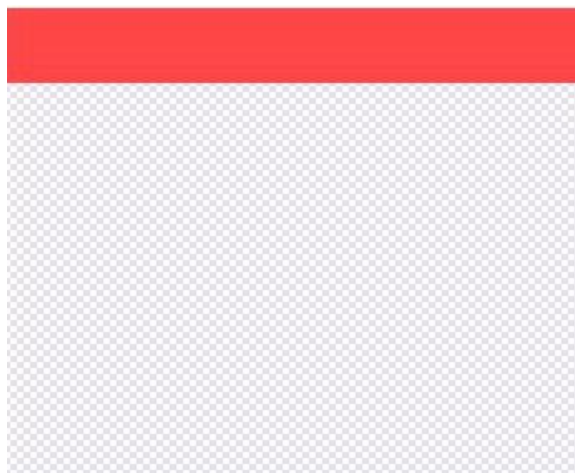
Figure 3.1a: Schematic representation of UV cross-linked barrier layer
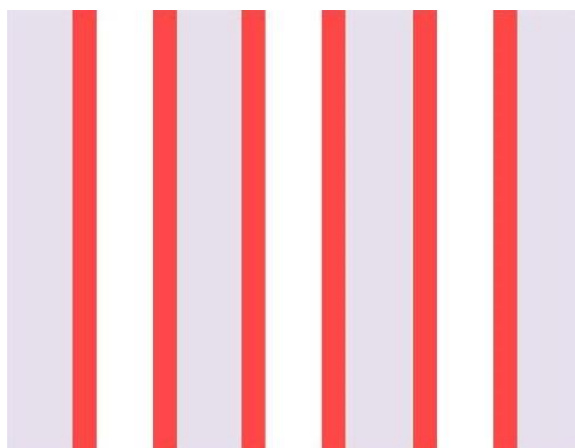
Figure 3.1b: Schematic representation of UV functionalized pores

The polymeric electrolyte membranes used in fuel cells are required to maintain the high concentration of charged groups so high conductivity is obtained but such a high concentration also leads to undesired swelling hence the barrier properties are compromised [224]. In order to overcome the swelling, photo-crosslinking of polyelectrolyte was carried out in a way that pores of the porous support membrane were filled with the photoactive polymer (Figure 3.1c) and thereafter photo cross-linked [48].
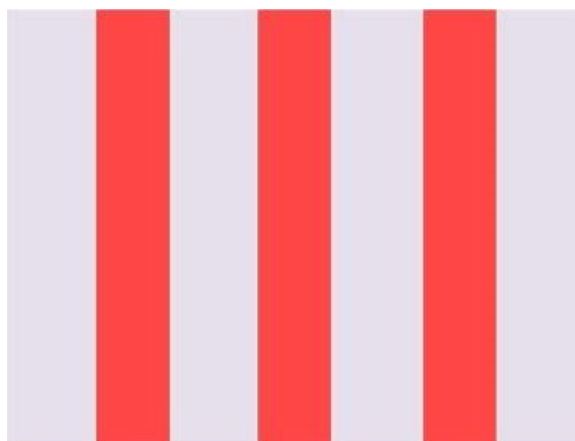
Figure 3.1c: Schematic representation of pores filled with photoactive polymer

UV irradiation has been also applied to fabricate novel membranes with reversibly "switchable" properties [225]. There is a growing interest in this kind of membranes as functional macromolecular systems could be designed in a number of ways to meet diversified application. Moreover it's reported that UV irradiation has potential application in special membranes used for integrated processes such as sensor system [226], bio-hybrid organs [227], (bio) catalytic reactors [228] and lab-on-chip systems [229].

3.2. Fundamentals of photo-polymerization and UV-curing

The photo–chemical reactions, as a general understanding, are the reactions induced by UV (200–400 nm), visible light rays (400–760 nm) and infrared rays (780–20,000 nm) [230]. In this thesis UV radiations are employed to functionalize Polysulfone so photo-irradiations in UV region are preferentially discussed in this chapter. The molecules of a system absorb light energy through electronic excitation. The efficiency of photo irradiation depends on the chemical structure of system to be irradiated as well as the energy (that is directly proportional to frequency and inversely proportional to the wavelength of radiations) and intensity of radiations.

The absorbed light leads to production of more reactive sites thus various photo–initiated reactions progress. The efficiency of these reactions depends upon the extent of competing irradiative (fluorescence or phosphorescence) and thermal deactivation processes. It is noteworthy that many of such photo–induced reactions occur (or efficiently proceed) only from the excited state of a molecule and not from the ground state.

The molecules rise to excited state after absorbing photons of light energy, whereas the energy contained in each photon is given in equation 3.1

$$E = h\nu \qquad\qquad\qquad \textbf{(3.1)}$$

Where h is planks constant and ν is the frequency of radiations.

This forms the basis of well-known chemo–selectivity of photo reactions – a practical term often used. The quantum yield provides the efficiency of a photo reaction and it is calculated as the ratio between amount of reactant consumed or product formed and the amount of photons absorbed. In photo-reactions two different reactive entities can be distinguished depending upon the mechanisms of reactions i.e. photo–sensitizers and photo-reactive molecules. Photo-sensitizers absorb the light selectively and subsequently trigger the chemical reaction of another substance thus energy is transferred through various mechanisms; most important of them are radiative and electron transfer.

On the other hand photo–reactive molecules (or functional groups in polymers) are likely to follow below possible conversions after absorption of light. These conversion processes are normally consisted of cleavage of at least one chemical bond. The types of conversions are;

1. Irreversible reaction (addition, substitution or elimination)

2. Reversible reaction (typically isomerization)

An important implication is the photo–initiated polymerization where one absorbed photon can lead to consumption of thousands of reactant molecules

(monomers). The light absorption by different substances is typically described by Lambert–Beer law given in equation 3.2

$$A = \varepsilon.C.l \qquad\qquad \textbf{(3.2)}$$

Where

A = Absorbance (unit-less)

ε = Molar absorptivity [L mol^{-1} cm^{-1}]

C = Concentration [mol L^{-1}]

l = Path length of the sample [cm]

The efficiency in terms of light absorption depends on matric effects, local concentration and many other factors. In case of more complicated samples with high turbidity there would be both absorption and scattering of light.

The emerging applications of UV and visible radiations are equipped with following advantages;

- Mostly no need of special solvents and added catalysts

- Under mild conditions (ambient temperature or also much below) a high selectivity of chemical reactions could be obtained

- Spatially addressable effects (2D and 3D structuring possible)

- Applicable to both large and very small scales

The different technical applications of photo–irradiation are;

- UV curing of coatings (2D reactions on thin films)

- Chemical synthesis

- Photo–catalysis

- Photo–Lithography

- Photo – polymerization of 3D objects like rapid prototyping and dental implants

- Data recording, transfer and storage

- Waste water treatment and disinfection of water (advanced oxidation)

- UV–sensitive "smart" materials

For photo–irradiation a large number of light sources are available and they could be applied for both fundamental investigation at lab scale and large technical applications. The light sources are mostly distinguished based on the emitted intensities [230–236] and the area to be emitted. While the amount of energy obtained depends upon intrinsic principle for example the traditional light bulbs produce light via electric heating of a filament usually made of tungsten. These bulbs exhibit moderate intensities up to few 100s of mW/cm^2 and used mainly for illumination in the visible range. The amplification of emission is possible by incorporating different additives to the filling gas. The lamps producing glow discharge are based on the plasma state of an inert gas whereas their emission energy is modulated by the addition of metals such as Mercury.

The configuration of such lamps depends on end-use like illumination or radiation-based curing. For UV–curing technologies (up to several 10s of W/cm^2) the high-intensity lamps for the entire wavelength range with tube length up to two meter are commercially available. The UV radiations are an exciting source of energy and over last two decades the use of UV has seen enormous growth in different new applications such as;

- Abrasives

- Metal coatings

- Fiberglass impregnation

- Electronics

- Car refinishing

The UV cured coatings and inks take into account solvents or waterborne systems. The polymerization is triggered by UV and binders polymerize forming an insoluble 3D network. In order to cure the UV radiations ensure quick transformation from liquid to solid. The UV belongs to 200–400 nm region of electromagnetic spectrum as shown in Figure 3.2.
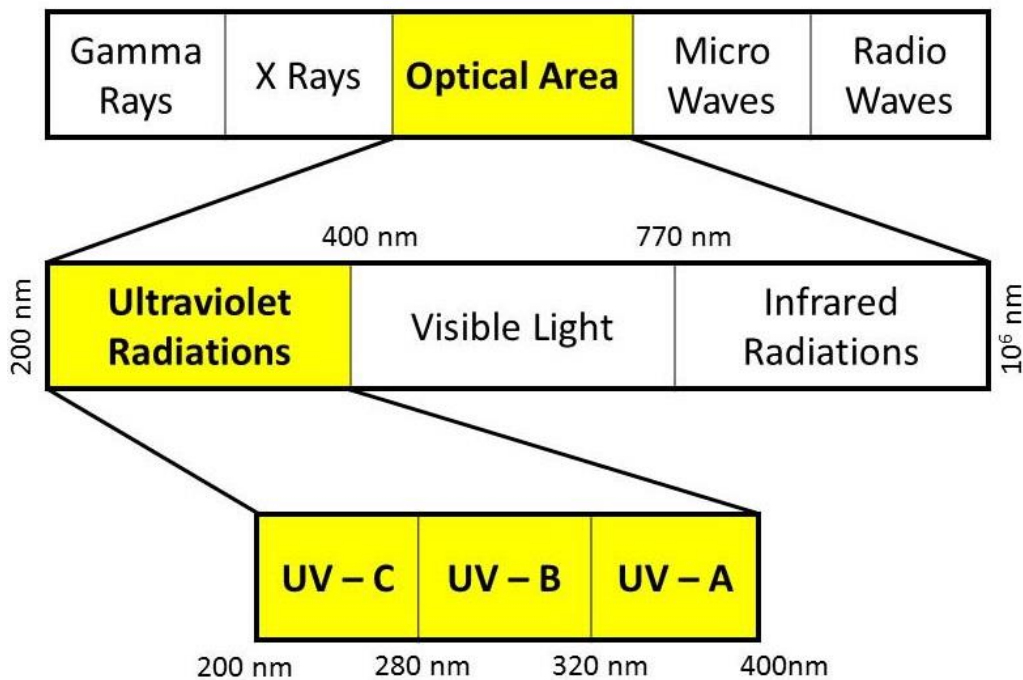
Figure 3.2: Different components of UV in electromagnetic spectrum

Thus UV curing comes up with several advantages over conventional chemical curing, for example;

- Immediate drying

- Low energy requirements

- In–line finishing

- Less space requirements

- High productivity / Rapid throughput

- Low VOCs content

- High and low gloss

- Unique performance

- Ability to coat heat–sensitive substrates

- UV technology can easily couple with existing production line

A schematic representation of photo–chemistry involved in UV curing is described in Figure 3.3.
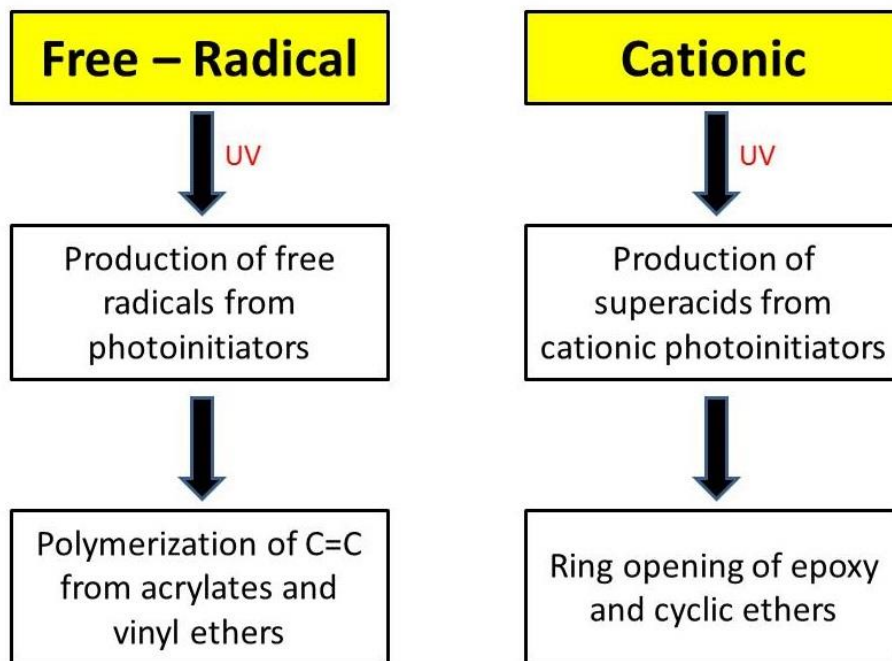
Figure 3.3: Photo–chemistry involved in UV curing

Besides certain advantageous aspects of UV as an efficient energy source, the regulatory environment (REACH, 2010 VOC regulations) is creating both opportunities and challenges for UV industry players.

3.3. The use of photo–irradiation for polymeric membranes

Photo–irradiation has been employed not only for preparation of membranes but also to improve the performance of existing membranes. The use of photo irradiation in the development of membranes largely depends upon choice of precursors that could be one or more and photo–chemical step is crucial in determining the final properties of developed membranes. The other application of photo–irradiation is post-modification (known as ''functionalization'') of an already fabricated polymeric membrane.

The performance parameters of polymeric membranes have seen substantial improvement through application of photo–irradiation depending upon the material of membrane.

The notable performance parameters are;

- Flux

- Selectivity

- Chemical and mechanical stabilities

- Anti-fouling

For post modification through photo–irradiation, the membrane must contain photo–responsive groups to undergo certain chemical and physical changes. The important roles of photo–irradiation in polymeric membranes are;

3.3.1. Photo–initiated polymerization

3.3.2. Photo crosslinking of polymeric membranes

3.3.3. Photo–functionalization of polymeric membranes

3.3.4. Photo degradation

3.3.1. Photo–initiated polymerization

The photo–irradiation based *in–situ* polymerization has been acknowledged as a good alternate of already established methods to prepare membranes. One particular advantage is that membranes could be prepared in one step from cross–linkable polymers. These photo–initiated polymerization reactions commence via photo initiators or/and photosensitizes and proceed efficiently thereafter. Some good reviews on various aspects of these processes have been already published [211, 212]. *In–situ* cross-linking polymerization carries versatility to fix interesting and sensitive morphologies such as sample preparation for transmission electron microscopy [48] and this concept could be extended to immobilize the self-assembled barrier structures. In order to have enzyme immobilization the photo–initiated preparation of membranes was reported by Arica et. al. [237, 238].

The hydrogel membranes, for biosensor and biomedical applications, represent an important application of photo–initiated polymerization technique in membrane preparation [215]. Poly HEMA membranes were prepared to immobilize the enzyme catalase [238]. For ion–selective sensor a membrane matrix free of plasticizer was prepared via free radical photo–initiated polymerization of a mixture of monomethacryloxypropyl, oligodimethylsiloxaes and dimethacryloxypropyl [239]. Another example is fabrication of self-supporting mixed matrix membrane consisting of ion conductive polymer electrolyte [240].

The micro-dialysis membranes were prepared via *in-situ* UV–initiated polymerization of the zwitterionic monomer and the cross linker using a focused 355 nm laser beam [241]. The molecular cut-off of these membranes could be engineered by controlling phase separation in the course of cross–linking polymerization i.e. manipulating the ratio between solvent and non–solvent. These membranes could be used for electrophoretic concentration of proteins in a microchip [242]. Photo–initiated polymerization have been also employed to prepare stimuli responsive membranes for controlling drug permeation, drug release [243], release of proteins [244, 245], recognition of cholesterol [246] or d-glucose [247]. UV irradiation was also used for sol–gel synthesis of silica particles as UV was employed during *in-situ* preparation of mixed matrix silica/poly(ethylene oxide) (PEO) – immobilized electrolyte membranes [248].

3.3.2. Photo-crosslinking of polymeric membranes

Photo-crosslinking is of great interest not only for membrane preparation (as mentioned in section 3.3.1) but also for the modification of already prepared polymer membranes in order to increase permittivity and selectivity or to introduce other desired properties. In order to achieve this target, crosslinking is generally aimed to change the physical property and chemical structure of polymeric membranes. The photo-crosslinking modifications of membranes from photo-reactive polymer and of polymeric membranes with added photoactive agent is covered in this section. There are two distinctive roles of photo crosslinking 1).Cross–linking via polymer radicals 2).Formation of interpenetrating polymer networks where additives, having monomer character, undergo polymerization.

Several works suggest the preparation of membranes from photo–reactive polymers where degree of crosslinking was much influenced by UV–irradiation time. Such membranes have been applied to separate the gases [249–262]. The PV membranes made from polyimide are also fabricated via exposure to UV light [263]. Another application is membrane for fuel cells prepared from UV irradiated crosslinking of multi–block copolymers of sulfonated poly (aryl ether ketone) (PAEK) containing Benzopheonone (BP) units [264].

The UV irradiation is also employed for development of membranes out of polymers with added photo–reactive agents for example Wycisk et. al. used UV light to crosslink poly (4-ethylphenoxyl)(phenoxy) phosphazenel (PEPP) mixed with benzophenone BP [265].

The sustainable membranes have been prepared by developing an interpenetrating polymer networks via UV–curing [266]. Photo–initiated crosslinking of Polyimide copolymers containing both alkenyated diamides and aromatic diamines have been prepared and applied for gas separation [216, 217]. The effects of photo–irradiation on the performance of PV and GS membranes have been reported in several studies using various polymers. Nevertheless the mechanism remains a subject of further debate in the literature because two proposed mechanisms are i) Polymer crosslinking via covalent bonds ii) polymer densification via non–covalent interactions. Moreover it is noteworthy that too high degree of crosslinking can make the membrane not only brittle but also less permeable. On the other hand too low degree of crosslinking may lead to plasticization over time resulting in the performance deterioration and loss of

selectivity. Thus it is imperative to optimize the degree of crosslinking. This thesis is also based on similar methodology and optimum crosslinking degree of UV–induced acrylate network in Polysulfone matrix is thoroughly studied.

3.3.3. Photo–functionalization of polymeric membranes

Photo–functionalization of a polymeric membrane is based on the photo-reaction between membrane material and functionalizing agent and such a reaction requires typical photo–reactive groups. Two routes can be classified depending upon location of these photo–reactive moieties; i) via photo–reactive functionalization agents and ii) via photo–reactive membrane polymer [48] (Figure 3.4).
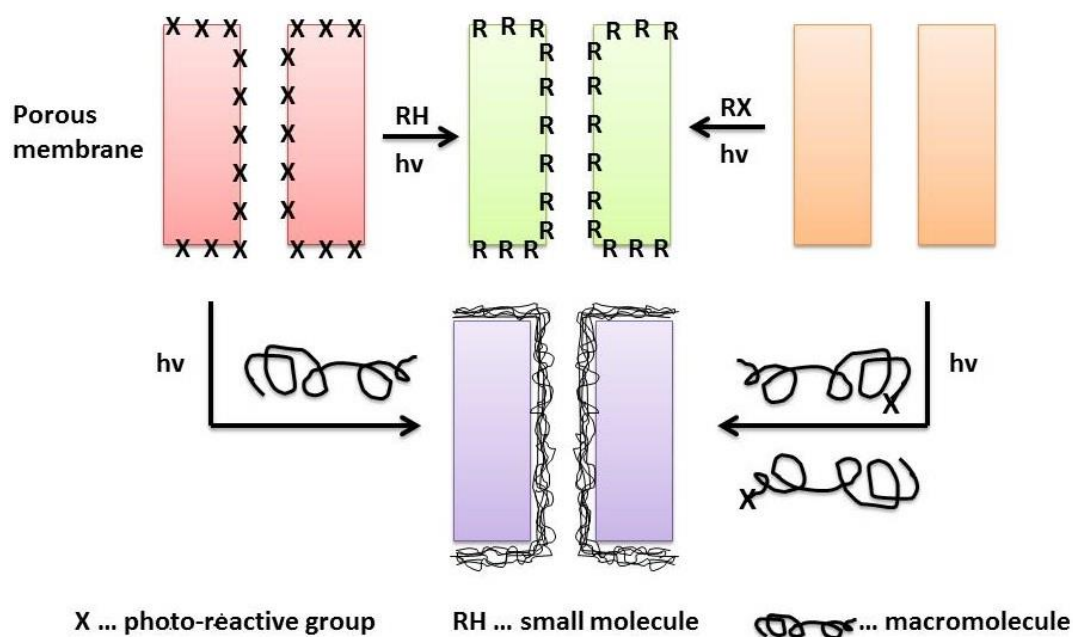
Figure 3.4: Two routes of UV functionalization i) via photo–reactive functionalization agents (from left) and ii) via photo–reactive membrane polymer (from right)

The photo–functionalization is relatively independent of the chemical composition of membrane material thus various functionalization agents could be attached on a

membrane surface via either photo–reactive moieties or a variety of membranes (porous and non–porous) can be modified by photo–reactive functional molecules.

There have been two distinctive approaches of functionalizing polymeric membranes i.e. "grafting-to" and "grafting-from". In the category of functionalization via "grafting–to", some notable methodologies followed are;

I. Development of photo–reactive thin film composite membranes and then post modification with functionalization agents [267, 268]

II. Preparation of non–porous membrane containing a photo–reactive moiety and then modified with functionalization agents [269]

III. The immobilization of photo–reactive groups on the surface of already prepared (and optimized) membranes [270, 271] and then subjected to UV or sunlight immobilization of proteins similar to a well–known technique for photo–affinity labeling of biomolecules [236]

IV. A number of works reported coating of membrane with a photo–reactive agent and then functionalization either through a cross-linker under UV irradiation [272] or photo–active surface agents [218, 219]

There are two crucial evaluation parameters for functionalization of polymeric membranes i.e. stability and controllability of grafted polymer layers. In "photo–grafting-to" technique, an extensive UV irradiation for covalent bonding of grafted layers often results into degradation of base polymeric membranes thus a tradeoff is sought and grafting density is compromised. The technique "photo–grafting-from" covers the aforementioned shortcoming for example a higher grafting density is obtained in contrast to "photo–grafting to". The anti–fouling modification for UF membranes is a typical example of "grafting-from".

Some noteworthy works on "Photo–grafting-from" are;

I. Development of low–fouling membranes where grafted polymers function as anti–fouling layer. The composition, surface coverage and thickness were optimized in a way that low fouling performance is ensured without compromising selectivity and flux [273, 274]

II.   Preparation of surface functionalized MF membranes absorbers for fast protein purification via photo-grafting of 2D or 3D layers having suited functional groups exhibiting reversible binding [223, 275]

III.   Development of membranes with grafting polymers as selective barrier to control undesired swelling and degradation in organic solvent while being applied in PV processes. An example is preparation of PAN UF membranes (with 5–15 nm pore diameter of active layer) for separation of organic mixtures in PV [276]

IV.   The iso–porous track–etched PP MF membranes with a large pore diameter (100 nm – 3 μm) have been functionalized via "grafting–from" process in order to make enzyme–membranes work as convective flow micro-reactors [277, 278].

3.3.4. Photo-degradation

Photo–degradation of polymeric membranes is generally an undesired process often leading to membrane material loss and subsequently a deterioration of its properties [232]. Most important reactions are cleavage or conversion of main chain, oxidation and loss or conversion of side groups. The photo–degradation mechanisms of typical membrane polymers such as Polyethersulfone, Cellulose and Polypropylene (PP) have been studied in detail [233–235]. It is imperative to consider mechanism of photo–degradation while coupling UV technology with the fabrication of polymeric membranes.

3.4. UV irradiation of Polysulfone based membranes

Polysulfone (PSF) and polyethersulfone (PES) are widely used materials for high performance UF and MF membranes because of good thermal, chemical and mechanical stability and excellent film forming properties. Nevertheless hydrophobicity of these materials causes fouling problems for example when applied to filtration of proteins the deposition and adsorption of contaminant yield membrane fouling. In order to reduce fouling, UV irradiation based approaches have been proved promising strategy thus have extended the application of these membranes. A valid strategy is to attach hydrophilic chains to the membrane's

surface which significantly increases the wettability of membrane surfaces and counteracts the fouling.

A number of works based on aforementioned methodology have employed UV irradiation to introduce hydrophilicity on the PSF and PES based membranes. For instance Crivello, Belfort and coworkers [279–280] developed a method of surface modification of Poly (arylsulfone) membranes where different hydrophilic polymers have been successfully photo–grafted from vinyl monomers in water or methanol onto Poly (arylsulfone) membranes endowing a high surface–selectivity. Ulbricht et. al. also investigated the mechanism of photo–grafting of PSF and PES including a comparison with and without photo–initiator [281].

A thorough investigation is done by group of Belfort for the sake of improvement in performance of Poly (arylsulfone) based composite membranes and to have a better understanding of mechanism. The characterizations of photo–grafted membranes revealed that grafting is not only surface bound instead it was extended to considerable depth in membrane [282]. This claim was also supported by the flux values of UF membranes before and after UV irradiation in the absence of a monomer. The results indicate that average pore size has undergone a marked increase because of localized degradation of membrane material [283] and this led to considerable reduction in selectivity.

Pieracci et. al. reported that grafting efficiency of N-vinylpyrrolidone (NVP) on the PES membranes was significantly higher if a high energy 254 nm UV lamp was used instead of 300 nm UV. But this approach also resulted into pore enlargement that led to increased flow rate and loss of rejection for bovine serum albumin (BSA) [283]. These side effects could be controlled using longer wavelength UV lamp or a UV filter for shorter wavelength UV lamp [48]. Taniguchi et. al. found a linear correlation between degree of grafting (DG) and the product of monomer concentration and irradiation energy [284].

$$DG \propto c \times E$$

Kaeseley et. al. reported another aspect i.e. much higher energy was required to achieved a desired DG on to PSF membranes as compare to PES membranes and it is because of high sensitivity of PES to UV irradiation [285].

Chapter No. 4

Research objective

The polysulfone (PSF) has major application in ultrafiltration membranes because of its ability to form a highly porous structure through NIPS. The PSF based membranes have reasonably good mechanical and chemical strength. However the membranes made of pristine polysulfone are not resistant to majority of organic solvents. The acrylic functionalization of polysulfone (PSF) has been an attractive strategy to improve the solvent stability of polysulfone based membranes but this modification has also led to significant drop in the flux when compared with pristine polysulfone. The previous attempt to bring solvent stability through UV-induced acrylic functionalization has resulted into material deterioration because of localized damage of membrane material i.e. polysulfone. Actually the amount and kind of acrylic functionality along with the parameters related to UV curing and NIPS were not fully investigated and correlated.

In order to overcome the aforementioned discrepancy; the current research was aimed to modulate the morphology and the performance of membranes in a way that a cross-linked network is developed for solvent stability and the pores morphology is retained for sufficient flux. The said objective could be achieved through optimization of UV–induced acrylic functionalization of polysulfone membranes. The acrylic functionalization could be introduced either as synthesis of functional macro-monmer or as separate addition of acrylic resin into polymer solution. The UV curing and membrane fabrication through NIPS were aimed to optimize and couple together in an efficient way. Following to these ideas, firstly

we introduced the acrylic functionality as synthesis of methacrylate polysulfone macro-monomer and two routes of membrane fabrication were investigated i.e. either UV curing followed by NIPS or vice versa. The first route was found better in terms of homogeneity but flux values in both cases were in the range of tight ultrafiltration. As a second approach, we incorporated two structurally different di-acrylates into pristine PSF solution in DMF and membranes were developed through UV curing followed by NIPS. Th membranes developed, via above two methods, were fully characterized, flux properties were determined through dead-end filtration process and solvent stability was assessed in a number of solvents.

After optimization of acrylic functionalization the best cross-linked membranes were subjected to coating of polydopamine (PDA) so the enhanced contaminant removal could be achieved. Furthermore, the best formulation out of phase separation membranes was also employed to produce electrospun nanofibrous mats through UV–induced reactive electrospinning setup.

Chapter No. 5

UV-cured methacrylated PSF membranes

5.1. Introduction

Porous polymeric membranes have attained an important place in the field of chemical technology in particular these are being frequently used in micro and ultrafiltration [34]. Though polymeric membranes are playing a vital role in the filtration of drinking water and wastewater treatment but existing membranes chemistries and structures also suffer from certain shortcomings that hinder further and widespread development of the separation technologies [2]. The progress in polymer science and technology could be useful in order to overcome limitations related to separation processes, fouling, chemical and mechanical stabilities of polymeric membranes.

There are several ways (c.f. 2.1) to prepare porous polymeric membranes but till today the majority of commercial porous membranes are being prepared via controlled phase separation of a polymer solution into two phases: one with low and other with a high polymer concentration. The concentrated (polymer–rich) phase solidifies shortly after phase separation and results into solid structure of membrane while polymer–poor phase leads to formation of voids. The separation performance of these membranes largely depends on the morphology out of phase

separation and subsequent solidification. The most common phase separation method is non-solvent induced phase separation (NIPS) [102–111]. The NIPS is carried out in a way that a thin wet film of polymer solution is cast on a support and immersed in a non-solvent (typically water). Precipitation takes place quickly because the good solvent for the polymer is exchanged with the non-solvent.

Polysulfone (PSF) is a widely used membrane material especially for microfiltration and ultrafiltration. The performance of PSF based membranes is quite stable because of workability over broad range of chemicals and pH conditions [286]. However, PSF is not resistant to many aprotic solvents [287, 288]. In order to improve the solvent stability as well as the mechanical performance of PSF–based membranes, the post-crosslinking process is often necessitated. For the said purpose electron-beam irradiation was proposed [289] but it requires expensive equipment and additionally the membrane structure is damaged during intensive irradiation. Alternatively, UV-irradiation was employed and mixtures of PSF and acrylic cross-linker were thus investigated [290, 291]. In those works solvent stability was somehow achieved but membrane material suffered from localized damaging and subsequently deterioration of separation properties. A different and more elegant approach could involve the incorporation of cross-linkable functionalities on the PSF-backbone during synthesis. Generally the incorporation of functional groups into PSF can be achieved through two approaches, (i) by using functional co-monomers during polycondensation, [292–296] and (ii) by post-synthesis modification [297–306].

In this chapter, we report a facile post-synthesis approach to incorporate methacrylic functionalities at the chain ends of PSF molecules. The attachment of cross-linking sites effectively provides fast curing while preserving the PSF properties. We describe here scalable fabrication of novel porous PSF membranes having cross–linked network developed via photo-induced cross-linking of the macro-monomer. We investigated two routes to fabricate membranes i) first phase separation and then UV-curing ii) First UV-curing and then phase separation. The cross-linked membranes were fully characterized and their morphology, viscoelastic properties, solvent stability, and flux performance were evaluated.

5.2. Experimental

5.2.1. Materials

The solvents acetone (99.9 %) and *N,N*-dimethyl formamide (DMF, anhydrous, 98.8%) were purchased from Sigma Aldrich. The photo–initiator (PhI), phenylbis(2,4,6-trimethylbenzoyl)phosphine oxide (BAPO) Irgacure 819, was kindly provided by BASF. The other materials methanol (Merck), dimethylacetamide (DMAc, 99%, Merck), Bisphenol A and bis(p-chlorophenyl) sulfone (Hallochem Pharma Co. Ltd, China), and triethylamine (TEA, Aldrich, HPLC grade) were used as it is without any purification. Methacryloyl chloride (+97%, Merck) and Dichloromethane (99%, Aldrich) were also used as received.

5.2.2. Synthesis of dimethacrylated polysulfone

The methacrylate functionalized polysulfone was synthesized via condensation followed by esterification. At first step hydroxyl functionalized polysulfone of different molecular weights (PSF-2000, PSF-4000, and PSF-14000) were prepared through condensation polymerization according to the modified procedure described in the literature [307]. The hydroxyl terminated polysulfone oligomers were obtained by adjusting concentrations of monomer. Thereafter, methacrylate functionalized polysulfone was synthesized by esterification of the oligomers with methacryloyl chloride in the presence of base (triethylamine). The overall schematic procedure is presented in Figure 5.1.

In order to synthesize PSF-2000, bis(p-chlorophenyl) sulfone (12.58 g, 43.81 mmol), bisphenol A (20.00 g, 87.61 mmol) and dried potassium carbonate (25.43 g, 183.98 mmol) were added to 50 mL toluene and 400 mL DMAc in a 2000 mL double necked round bottom flask, fitted with a nitrogen inlet, condenser, a dean and stark trap and an overhead mechanical stirrer. The reaction mixture was heated at 150 °C for 4 hr under reflux with removal of water. After almost two hours the reaction was stopped and cooled to room temperature. The solution was filtered to remove most of the salts and poured into a mixture of water and methanol (1:4). The precipitated polymer was filtered, and several times washed with water so the remaining salts and other impurities are removed. Finally, the polymer was washed with methanol and dried at 60 °C in a vacuum oven for about 12 hr to give PSF-2000 oligomer (15.62 g). The similar procedure employing appropriate ratios of the monomers was followed for the synthesis of

PSF-4000 and PSF-14000. The observed FTIR peaks in polysulfone are given in Table 5.1

Table 5.1: FTIR peaks of polysulfone

Wave number (cm^{-1})	The structure
1014	Aromatic
1151 & 1175	O=S=O Symmetric
1240	C – O – C
1293 & 1322	O=S=O Asymmetric
2945	– CH3 symmetric
2975	– CH3 Asymmetric
3000 – 3200	Aromatic
3435	– OH

In order to synthesize PSF-DM-2000, 1.52 g (1.25 mmol) PSF-2000 was added to 20 mL CH$_2$Cl$_2$ contained in a 50-mL two necked round bottomed flask stirring in an ice bath, fitted with a nitrogen inlet and condenser thereafter mixed for roughly 5 minutes. Then, 0.87 mL (excess amount) triethylamine was added. 0.62 mL (6.24 mmol) (excess amount) methacryloyl chloride dissolved in 5 mL CH$_2$Cl$_2$ was added slowly to the reaction flask in a time period of 10 minutes. The reaction mixture was stirred for 24 hr. Subsequently the reaction mixture was filtered to remove salts and it was poured into methanol in order to precipitate the methacrylate oligomer. The precipitated oligomer was filtered and washed several times with water in order to remove salts and impurities. Thereafter the polymer was washed with methanol and dried in a vacuum oven at room temperature for about 12 hr. 1.29 g PSF-DM-2000 was thus obtained. An analogous procedure using appropriate ratios of the monomers was also used for the synthesis of PSF-DM-4000 and PSF-DM-14000. The FTIR peaks of dimethacrylated PSF are given in Table 5.2

Table 5.2: FTIR peaks of dimethacrylated polysulfone

Wave number (cm^{-1})	The structure
1014	Aromatic
1151 & 1170	O=S=O Symmetric
1244	C – O – C
1295 & 1324	O=S=O Asymmetric
1730	– C=O
2872	– CH3 symmetric
2968	– CH3 Asymmetric
3000 – 3200	Aromatic

5.2.3. Preparation of UV-cured membranes

The functionalized PSF was synthesized in three different categories of molecular weights. At first, each category of PSF was used in different concentrations to prepare membranes so the workable molecular weight and optimum concentration could be established. Regarding structural integrity of membranes there were some notable observations during fabrication of membranes

- The different concentrations of functionalized PSF having molecular weight 2000 or 4000 were employed to prepare the membranes but the developed membranes were highly fragile and the membranes were shattered during phase separation

- The functionalized PSF having molecular weight 14000 was also used in different concentrations and 25 wt % concentration was found suitable to develop structurally stable membranes otherwise lower concentrations had similar behavior as that of polysulfone having lower molecular weights

All PSF solutions were prepared in a way that polymer was dissolved in DMF with continuous stirring at temp 60 °C. After evaluation of different PSF molecular weights only PSF–DM–14000 was employed for membranes development. A 25 wt. % solution of PSF–DM–14000 in DFM was prepared and

once the homogenous solution was obtained the photo–initiator was added as 3 wt. % with respect to PSF and sonicated for 15 min so the solution is homogenous again. From this solution 100 μm thick films were cast on the glass plate and thereafter these films were subjected to either of two sequences i.e. NIPS followed by UV curing (NIPS – UV) and UV curing followed by NIPS. NIPS was carried out in a coagulation bath of non–solvent i.e. water. During wet casting of membranes and thereafter phase separation the relative humidity of atmosphere was 40±10 % and the temperature was 25±3 ^{o}C. The cross–linking of functionalized PSF was performed via UV curing. The UV curable membranes were irradiated under nitrogen atmosphere in a static UV lamp for one minute. The irradiation light was in the range of UVA i.e. 320–390 nm. The energy of irradiation was recorded as 10.05 J / cm^2. The composition of cast solutions and fabrication methods are summarized in Table 5.3. The schematic representation of steps involved in membrane fabrication is given in Figure 5.1

Table 5.3: The composition of casting solutions and sequences followed

Membrane Code	PSF wt. %	DMF wt. %	PhI wt. % of PSF	Sequence I NIPS–UV	Sequence II UV–NIPS
M1	25.0	75.0	3.0	✓	–
M2	25.0	75.0	3.0		✓

5.2.4. Fourier transform infrared (FTIR) analysis

A spectrophotometer furnished with attenuated total reflectance (ATR) accessory made by Thermo Electron Corporation was used for FTIR and ATR–FTIR analysis. The ATR assembly had diamond crystal based internal reflection element. In UV–NIPS sequence the wet polymeric films (not yet precipitated) were applied onto a silicon crystal, UV irradiated and analyzed via FTIR. Alternatively the membranes developed through NIPS–UV procedure were directly analyzed through ATR–FTIR. The cross-linking degree was measured by scanning each sample 32 times with a resolution of 4 cm^{-1} and the spectra were collected in the wave number range 650 to 4000 cm^{-1}. A background was run before every individual sample was analyzed. The acrylic double bond conversion

was calculated though decrease of the peak area for C=C group at 810 cm^{-1} and normalized with the peak area for C=O group at 1730 cm^{-1}.

5.2.5. Dynamic mechanical thermal analysis (DMTA)

The triton DMTA apparatus was employed to carry out dynamic mechanical thermal analysis (DMTA). The instrument has tension–film clamp assembly and it operates in multi-frequency strain mode. The size of samples to be tested was measured using an electronic caliper and almost all the samples have dimensions approximately 10×10^{-3} m by 6×10^{-3} m. Each sample was held in tension mode and a sinusoidal stress was applied whereas applied preload force was set at 0.001 N. Both the loss modulus and storage modulus were collected over the required temperature range 25 – 200 ^{o}C. The rate of increase of temperature was set as 3 ^{o}C per minute. Each sample was tested three times and the selected results are presented.

5.2.6. Field emission scanning electron microscopy (FESEM)

The morphology of membranes cross–sections was investigated through FESEM. The instrument for FESEM is a MERLIN model by ZEISS furnished with the state of the art GEMINILIS column that ensures good control of both current and spot. The samples were immersed in liquid nitrogen and snapped within seconds after immersion thus sharp edged samples were obtained for cross–sectional morphological analysis. These samples were mounted on the studs in a way that cross section faces upward. In order to counteract charging effect during FESEM analysis the samples were coated with chromium up to thickness of 8.0 nm.

5.2.7. Permeability tests

The hydraulic permeability of developed membranes was experimented in a stirred cell apparatus – Model 8010 by Amicon® Millipore Co. In order to drive the flow the cell was pressurized with Nitrogen gas. The pressure drop of 250 kPa (35 psi) was established and monitored using a pressure gauge. The filtration experiments were carried out using deionized water obtained from a Milli-Q ultrapure water purification system. The flow rate was determined by measuring the permeate mass in a given time after reaching steady-state.

5.3. Results and discussion

The PSF membranes are widely used because of their strength and resistance towards a relatively broad range of chemical and pH conditions but PSF is inherently soluble in aprotic solvents and therefore a crosslinking process is required to enhance its solvent stability. Our strategy is focused to develop UV-induced cross-linked membrane from methacrylated PSF macro-monomer.

5.3.1. Synthesis of dimethacrylated polysulfone

PSF dimethacrylate (PSF-DM) macro-monomer was synthesized by condensation polymerization and subsequent esterification. The schematic representation of synthesis is given in Figure 5.1. The parameters collected in Table 5.4 were adjusted so as to obtain PSF with sufficient molecular weight and desired functionality in order to have efficient cross-linking and extended properties of PSF in the final membrane.
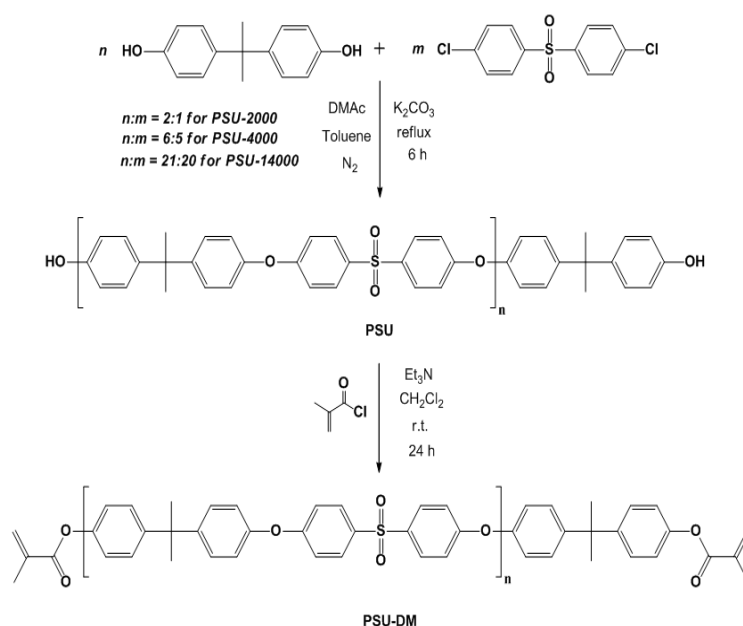
Figure 5.1: Schematic representation of synthesis of PSF and PSF-DM oligomers

Table 5.4: Molecular weight characteristics and synthesis[a] of phenol and
methacrylate functional polysulfones

Polymer	BisphenolA/ Chlorosulfone (mol/mol)	Yield[b]	$M_n{}^c$ (g/mol)	$M_w{}^c$ (g/mol)	PDI
PSF-2000	2/1	47.9	2080	2615	1.26
PSF-4000	6/5	80.4	4173	6475	1.55
PSF-14000	21/20	60.7	14125	21503	1.52
PSF-DM-2000	-	84.1	2451	2986	1.22
PSF-DM-4000	-	90.0	4494	6641	1.48
PSF-DM-14000	-	84.7	15039	23045	1.53

[a]Reaction temperature: 170 °C, time: 6 h.
[b]Determined gravimetrically.
[c]Determined from GPC measurements based on polystyrene standards

A scheme of UV–induced crosslinking reaction is presented in Figure 5.2.
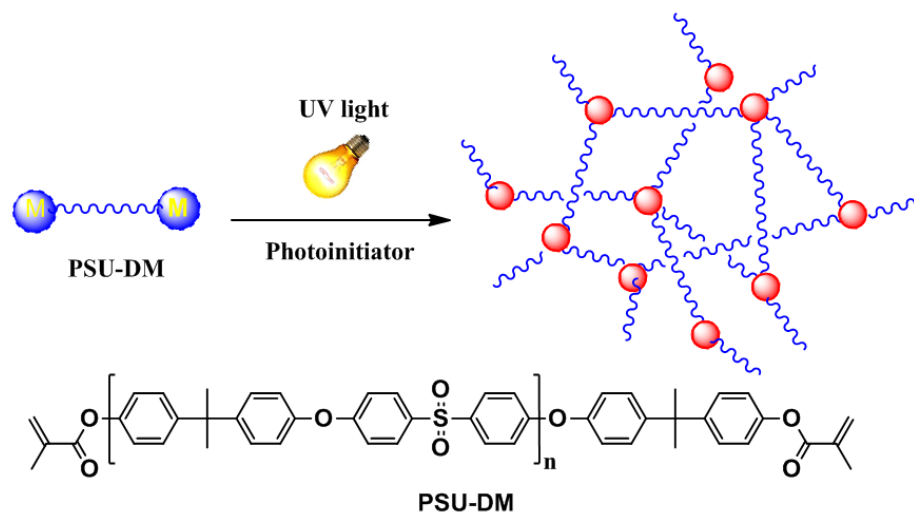
Figure 5.2: Scheme of UV–induced cross–linking of PSF-DM

5.3.2. Evaluation of sequences of fabrication

The synthesized macro-monomer was dissolved in DMF and the membranes were prepared via two sequences i.e. either phase separation was followed by UV-curing process or vice versa. A schematic representation of the both sequences is reported in Figure 5.3.
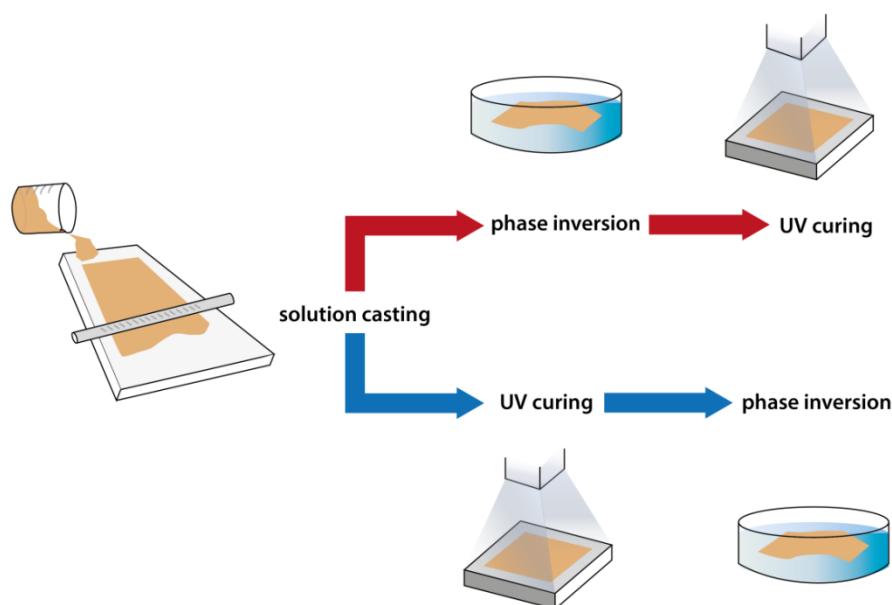
Figure 5.3: Schematic representation of the two sequences procedure

In a typical UV–induced cross–linking reaction, a radical initiator is photo-generated and the polymerization reaction proceeds via a classical chain-growth addition reaction of the radicals on methacrylic double bond. The radical photo-initiator was selected with absorption in a different spectral window from PSF absorption and with a very limited solubility in water in order to avoid leaching out in the coagulation bath during the NIPS process. For membrane preparation the oligomer PSF-DMA-14000 was chosen because of its high molecular weight. All the results related to membrane structure and properties refer to that particular macro-monomer.

The acrylic double bond conversion was calculated via FT-IR. The C=C (810 cm^{-1}) peak was analyzed to measure the conversion degree while C=O (1730 cm^{-1}) peak was taken as reference. When NIPS-UV sequence was followed, the casting solution was immersed in water in accordance with the usual preparation conditions reported in the literature for PSF membranes [308, 309].

The obtained membrane was irradiated and the methacrylic double bond conversion was measured through ATR-FTIR analysis done before and after UV irradiation. A conversion of about 41% of acrylic double bonds was achieved after one minute of irradiation under nitrogen (Table 5.5). The limited methacrylic double bond conversion could be attributed to a limited mobility in the PSF membrane with Tg around 185 °C. In order to increase the methacrylic double bond conversion, the reverse sequence was also applied, involving curing reaction at first and subsequently the phase separation of the cross–linked matrix. For this purpose a film of the polymer solution in DMF was cast on a silicon wafer and the curing reaction was analyzed via FT-IR analysis collecting spectra before and after one minute of UV-irradiation. A conversion of about 62% was recorded during this sequence (Table 5.5).

5.3.3. Viscoelastic behavior of the membranes

The viscoelastic properties of the PSF membranes were investigated through DMTA which allows the evaluation of both the elastic and viscous components of the modulus of the material on a reasonable large temperature interval. The tanδ (Equation 5.1) curves of membranes developed through NIPS-UV (M1) and UV-NIPS (M2) sequence are given in Figure 5.4

$$\tan\delta = \frac{Loss\ Modulus}{Storage\ Modulus} = \frac{E''}{E'} \qquad\qquad \textbf{(5.1)}$$
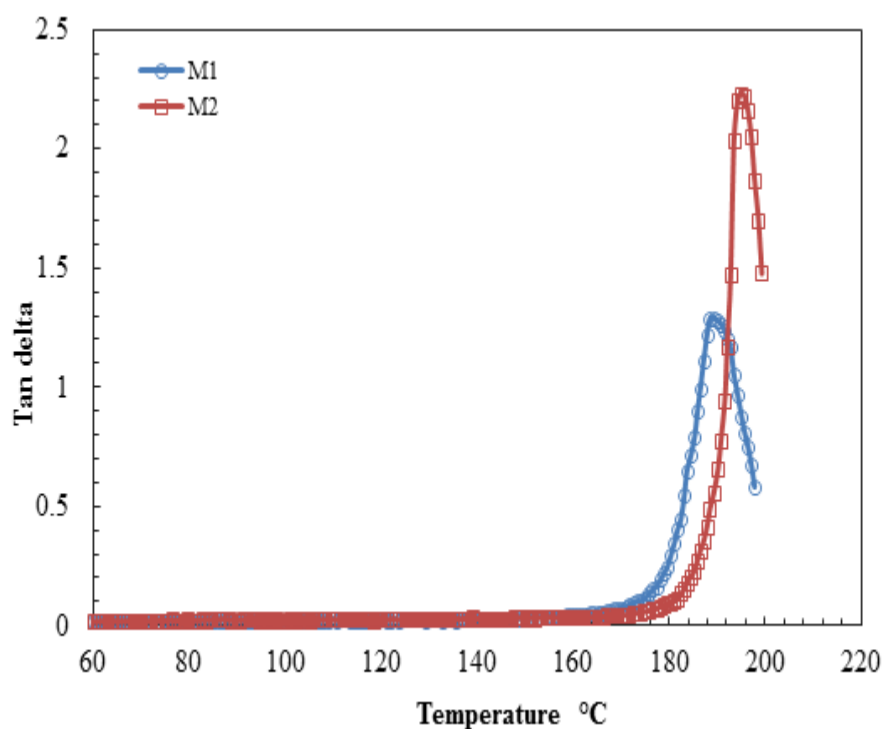
Figure 5.4: tanδ curves of membranes developed via NIPS-UV (M1) and UV-NIPS (M2)

The region, tanδ curve shows a maximum, is assumed to be T_g of the cured films. When phase separation was performed before UV–curing, a Tg value of about 185 °C was measured (See Figure 5.4 and Table 5.5). The Tg slightly shifted to higher temperature (around 195 °C) when the UV-curing process was performed before the phase separation process.

This difference is in accordance with the higher cross–linking density achieved when the membranes were prepared through the UV–NIPS sequence. Furthermore, a narrower tanδ peak was obtained for the membranes developed through UV–NIPS confirming the uniformity of the membranes developed through this sequence.

5.3.4. Membranes morphological analysis

Morphological investigations on cross-sections of the developed membranes were performed through FESEM analysis. The micrographs are reported in Figure 5.5 and 5.6, respectively for the membranes obtained via NIPS–UV and UV–NIPS sequence. It is evident that the UV–NIPS sequence (Figure 5.6) produced a more uniform porous distribution with pore dimension ranging from 800 nm to 1.2 µm. On the other hand when NIPS–UV sequence was adopted (Figure 5.5), the membranes came up with some larger pores, even larger than 2 µm, as well as a less uniform distribution.
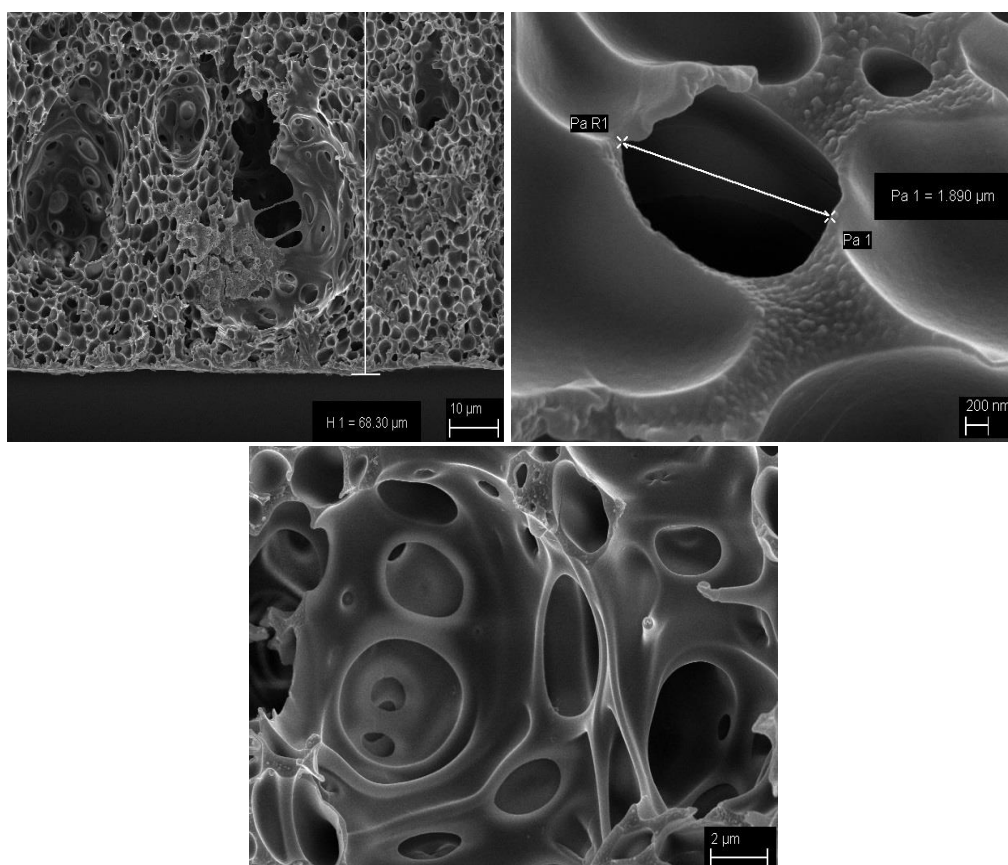
Figure 5.5: Cross–sectional morphology of methacrylated membranes developed via NIPS–UV
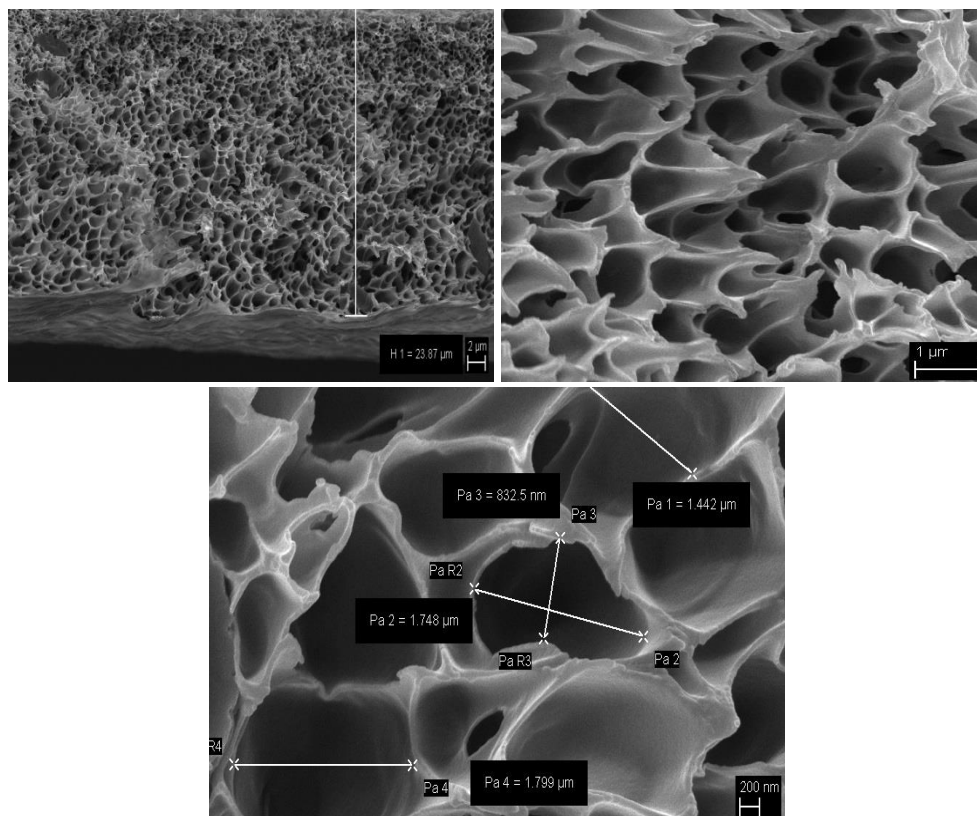
Figure 5.6: Cross–sectional morphology of methacrylated membranes developed via UV–NIPS

Table 5.5: Parametric analysis of membranes characteristics

Membrane Code	Conversion[1] %	Tg[2] °C	Pore dimension[3] μm
M1	41	185	2.0±0.5
M2	62	195	1.2±0.2

1: Calculated through FTIR and ATR–FTIR analysis

2: Determined as the maximum of tanδ curve in DMTA analysis

3: Determined by FESEM morphological analysis

5.3.5. Dead–end filtration tests

The developed membranes were tested in dead–end filtration mode using stirred cell apparatus. A schematic representation of lab scale dead–end stirred cell apparatus is shown in Figure 5.7. The preliminary tests showed that the pure water permeability of modified membranes was 2.5±0.1 and 9.5±0.1 L m^{-2}h^{-1}bar^{-1}, respectively, for NIPS–UV and UV–NIPS sequences. These permeability values lie in the range of tight ultrafiltration membranes.
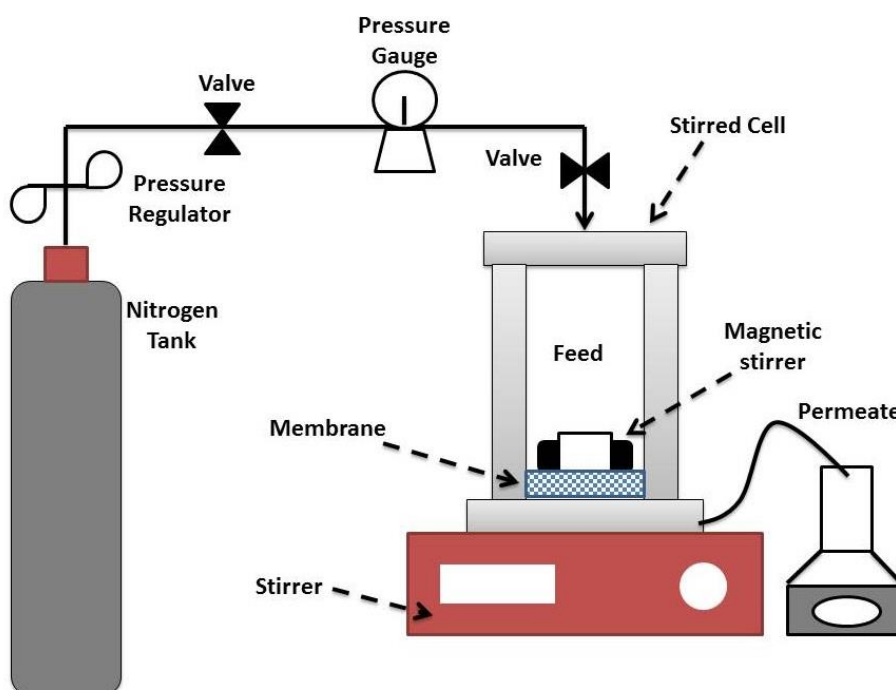
Figure 5.7: Schematic representation of lab scale dead–end filtration apparatus

The flux values confirm that our fabrication procedure is a viable route, yielding performance comparable to traditional polysulfone membranes. A higher permeability is viable through further optimization of polymer synthesis, UV curing time and membrane fabrication. The resulting UV-crosslinked membranes were insoluble in DMF, DMSO and boiling water, showing always a gel content value of 100%. These results highlight the high solvent resistance of cross-linked membranes.

5.4. Conclusion

Cross-linked polysulfone membranes were prepared through scalable non-solvent induced phase separation (NIPS) and UV curing processes. Methacrylate functionalized polysulfone precursors were synthesized by condensation polymerization and subsequent esterification and the macro-monomer was fully characterized. Porous membranes were obtained by subjecting the wet films, from solutions of macro-monomer in DMF, to the successive phase separation and UV-curing processes NIPS-UV and vice versa (UV-NIPS). The resulting UV-cross-linked membranes, obtained through either of sequences, were insoluble in DMF, DMSO and boiling water, showing always a gel content value of 100%. The viscoelastic properties of the membranes were characterized by DMTA. When phase separation was performed before the UV-curing, a T_g value of about 185 °C was recorded and the T_g got shifted to a higher temperature (around 195 °C) in the reverse fabrication mode. These T_g values are in accordance with the degree of crosslinking calculated through FTIR analysis. Morphological investigations showed that the UV–NIPS sequence produced a more uniform pores distribution with pore dimension ranging from 800 nm to 1.2 μm. On the other hand, when NIPS–UV sequence was adopted, the membranes showed some larger pores, even larger than 2 μm, as well as a less uniform distribution. The pure water permeability of membranes obtained with both procedures was in the range of tight ultrafiltration membranes. Furthermore the water permeability recorded for both membranes is not exactly in accordance with the average cross–sectional pore size calculated via FESEM analysis. This could be attributed to two aspects one is related to phase separation, this technique is an empirical art and the pores distribution out of phase separation is quite uncontrollable and other belongs to the fact that flux across an ultrafltration membrane depends not only on macro voids in the bulk but also nano pores on the surface. Hence, the current approach is not a best technique to produce solvent stable ultrafiltration membranes. Nevertheless a notable enhancement of mechanical behavior and solvent stability of PSF-based membranes were already achieved in this work. Further study (chapter no. 6) was done in order to selectively control the pores dimensions and performance of cross-linked membranes.

Chapter No. 6

UV–cured di–acrylate polysulfone membranes

The previous chapter described the UV–induced fabrication of membranes from functionalized polysulfone. The idea was based on incorporation of methacrylate functionality at the backbone of polysulfone so the enhanced performance could be achieved regarding solvent stability of membranes. The membranes were prepared via NIPS process and cross–linking of functional macro-monomer was obtained through UV irradiation. Both these techniques, NIPS and UV irradiation, were combined in two different sequences i.e. either first NIPS then UV irradiation or vice versa. Though solvent stability was increased but flux across the membrane was reduced drastically in contrast to pristine polysulfone without any added functionality. In this chapter we report another way to add acrylic functionality i.e. incorporation of acrylate cross-linkers into pristine polysulfone solutions and then fabrication of membranes through combined effect of NIPS and UV irradiation so the cross-linked network of acrylate system is developed for solvent stability and pores morphology could be retained for sufficient flux.

6.1. Introduction

As a membrane material, polysulfone could be easily fabricated into a highly porous structure through NIPS and it is stable over broad range of solution pH

[310] but instability of polysulfone in many of organic solvents restricts wide spread application of polysulfone based membranes.

In order to improve the solvent stability of PSF membranes prepared via NIPS, post-synthesis treatments are required to crosslink the polymer. In previous chapter, we apportioned a two-step method involving UV curing and NIPS for preparation of membranes from functional methacrylated PSF macro-monomer [102]. The flux properties of cross-linked membranes for pure water were found in the range of tight ultrafiltration membranes but an adequate solvent stability was achieved. In another important contribution Vankelecom [290, 291] reported a thorough investigation of the influence of UV curing on the morphology and reported the performance of PSF membranes containing different acrylates with varying functional groups. Those works did not present any study on the effect of the cross-linker content into PSF formulations. Besides content and type of acrylate system the sequence of applying NIPS and UV was also found to affect not only morphology but also structural integrity of the membranes. Moreover it was reported that UV–induced crosslinking resulted into localized deterioration of membrane surface. In previous chapter, we came up with a conclusion that UV irradiation, for the sake of cross-linking, should precede the NIPS in order to obtain more uniform and structurally stable cross–linked membranes.

In this chapter, we demonstrate an extended analysis based upon the previous studies. In contrast to previous approach based on *in-situ* methacrylated functionality here we report a systematic investigation on the effect of two different di–acrylate resins, both in terms of structure and concentration, on the PSF-based membranes. We incorporated two structurally different di-acrylates into pristine polysulfone solution in DMF and established the protocol of membrane fabrication in which the membranes were prepared via UV curing followed by NIPS process. The crosslinking of pure acrylic resin was evaluated through FTIR analysis and it was compared with the conversion obtained for the modified polymer solutions used to fabricate membranes. The UV cross–linked di-acrylate PSF membranes were characterized to analyze their viscoelastic properties, morphology, solvent stability, water flux and selectivity. The study provides an understanding of the influence of acrylic monomer type and content on the membrane structure and performance.

6.2. Experimental

6.2.1. Materials
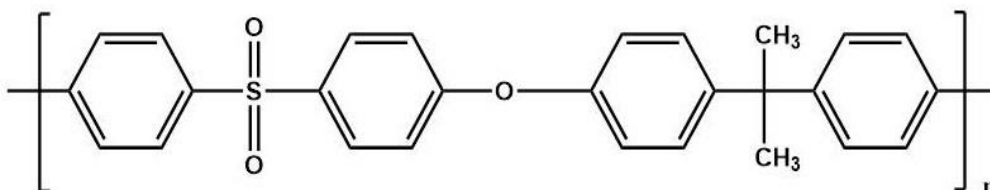
- Polysulfone (PSF, Mn=22000 g mol^{-1}) `
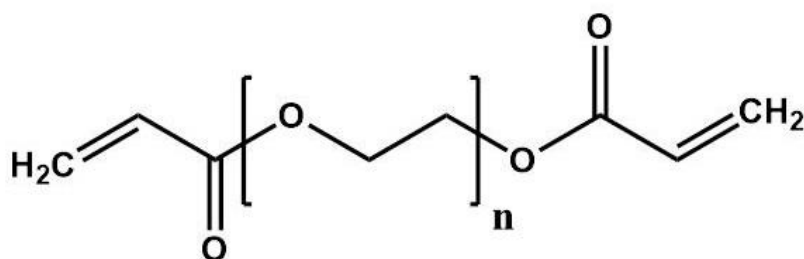
- Poly(ethylene glycol) diacrylate (PEGDA, Mn=700 g mol^{-1})
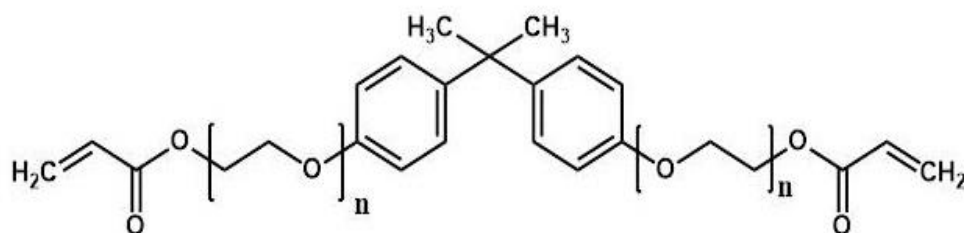
- Bisphenol-A-ethoxylate (2EO/phenol) diacrylate (BEDA, Average $Mn=512$ g mol^{-1} inhibited with 1000 ppm MEHQ).
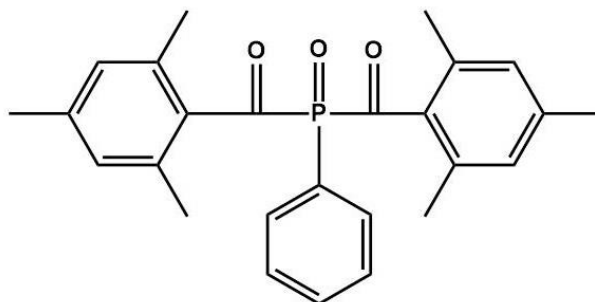
- Photo initiator (PhI) phenylbis (2,4,6-trimethylbenzoyl)phoshineoxide (BAPO)

A glass plate was used as casting substrate to prepare the membranes. All the chemicals were purchased from Sigma Aldrich while the photo–initiator was provided by BASF.

6.2.2. Preparation of UV cured acrylic modified PSF membranes

The membranes based on modified polysulfone (PSF) solutions, containing acrylic cross-linker, were prepared via UV curing and NIPS processes. A 15 wt. % solution of pristine PSF in DMF was prepared by gradual addition of PSF beeds and continuous stirring at 60 $^{\circ}$C for 7 hrs. Then the solution was cooled overnight. The PSF solutions were modified by incorporating a di-acrylate

monomer cross-linker along with a photo-initiator. Two structurally different cross-linkers, BEDA and PEGDA, were investigated. These were added individually to modify the polymeric solutions and the effect of three concentrations, namely 10, 20 and 30 wt. % was studied. The photoinitiator was always added at 3 wt. % with respect to the weight of acrylic content. The sole objective of the photoinitiator was to induce crosslinking so there was no need to add photoinitiator into pristine PSF solution. The solutions were sonicated for 15 minutes and then left in normal condition for 10 min so the trapped air bubbles could be released. The homogeneous solutions were then cast on the glass plate with a nominal film thickness of 100 μm. The wire-wound applicator was applied to control film thickness. The compositions of the different casting solutions are given in Table 6.1.

The crosslinking was performed before phase separation by employing a mercury medium pressure UV lamp. The UV curable films, obtained from modified solutions, were irradiated in a static UV lamp for one min under nitrogen atmosphere. The UVA (320–390 nm) was the irradiation source. The energy dose being absorbed to cure the membranes was recorded at 10.05 J / cm^2. The degree of crosslinking was measured via FTIR analysis. Shortly after UV curing, NIPS was carried out in a coagulation bath containing distilled water. The membranes were stirred in a bath containing plenty of distilled water for 24 hrs so no DMF was left in the membrane. During the wet casting of membranes and process of phase separation, the temperature of air was 25±3 ^{o}C and the relative humidity was 40±10 %. A schematic representation of methodology is given in Figure 6.1.

Table 6.1: The composition of different membrane casting solutions

Membrane Code	PSF wt. %	BEDA wt. %	PEGDA wt. %	PhI wt. %
M00	15.0	-	-	-
M11	15.0	10.0	-	3.0
M12	15.0	20.0	-	3.0
M13	15.0	30.0	-	3.0
M21	15.0	-	10.0	3.0
M22	15.0	-	20.0	3.0
M23	15.0	-	30.0	3.0
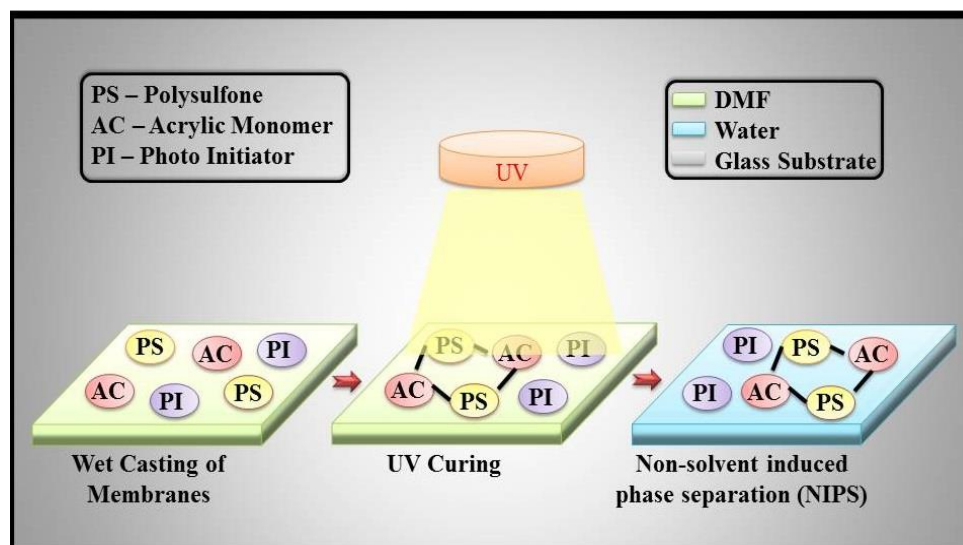
Figure 6.1: Schematic representation of preparation of di-acrylate PSF membranes via UV curing followed by NIPS

6.2.3. Characterizations of modified PSF membranes

FTIR analyses were performed using spectrophotometer by Thermo Electron Corporation. The solutions were analyzed in a way that a 50 µm film was coated on the silicon wafer and UV cured thereafter FTIR analysis was carried out following the parameters same as described in section 5.2.4. A background run was applied before each individual sample was subjected to scanning. The conversion of acrylate double bonds was calculated by following the decrease of the peak area of C=C group at 810 cm^{-1} and normalized with the peak area of C=O group at 1730 cm^{-1}.

The viscoelastic properties of membranes were evaluated through dynamic mechanical thermal analysis (DMTA) using Triton DMTA apparatus. The operational parameters were kept same as described in section 5.2.5. The ending temperature was set at 200 ^{o}C while the starting temperature was set with respect to type of di-acrylate system in the casting solution. For example, with PEGDA the starting temperature was set at – 60 ^{o}C while for BEDA it was 20 ^{o}C. The temperature range, applied for analysis, is important to confirm the bis-phasic nature of PSF membranes modified with acrylate monomer. The rate of increase of temperature was fixed as 3 ^{o}C per min.

The morphology of membranes surfaces and cross-sections was analyzed through field emission scanning electron microscopy (FESEM). The samples were prepared and coated in the same way as mentioned in 5.2.6.

6.2.4. Solvent resistance test

The solvent resistance of cross-linked membranes was accessed by immersing membranes cutouts in a variety of solvents. The samples were kept immersed in solvents at room temperature for at least 120 hrs. A qualitative evaluation was made via visual inspection of the membranes. For a specific solvent the membranes were categorized into three grades;

      1) Stable

      2) Swollen

      3) Dissolved

6.2.5. Permeability and rejection tests

The water permeability of the membranes was tested in a stirred cell apparatus i.e. Amicon 8010 Millipore Co. having sample size of 1 inch diameter. In order to drive the flow, the cell was pressurized with N_2 (g) to reach a pressure drop of 15 psi, monitored using a pressure gauge. Once the pressure is reached, the membranes were subjected to pre-compaction for 10 min at this pressure. Thereafter, the rejection and flux tests were performed at constant applied pressure of 8 psi. The flux across the membranes was determined by measuring the change of permeate mass in time and permeability was calculated in a way that value of flux was divided by the sample area and the applied pressure. The experiments were performed using deionized water; obtained from a Milli-Q ultrapure water purification system. The experiment was repeated four times for each membrane type and the values were averaged.

The rejection by membranes was tested with a solution of polystyrene latex beads having nominal diameter of 27±4 nm from transmission electron microcopy (TEM) measurements and average hydrodynamic diameter of 39 nm, the later

evaluated by light scattering. The nanoparticles were chosen because of inert nature, i.e. they did not interact with the membrane material. That's why their rejection was solely based on size exclusion, thus providing information on the average size of the pores at the membrane/water interface. The beads were chosen based on a size typically separated by ultrafiltration. A spectrophotometer was used to measure the absorbance of both the feed solution (c_f) and the permeate solution (c_p) at a wavelength of 260 nm. A previously obtained linear correlation allowed calculation of the particle concentration from the value of absorbance. The rejection of latex particles, R, was then calculated following the equation 1.5.

6.3. Results and discussion

The membranes from PSF solutions containing an acrylate system were prepared in a way that UV–induced cross-linked network was developed for solvent stability and the pores morphology was retained for sufficient flux. The all three steps of membranes development, shown in Figure 6.1, were thoroughly investigated, optimized and correlated. The wet thickness was fixed at a value neither too high to lose in–depth UV curing nor too low to compromise the structural integrity. The UV–curing was carried out in an efficient manner and the amount of energy absorbed is controlled by changing vertical distance from lamp to the substrate. The irradiation was done to achieve optimum crosslinking of acrylic resin and shortly after UV–curing the wet membranes were subjected to NIPS. A quick transfer from UV–curing to NIPS is an important step in the development of nano pores on the surface of membranes which are imperative for good water permeability.

6.3.1. Cross linking degree of modified PSF membranes

The pure acrylate system has characteristic C=C peaks at wave number 810 and 1640 cm^{-1}. After the acrylate system was incorporated into PSF solution, the later peak was not so evident so only the peak at 810 cm^{-1} was analyzed to measure the conversion percentage. Firstly the optimum degree of conversion was obtained for pure acrylates. The time of irradiation and intensity of rays were controlled to achieve maximum conversion of C=C.

The FTIR spectra for pristine BEDA and PEGDA formulations containing photo-initiator, before and after 1 min of UV-irradiation, are given in Figure 6.2a and 6.2b respectively. After 1 min of irradiation, the average acrylic double bond conversions for BEDA and PEGDA were measured as 85% and 100%, respectively. The lower acrylic double bond conversion with BEDA is because of well-known vitrification effect as BEDA cross-linked network is characterized by a Tg (85 °C) considerably higher than room temperature reported later in the section 6.3.2. The cross-linked PEGDA possesses a very low Tg (–40 °C) thus it ensures the mobility of the macro-radical growing chains and therefore almost a complete addition reaction is observed with PEGDA. The high percentage of conversion, achieved with pure acrylates, suggests that 1 min of irradiation is sufficient time to obtain desired cross-linking during membrane fabrication.

The acrylic double bond conversion was also calculated for all the PSF formulations containing different weight percentage of both acrylic monomers. As an example, Figures 6.3a and 6.3b represent the FTIR spectra before and after 1 min of UV-irradiation for the PSF solution containing 20 wt. % of BEDA and 20 wt. % of PEGDA respectively. The conversion for the acrylic monomers in PSF solutions were convincingly high and in accordance with the conversion of pristine monomers. All the data are presented in Table 6.2.
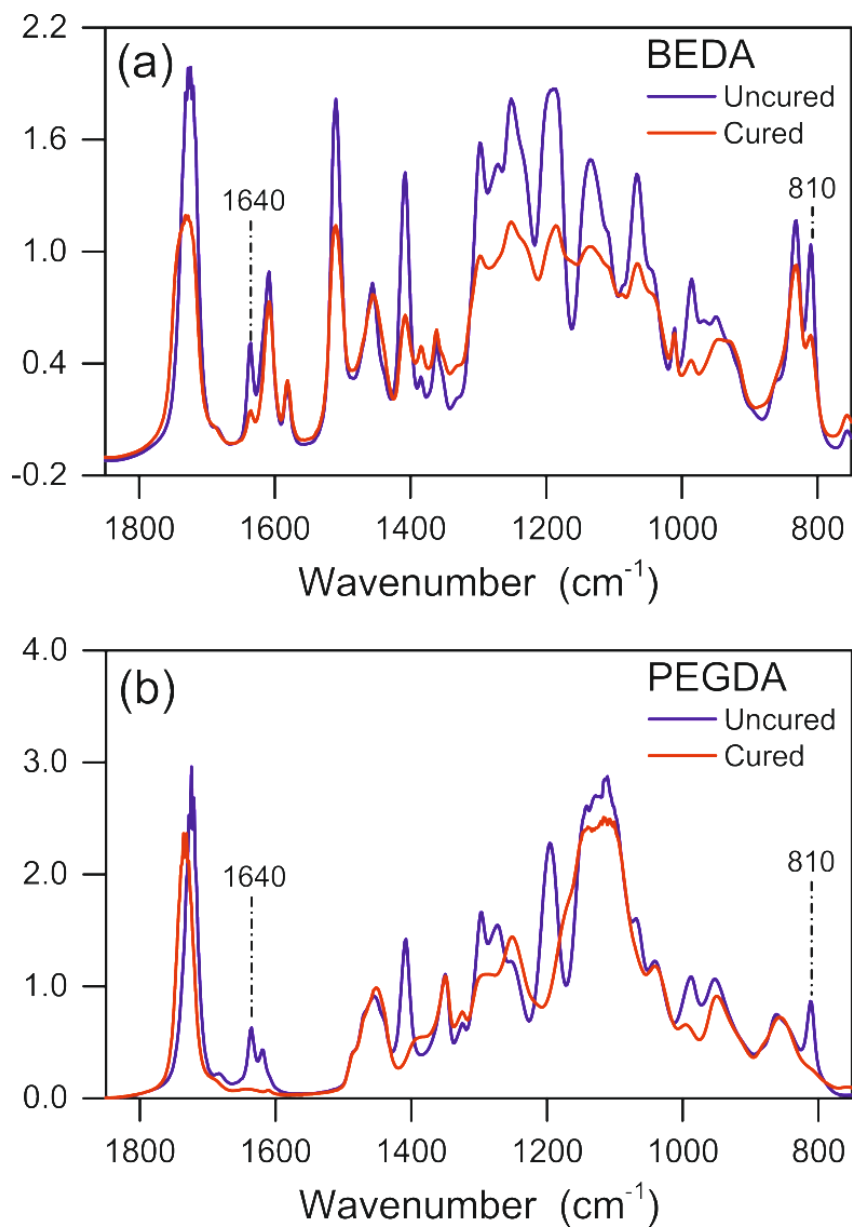
Figure 6.2: FTIR spectra of (a) pristine BEDA and (b) pristine PEGDA films of nominal thickness 100 μm before and after 1 min of UV irradiation
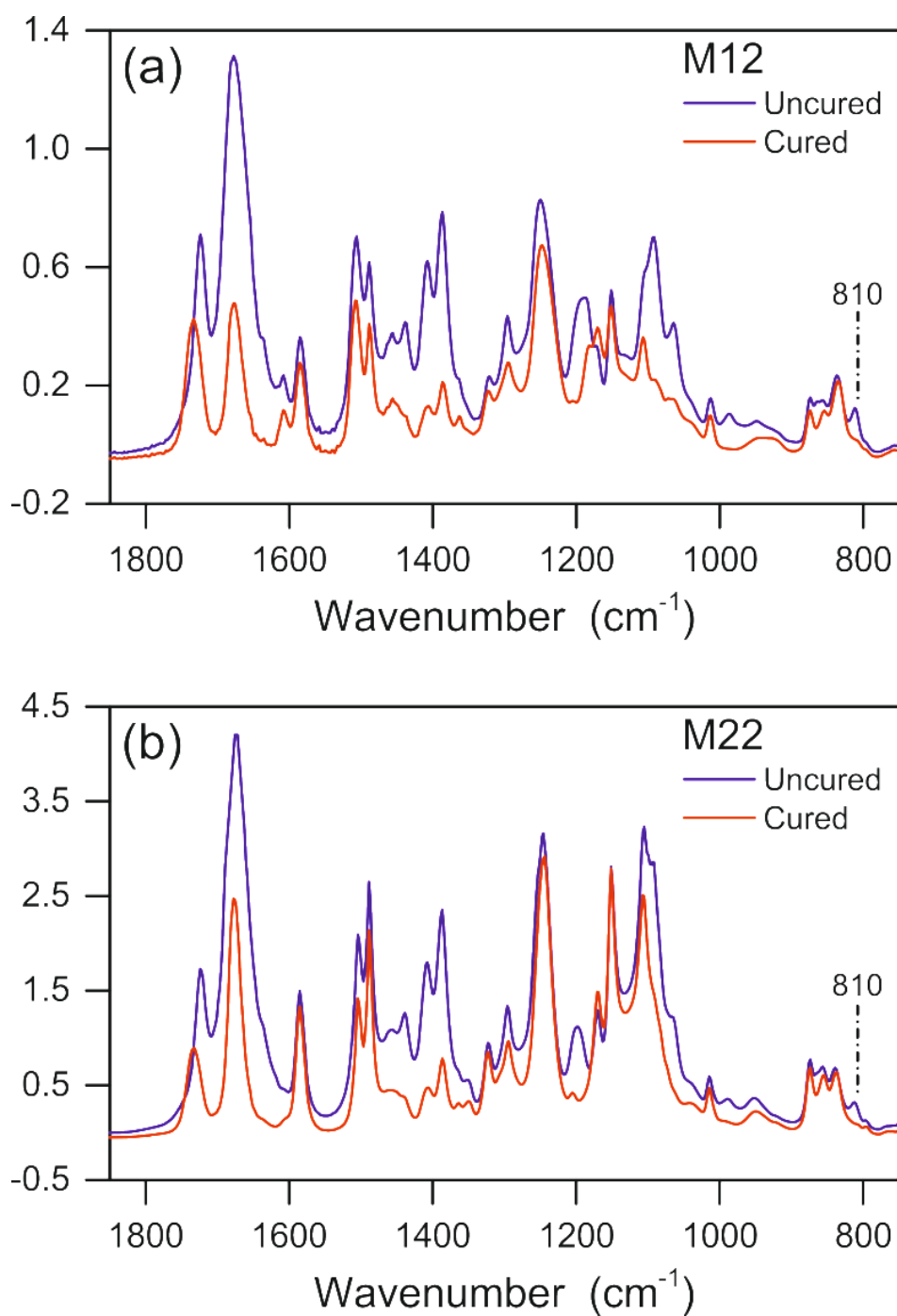
Figure 6.3: FTIR spectra of PSF solutions containing (a) 20 wt. % of BEDA (M12) and (b) 20 wt. % of PEGDA (M22) of nominal film thickness 100 μm before and after 1 min of UV irradiation

6.3.2. Viscoelastic behavior of membranes

The viscoelastic behavior of membranes was characterized through dynamic mechanical thermal analysis (DMTA) which provides both elastic and viscous modulus of the material over a large temp interval and the tan δ curves of all the cross-linked membranes. The tanδ curves from DMTA analysis of the cross-linked membranes are presented in Figure 6.4a and 6.4b.

From DMTA curves of both acrylates, it is evident that all the cross-linked membranes exhibited a biphasic nature due to the interpenetration of the UV–induced cross-linked acrylic network and the PSF polymeric chains. The peak region of tanδ corresponds to Tg and it is clear from the curves that each PSF membrane containing an acrylate network has two Tgs where one belongs to acrylate system and other to PSF. All the data are collected in Table 6.2. With BEDA cross-linker, the first tanδ curve was centered at around 85 °C, on the other hand when PEGDA was used, the first tanδ curve was centered at around –44 °C. These Tg values are in accordance with the Tgs of the corresponding pristine cross-linked acrylates [311] and therefore these values could be attributed to the UV-cured acrylic network in the modified membranes.

The second tanδ curve belongs to the PSF domain. With BEDA cross-linker, the maximum of tanδ curve related to the PSF domain was shifted to higher temperature with the increase of weight percentage of the acrylate monomer. This could be related to the higher cross-linking density achieved in the presence of BEDA which shows a lower molecular weight between crosslinks. Additionally the BEDA has rigid aromatic backbone in contrast to linear PEGDA that introduced stiffness to PSF domain. When PEGDA was used as cross-linker the tanδ curve related to PSF domain was always centered around 160 °C, which is is typical Tg of pure PSF [292].
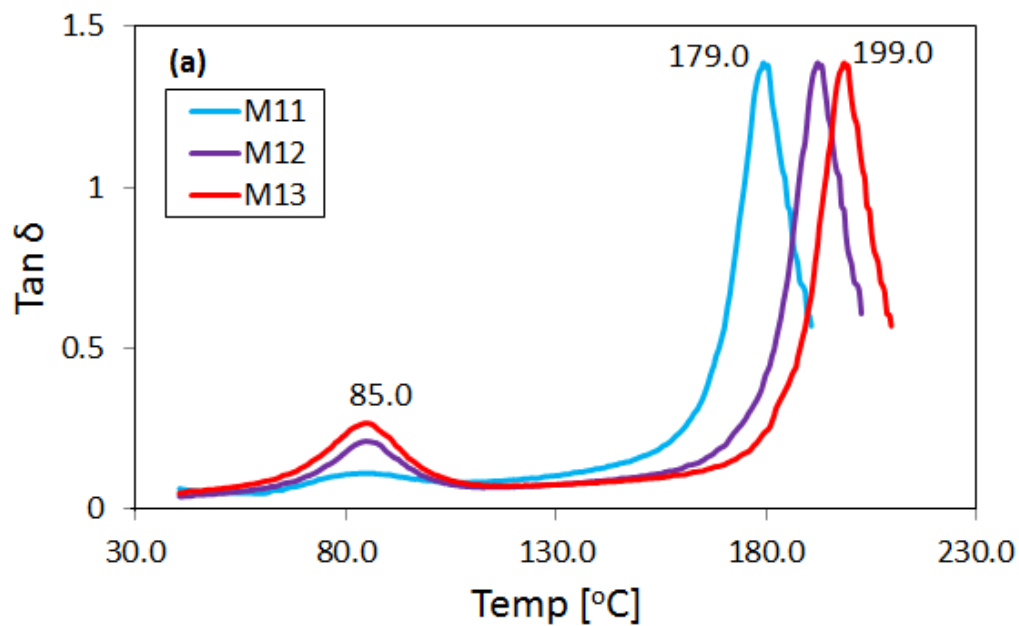
Figure 6.4(a): DMTA curves of membranes from PSF containing BEDA
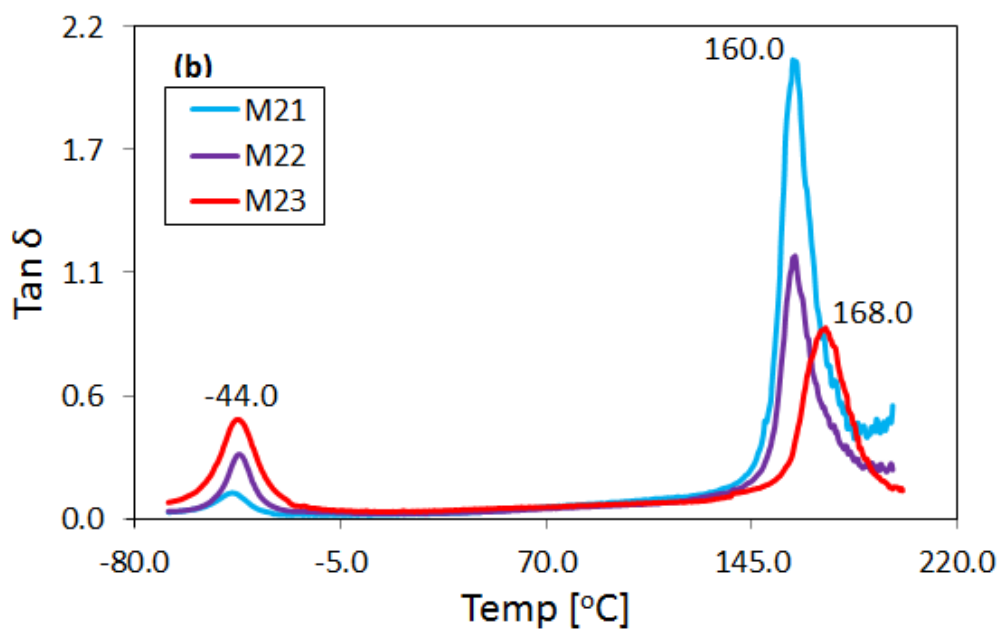
Figure 6.4(b): DMTA curves of membranes from PSF containing PEGDA

Table 6.2: Parametric breakdown of characterizations and performance evaluation of reference and UV cured membranes

Code	BEDA wt. %	PEGDA wt. %	Conversion (%)	First Tg [°C]	Second Tg [°C]	Water Flux [L/m^2.h.b]	Rejection of 27 nm Particles [%]
M00	-	-	-	185.0	-	337.90	96.53
M11	10.0	-	95	85.3	179.3	238.79	92.47
M12	20.0	-	90	84.8	193.2	169.30	98.35
M13	30.0	-	90	84.8	199.4	0	-
M21	-	10.0	100	−44.0	160.0	230.81	96.75
M22	-	20.0	100	−42.0	161.0	110.90	95.84
M23	-	30.0	100	−42.0	168.0	0	-

6.3.3. Membranes morphology and performance

The morphological investigations on membranes were performed by FESEM analysis. Both the surface and the cross-section were examined for pristine PSF membranes and cross-linked membranes prepared from UV–curing and NIPS of modifed PSF solutions. The representative micrographs of membranes made of pristine PSF and PSF containing 10 wt. % of BEDA and 10 wt. % of PEGDA acrylic resins are shown respectively in Figures 6.5 (a-c), 6.6 (a-c) and 6.7 (a-c),

The cross-sectional images of all membranes revealed a sponge-like structure with pores sized in the micrometer range. This structure was comparable for membranes made of pristine PSF and PSF modified with crosslinkers. No significant difference was observed for the two acrylic resins. On average the micro pores were smaller upon addition of the crosslinkers but the size difference was not significant for the lowest investigated concentration i.e. 10 wt. %. The cross-sectional micrographs also suggest that thickness did not change considerably between pristine and modified membranes. These qualitative observations were corroborated by measurement of water flux which was used in this study as a proxy to evaluate the overall membrane porosity and to assess the potential membrane performance in ultrafiltration systems. The flux values of

membranes containing 10 wt. % of acrylic crosslinkers were lower than that of pristine PSF membrane but they remained in the ultrafiltration range. On the other hand, when the acrylic resin content was increased to 20 wt. %, a strong reduction in flux was observed while no flux was measured when 30 wt. % of the acrylic resins were added to the PSF formulations. When the acrylic content is high the pores got closed by the acrylic network formation as shown in Figure 6.8. Moreover, figure 6.9 shows the water permeability decreased in a linear fashion with increased acrylic content in the polysulfone solution. These results suggest that a tradeoff exists between the amount of acrylic agent added to the polymer dope and the final chemical robustness of the membrane and its characteristics in terms of porosity and productivity. They also suggest that an optimum exists around a value of 10 wt. % of crosslinker which still guarantees the fabrication of porous ultrafiltration membranes.
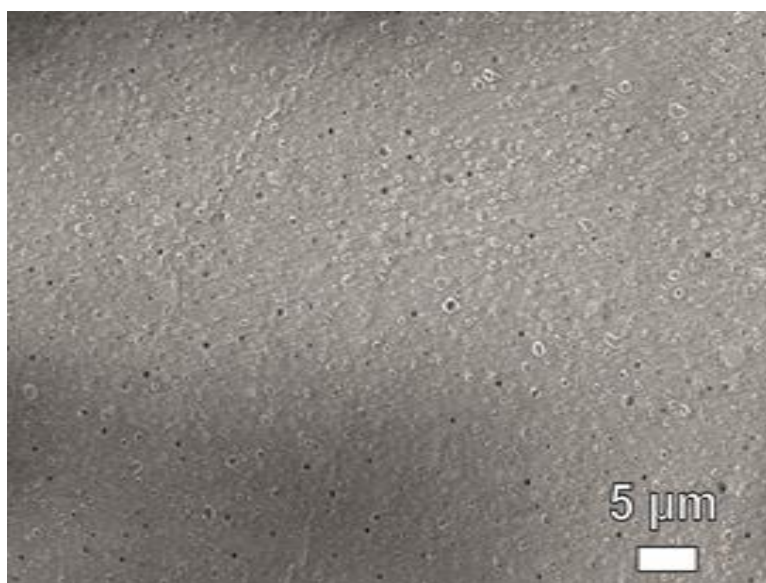
Figure 6.5(a) FESEM micrograph of surface of M00–Pristine PSF
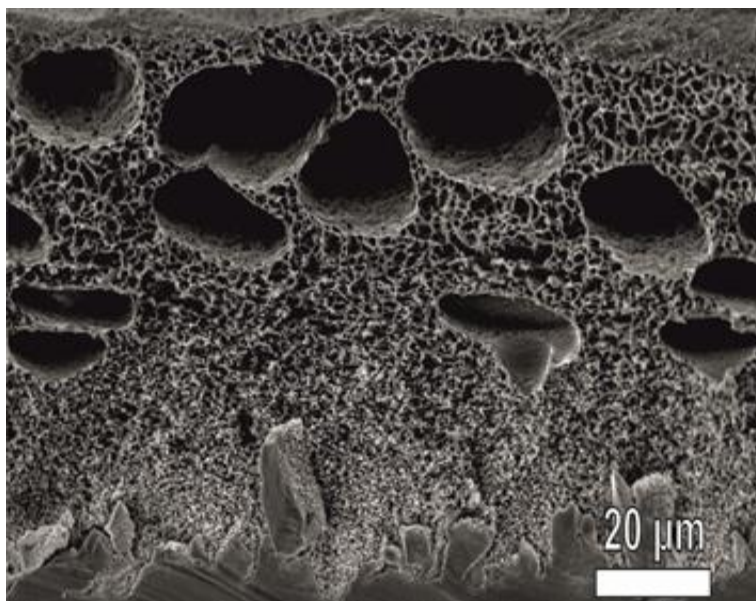
Figure 6.5(b) FESEM micrograph of cross–section of M00–Pristine PSF
(10K magnification)
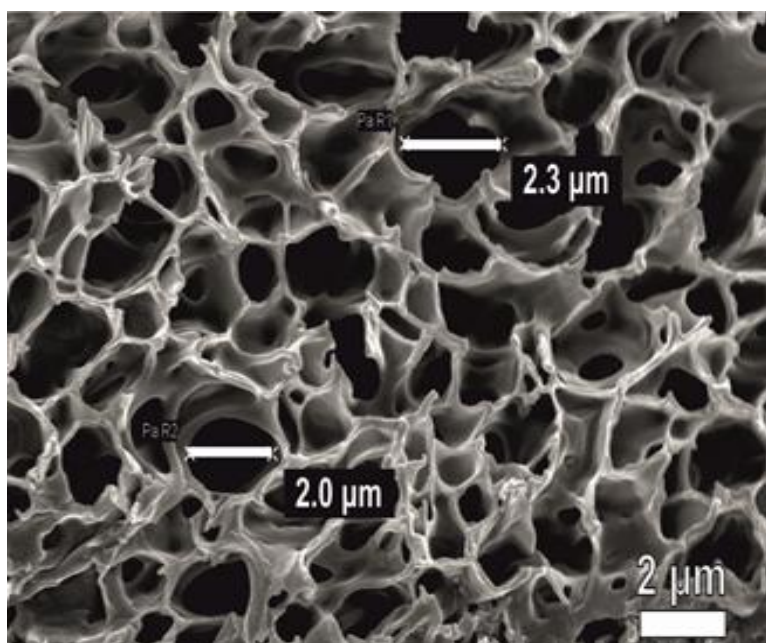
Figure 6.5(c) FESEM micrograph of cross–section of M00–Pristine PSF
(20K magnification)
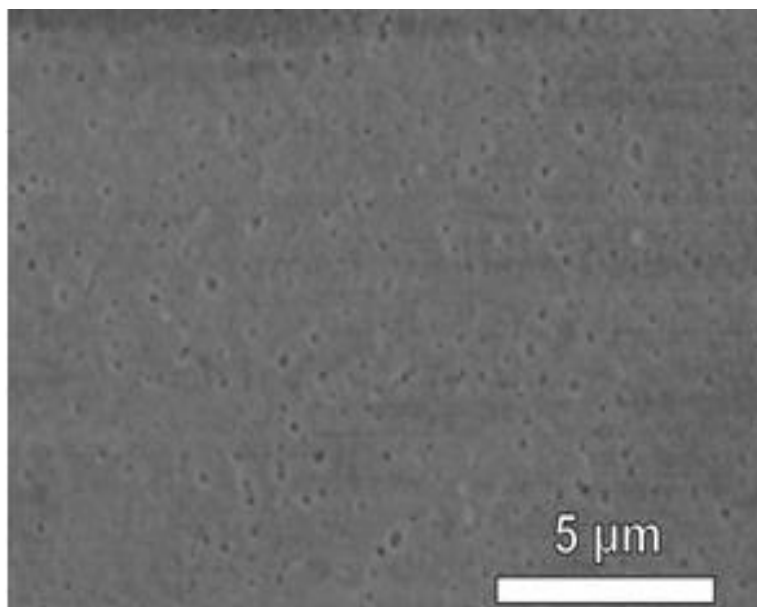
Figure 6.6(a) FESEM micrograph of surface of M11–PSF+10 % BEDA
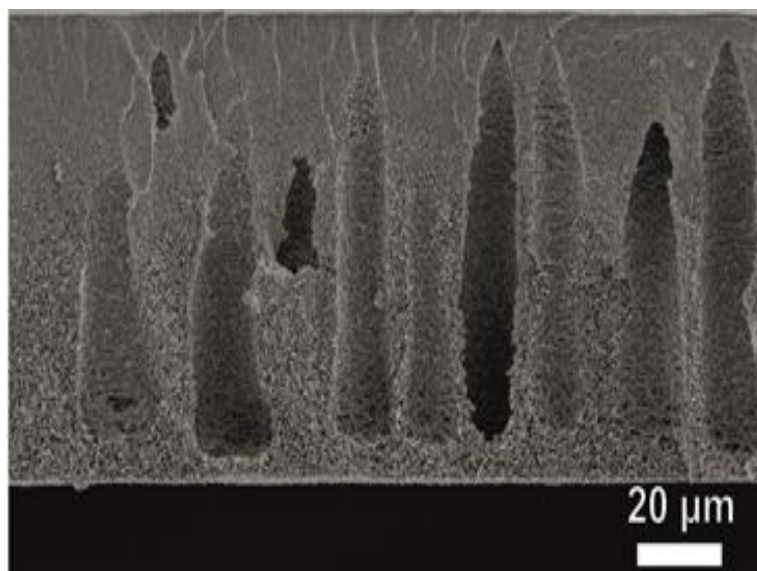
Figure 6.6(b) FESEM micrograph of cross–section of M11–PSF+10 % BEDA
(10K Magnification)
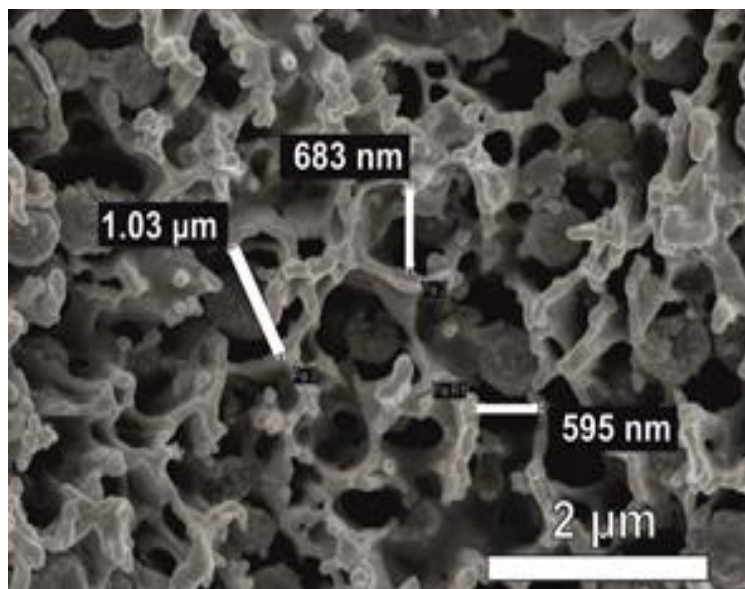
Figure 6.6(c) FESEM micrographs of cross–section of M11–PSF+10 % BEDA (20K Magnification)
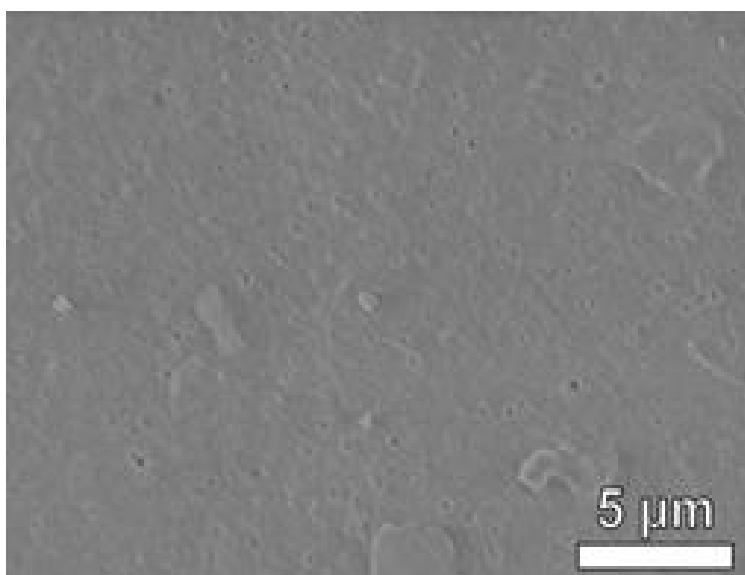
Figure 6.7(a) FESEM micrograph of surface of M21–PSF+10 % PEGDA
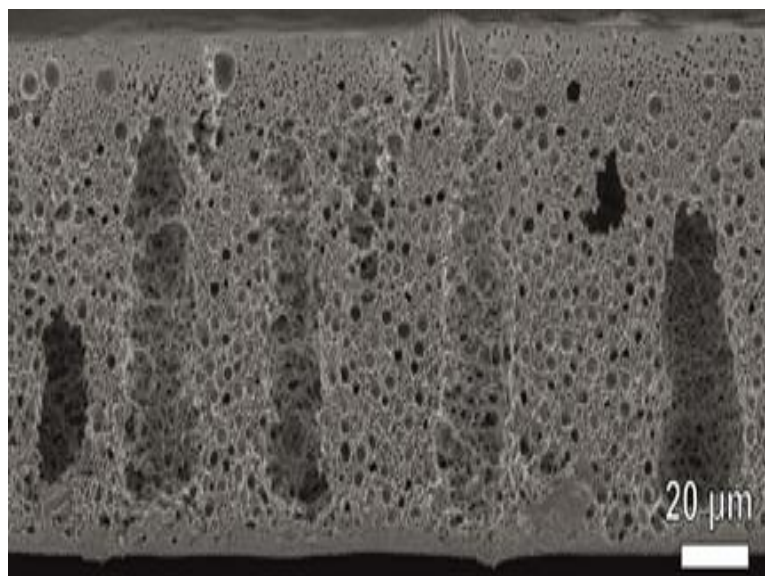
Figure 6.7(b) FESEM micrograph of cross–section of M21–PSF+10 % PEGDA
(10K Magnification)
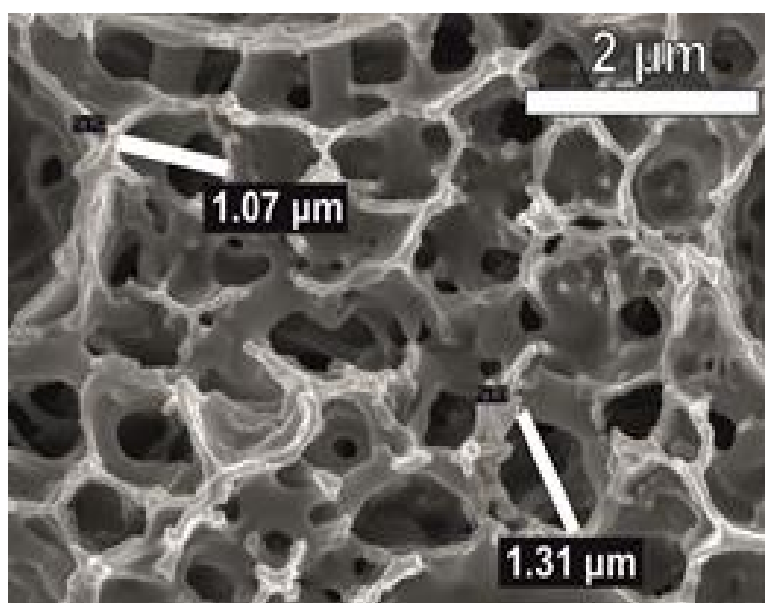
Figure 6.7(c) FESEM micrograph of cross–section of M21–PSF+10 % PEGDA
(20K Magnification)
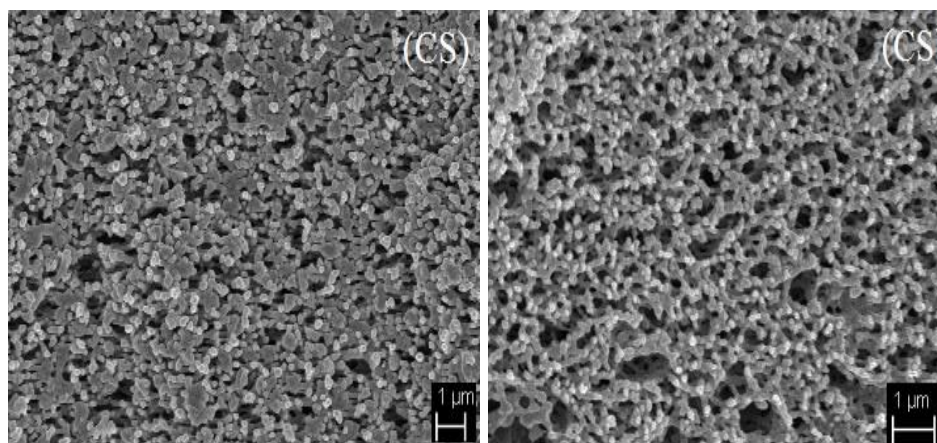
Figure 6.8: FESEM micrograph of cross–section of M13–PSF+30 % BEDA (left) and M23–PSF+30 % PEGDA (right) (30K Magnification)
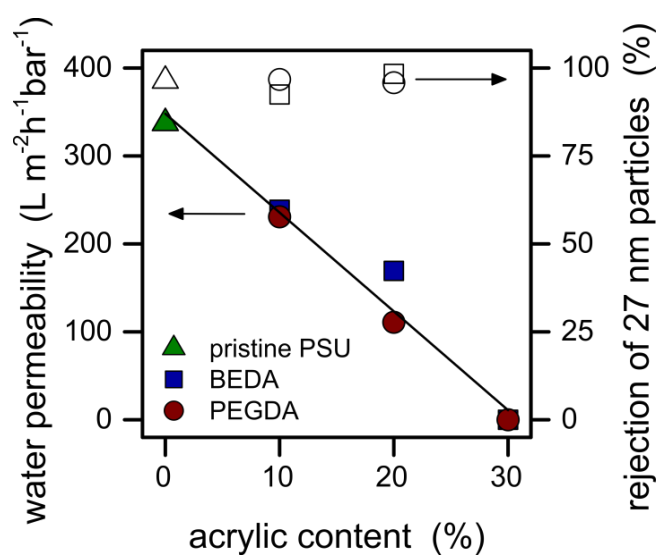
Figure 6.9: Influence of acrylic content on water permeability of the membranes and their ability to reject inert particles with a diameter of 27 nm. The solid line is the best fit of the combined data of permeability, having a slope of approximately -11 L m^{-2}h^{-1}bar^{-1} for each percentage point of acrylic compound added.

The rejection of 27 nm particles recorded at a high level (> 90%) with all samples having measurable flux suggests that the functionalization with resins did not

affect the selectivity of the membranes. No obvious correlation was observed between acrylic content and rejection of 27 nm particles, whose values are within experimental error; see Figure 6.9. These data suggest that though porosity was reduced as the content of acrylic compound was increased but the change in the average pore size at the membrane surface was instead negligible. Therefore, the addition of the crosslinker did not affect significantly the selectivity of the membranes. All the crosslinked membranes were found completely insoluble in DMF, THF, acetone, DMSO and toluene, demonstrating that the crosslinking reaction allowed to achieve solvent stable PSF based membranes.

6.4. Conclusion

We performed a systematic investigation of the effect of content and structure of acrylate resin on PSF-based membranes with the aim to obtain increased chemically stable crosslinked membranes without compromising their flux properties. The membranes were developed through UV curing followed by NIPS process. The acrylic double bond conversion was evaluated via FTIR analysis and the crosslinked membranes were fully characterized. The double bond conversions achieved with acrylic monomers incoporarted into PSF solutions were high and in accordance with the conversion of pristine monomers. The viscoelastic behavior of membranes was studied through dynamic mechanical thermal analysis (DMTA). All the crosslinked membrans exhibited an evident biphasic nature on the behalf of interpenetration of the crosslinked acrylic network and the PSF polymeric chains. Morphological investigations were performed by FESEM on the surface and the cross-sections, both for the pristine PSF membranes and the crosslinked membranes containing different weight percentages of BEDA and PEGDA acrylic resins. The porosity suitable for ultrafiltration application was very much retained after crosslinking of 10 wt. % of acrylic monomers and it was found consistent with the water flux values that were comparable to that of pristine PSF membrane. By increasing the acrylic content above 10 wt. %, the pores were closed by the polymer–acrylate network formation. High rejection of 27 nm particles (> 90%) was measured on all the modified samples having measurable flux suggesting that the functionalization with resins did not affect the selectivity of the membranes. All the cross-linked membranes displayed excellent stability in various solvents. In conclusion we have observed the most suitable acrylic monomer content to enhance the solvent stability without affecting the flux and rejection behavior of membranes.

Chapter No 7

PSF membranes functionalized with polydopamine for dye removal

The previous chapter discussed the preparation of ultrafiltration membranes based on UV–induced acrylic functionalization of PSF where di-acrylate cross-linker was added into pristine PSF solution and cross-linked membranes were developed through combined effect of UV–curing and NIPS. The modified membranes exhibited increased chemical stability without compromising the flux properties. Among casting solutions, the PSF solution containing 10 % BEDA cross-linker was found to be the best formulation in terms of solvent stability and optimum permeability of the modified membranes. After controlled fabrication, the membranes of aforementioned composition retained the typical morphology and porosity required for ultrafiltration application. In this chapter we extended the functionality of the membranes from PSF + 10 % BEDA by depositing a layer of polydopamine on the surface of membrane thus allowing the removal of contaminants not only based on size exclusion but also on specific chemical interactions between contaminant and the membrane surface.

7.1. Introduction

Polydopamine (PDA) layers of controlled thickness have been successfully deposited on almost all types of inorganic and organic substrates by initiating oxidation of dopamine under mild alkaline conditions (pH typically in the range 7.5–8.5) using oxygen as the oxidant [312]. Following the said conditions, the

dopamine monomers undergo self-polymerization so PDA is formed spontaneously. The chemical structure of PDA contains amine, catechol and imine functional groups (see Figure 7.1) [313]. In the near past the PDA coatings have been also adjoined to several polymeric materials including polytetrafluoroethylene (PTFE), polydimethylsiloxane, polyethylene terephthalate (PET), polyetheretherketone, polyurethanes and polyimides [314, 315].

Due to their zwitterionic behavior, PDA coatings bring about interesting functionalities to membrane applications for instance, at higher pH, PDA is negatively charged and retains positively charged molecules while at lower pH the PDA layers are positively charged thus allow small positively charged molecules to pass through [316]. This behavior could be exploited further in a way that contaminants are removed and PDA functionalized membranes are regenerated. McCloskey et al. studied the effect of PDA deposition conditions on pure water flux and resistance to foulant adhesion during reverse osmosis, ultrafiltration, and microfiltration operations [317]. The research group investigated a number of polymeric membranes such as PVDF, PTFE and PP microfiltration membranes, PSF ultrafiltration membranes and polyamide based TFC desalination membranes. The correlation between PDA deposition conditions and fouling of membranes was thoroughly investigated for prevention of bio-fouling in particular in terms of drop of trans–membrane pressure during the filtration of micro-organisms and proteins [318]. Similar works on coating of membranes with PDA were reported by Choi et al. [319] and Wei et al. [320]. Though all those works have been showing the excellent characteristics of PDA-coated micro and ultrafiltration membranes but so far no one reported performance of PDA-coated membrane being applied in a continuous filtration mode. In fact, previously reported all the experiments were focused on the changes in membrane performance under static conditions.
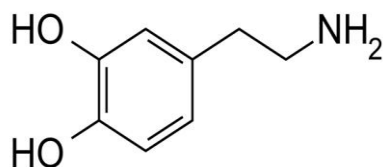
Figure 7.1(a) Structure of dopamine
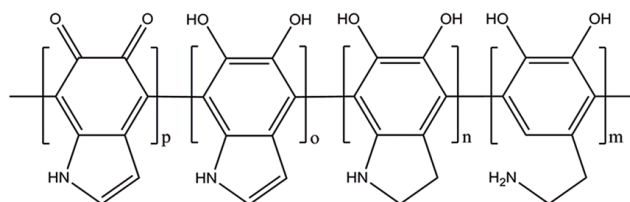
Figure 7.1(b) Structure of polydopamine

This chapter illustrates the filtration performance of a PDA functionalized membrane that combines the typical size–exclusion selectivity mechanism of ultrafiltration with chemical interaction based additional removal of contaminants while performing depth filtration in the membrane cross-section. We used high performance UV–crosslinked PSF–based membranes (discussed in chapter no. 6) as a substrate and investigated two procedures to functionalize these membranes with PDA. In a two-steps method, the PDA functionalized membranes were prepared via phase separation of UV–crosslinked PSF membrane followed by PDA coating. An advantageous and more facile one–step method was also investigated; in which UV–crosslinked PSF membranes were subjected to phase separation in an aqueous solution containing dopamine, so that phase inversion and PDA functionalization proceed at the same time. The functionalized membranes were fully characterized with evaluation of their morphology, surface properties, water flux and selectivity. In order to study the increased membrane adsorption behavior, methylene blue (a positively charged dye) was employed as a representative target contaminant. Using PDA coated membranes the removal of methylene blue was extensively studied both in batch and under filtration.

7.2. Experimental

7.2.1. Materials

- Polysulfone (PSF, Mn = 22,000 g mol^{-1})

- N,N-dimethyl formamide (DMF, Anhydrous, 98.8%)

- Acetone (99.9 %)

- Bisphenol-A-ethoxylate diacrylate (BEDA, Average Mn=512 g mole^{-1})

- Photo-initiator – phenylbis(2,4,6-trimethylbenzoyl)phoshineoxide (BAPO)

- Dopamine hydrochloride

- Tris(hydroxymethyl)aminomethane base

- Methylene blue (MB)

All the chemicals were purchased from Sigma Aldrich while the photo–initiator was provided by BASF.

7.2.2. Preparation of UV cured PSF based membranes

The polysulfone–based UV–crosslinked membranes were prepared via procedure same as described in section 6.2.2 i.e. UV curing of PSF solution containing BEDA crosslinker followed by NIPS process. A 15 wt. % solution of PSF in DMF was prepared by gradual addition of PSF beeds and continuous stirring at 60 $^{\circ}$C for 7 hrs. The solution was then cooled down overnight and 10 wt. % of BEDA was added as acrylic cross-linker together with the photoinitiator (Irgacure 819) at 3 wt. % with respect to the amount of the acrylic resin. The modified solution was sonicated for 15 min and left to release trapped air. After obtaining a homogenous solution, a film of 100 μm thickness was cast on the glass plate using a wire wound applicator. The wet film was UV cured for one minute under nitrogen (using a mercury medium pressure lamp) and thereafter subjected to NIPS to produce crosslinked membrane. The amount of energy consumed to cure the membranes was 10.05 J/cm^2. During wet casting and NIPS, the relative humidity in air was 40±10 % and temperature was 25±3 $^{\circ}$C.

7.2.3. Polydopamine functionalization of cross-linked membranes

The polydopamine coating was aimed to provide a large density of sorption sites for contaminant removal during cross–sectional depth filtration. As such the functionalization ensured the effectual formation of PDA layer thus coating the inner pores of the membrane all across the membrane thickness. This functionalization was performed following two different strategies, namely a two-steps and a one-step method. In the two-steps method, NIPS and PDA coating were performed as two independent processes one after the other. After UV curing the membrane was immersed in a non-solvent bath, containing distilled water, to obtain NIPS. Subsequently the cross-linked porous membrane was coated after being immersed in a dopamine solution under alkaline conditions (dopamine = 2.0 g/L in 50 mM TRIS-HCl buffer with pH = 8.5) and gently stirred at 50 °C. A number of immersion times (3, 6, 12, or 24 hrs) were investigated to understand the effect of the extent of PDA coating on the filtration performance of the membranes. After the functionalization, the membrane was washed with gentle stirring in a deionized water bath for 24 hrs in order to remove the residual PDA that has been adhered to the membrane.

The one-step method is exclusively a single stage process in which NIPS of the UV cross-linked films was performed directly inside dopamine solution in water. After UV irradiation, the membrane was immersed, for different time intervals (3, 6, 12 and 24 hrs), in a water bath containing dopamine monomer under alkaline conditions. The concentration of dopamine was 2.0 g/L in 50 mM Tris-HCl buffer and a pH 8.5 was maintained. The system was gently stirred at 50 °C. After this stage, the membrane was washed in a deionized water bath for 24 hr. The formulations of all the membranes functionalized with PDA are summarized in Table 7.1. The pristine PSF membrane was also fabricated and referred to as M0, while control UV cross-linked membranes containing 10 wt. % BEDA acrylate is referred to as M01.

Table 7.1: Composition of casting solutions and the corresponding PDA coating methodologies (all the membranes contain 15 wt. % PSF and 10 wt. % BEDA)

Membrane	PDA Coating time (hr)	two-steps method	one-step method
M1-3	3	–	✓
M2-3	3	✓	–
M1-6	6	–	✓
M2-6	6	✓	–
M1-12	12	–	✓
M2-12	12	✓	–
M1-24	24	–	✓
M2-24	24	✓	–

7.2.4. Characterization of PDA coated membranes

A Thermo Electron spectrophotometer was used for Fourier transform infrared (FTIR) spectroscopy and attenuated total reflectance (ATR) FTIR analysis to evaluate the degree of crosslinking. The instrument is equipped with an ATR accessory containing an internal reflection element based on diamond crystal. The analysis was carried out with a resolution fixed at 4 cm^{-1} and samples were scanned 32 times in the wavenumber range between 650 and 4000 cm^{-1}. The conversion of acrylic double bonds was calculated following the decrease of the area of the peak relative to C=C stretching group at 810 cm^{-1}, normalized with the area of the C=O peak at 1730 cm^{-1}.

The morphology, of both surface and cross-section, of each membrane was analyzed through field emission scanning electron microscopy (FESEM). The instrument used is MERLIN model by ZEISS, equipped with state of the art GEMINILIS column ensuring accurate control of spot and current. The operational voltage was adjusted for each sample based on its properties and the desired magnitude. The samples were snapped after immersion in liquid nitrogen

and mounted onto SEM stubs. For cross-sectional analysis, the samples were clamped with edges in upward position. The samples were sputter coated with a layer of chromium upto thickness of 8.0 nm.

The hydrophobicity of the membranes was determined at room temperature via static contact angle measurements through a KRUSS DSA–100 apparatus. This system makes use of different methods to obtain drop shape analysis across three phases: dry membrane/air/water drop. The sessile drop fitting method was chosen to measure the contact angle and the results were also verified by other methods: tangent method–I and tangent method–II. All the contact angles were measured in equilibrium mode and the average values are presented.

7.2.5. Batch adsorption

Batch adsorption experiments were performed using PDA functionalized membranes targeting methylene blue (MB), a cationic dye chosen as a model contaminant. A cut-out of coated membrane (20-30 mg) was immersed into a solution with known concentration of MB while the concentration of MB in the solution was monitored by UV spectrophotometer at the wavelength of 664 nm. In order to calculate the amount of dye adsorbed on the membranes, a simple mass balance was carried out taking into consideration the values of the dissolved dye in the beginning and at the end of the test. Initial experiments were conducted by immersing the samples functionalized for different coating times (namely, 3, 6, 12 and 24 hr) in the MB solution at pH 10 and left for 24 hrs to study the influence of coating time on the maximum amount of dye adsorbed. The rate of adsorption at pH 10 was estimated by monitoring the amount of MB adsorbed as a function of time. Then, the effect of pH of MB solution was studied by immersing the membranes functionalized with a coating time of 24 hr in MB solutions of pH 4, 6 and 10. Finally, the reusability of the membranes was evaluated by regenerating the membrane under acid conditions after being saturated with MB solution at pH 10. HCl solution, at pH 3, was used to promote desorption of MB and subsequently to regenerate the membrane. The process of desorption was run for 12 hrs followed by a rinsing step in distilled water for 12 hr. The same membrane piece was used to perform seven adsorption–desorption cycles.

7.2.6. Filtration tests

The filtration tests to measure the permeability adsorption characteristics of the membranes were carried out in a stirred cell apparatus, Amicon Model 8010 (Millipore Co.), with samples having a diameter of 1 inch. The cell was initially pressurized with $N_2(g)$ to reach a pressure drop of 15 psi, monitored using a pressure gauge. At this pressure, the membranes were subjected to pre-compaction for 10 minutes. Thereafter, the pressure was reduced to 8 psi and the flux through the membranes was determined by collecting the permeate and measuring the change in mass over time after the steady-state is reached. The experiments were performed using deionized water obtained from a Milli-Q water purification system. The permeability was calculated as the flow rate divided by the membrane area and by the applied pressure, and it is reported in $L\ m^{-2}h^{-1}bar^{-1}$. The ultrafiltration selectivity of the membrane was tested with polystyrene latex beads with a nominal diameter of 27 ± 4 nm from TEM measurements, suspended in deionized water. Rejection was purely based on size–exclusion, thus providing information on the average size of the pores at the membrane active surface, which should not change upon functionalization with PDA. A spectrophotometer was used to measure the absorbance of both the feed solution (c_f) and the permeate solution (c_p) at a wavelength of 260 nm. A previously obtained linear correlation allowed calculation of the particle concentration from the value of absorbance. The rejection of latex particles, R, was then calculated through the equation 1.5

In the same filtration system, MB depth adsorption tests were conducted. Firstly, a solution of deionized water at pH 10 was filtered through the membrane for 1 hr at an applied pressure of 10 psi so the excess PDA is removed and thus sample is thoroughly cleaned. Thereafter, the feed was substituted with a 0.5 g/L solution of MB at pH 10. The solution was directed to flow through the membrane for 3 hr. The permeate samples were collected continuously at fixed intervals of three minutes and their absorbance was measured using a spectrophotometer following wavelength of 664 nm to evaluate the concentration of MB. A previously obtained linear correlation guided to the calculation of the dye concentration from the value of absorbance. A tracer test was conducted as follows: after the membrane is saturated with the dye during the adsorption experiment, both the ultrafiltration system and the membrane were flushed using a dye-free solution at pH 10. During this flushing no significant release of the previously adsorbed dye was observed. Subsequently, the initial feed solution containing 0.5 g/L MB was again filtered

through the already saturated membrane. As all PDA sites were saturated with the dye, so the hypothesis is made that the dye did not interact with the membrane, thus this second filtration step can be used as tracer filtration. Also in this case the permeate samples were collected and analyzed with the same procedure used for the previous adsorption tests. At the end of this tracer filtration, the membrane was removed from the cell and rinsed in deionized water at pH 10. A dye desorption test was then conducted by leaving the membrane sample in a bath containing deionized water at pH 3 for 24 hr with gentle stirring. The absorbance of this solution was measured to estimate the amount of dye that desorbed from the membrane.

7.3. Results and discussion

In this work, we combined the ultrafiltration performance of a solvent stable UV-cured PSF-based membrane with the adsorption behavior of PDA used to functionalize the membrane. We practiced two different strategies for the preparation of these multifunctional membranes. A schematic representation of both methods is given in Figure 7.2. In two-steps process, at first membrane was fabricated by subjecting UV cross-linked film to NIPS and in the next step PDA functionalization was carried out by immersing the already formed membrane into an aqueous dopamine solution so a pH-induced self-polymerization takes place. An alternative and advantageous approach employed is one-step process where NIPS and PDA functionalization were merged in a single step process. In both approaches, the PDA coating was done for different intervals of time namely 3, 6, 12 and 24 hrs.
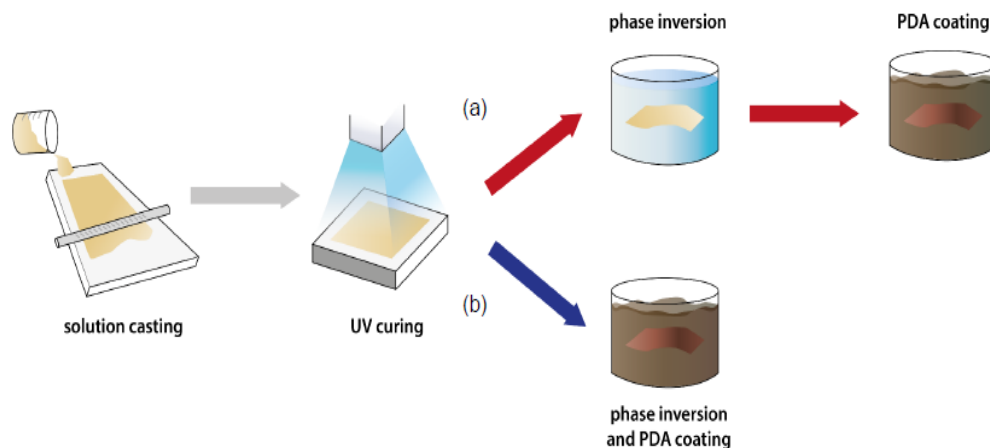
Figure 7.2: Schematic representation of the preparation of PDA functionalized membranes a): NIPS followed by PDA coating in dopamine solution b): NIPS in dopamine solution – a unique approach of PDA functionalization

7.3.1. Membranes preparation and characterization

The degree of conversion of the BEDA functionalized PSF-based membrane has been previously evaluated and reported in section 6.3.1, a final conversion of about 85% was achieved after one minute of irradiation [c.f. 6.3.1]. In case of PDA functionalized membranes the evidence of PDA coating was confirmed via ATR–FTIR analysis: the spectra of the PDA coated membranes M1-6, M2-6, M1-24 and M2-24 were recorded and compared with that of the pristine PSF membrane (M0). The spectra are given in Figure 7.3. After PDA functionalization peaks at 1600 cm^{-1} and 1450 cm^{-1} are evident due to the C=C from phenyl groups and N–H from amino groups, respectively, present on PDA. The signal at 1730 cm^{-1} was related to the C=O from the acrylate crosslinker.
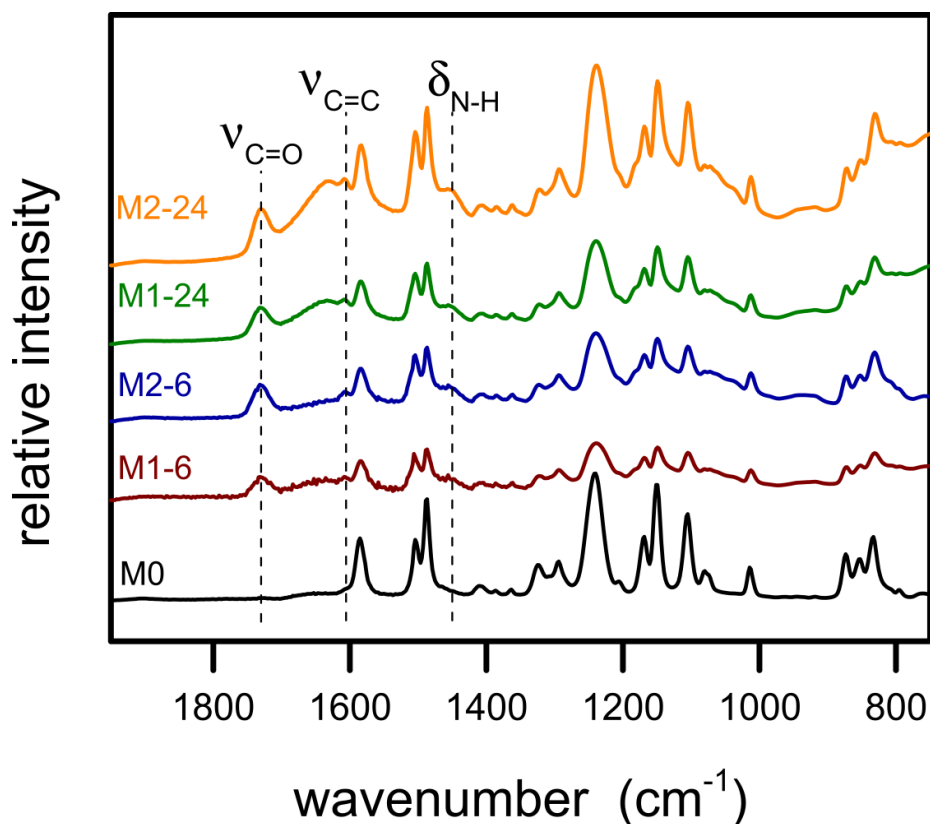
Figure 7.3: ATR-FTIR spectra of pristine PSF (M0) and PDA-coated crosslinked PSF based membranes

The morphology of both the surface and cross–section of the membranes was investigated through FESEM. The representative micrographs are shown in Figure 7.4 that include pristine PSF membrane, the cross–linked PSF membrane and the PDA coated membranes obtained with both methods after 24 hrs of functionalization. As reported in the previous chapter, the pristine PSF exhibited typical ultrafiltration morphology i.e. macro voids in the bulk and nano pores on the surface (Figure 7.4a) and the cross-linked membrane also presented dense sponge-like structure (Figure 7.4b) in the bulk similar to that of pristine PSF and the density and the size of the pores at the active surface did not change significantly, thus cross-linked membrane retained high water flux; see Table 7.2. Both of these morphologies have been discussed in detail in section 6.3.3. The morphology of PDA coated membranes is given in Figure 7.4c (coating for 24 hrs following two steps method) and Figure 7.4d (one step coating for 24 hrs).
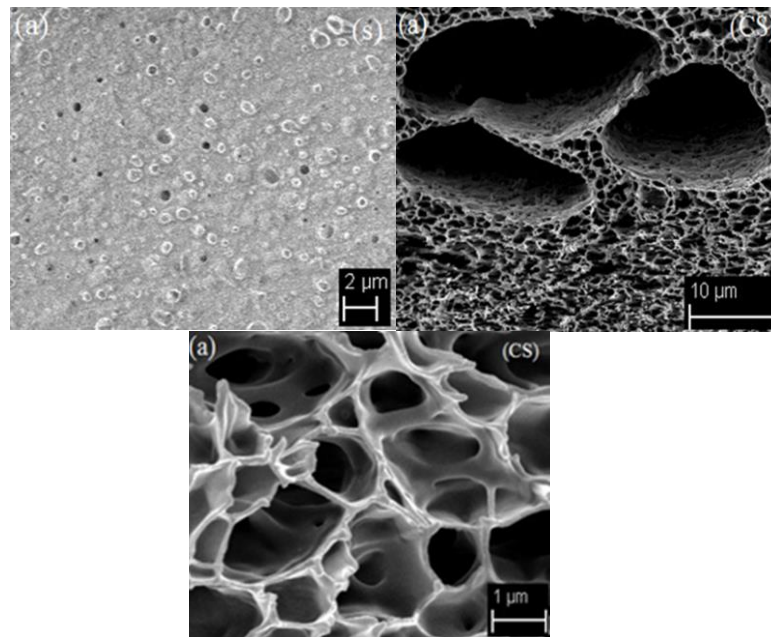
Figure 7.4a: SEM micrographas of surface (S) and cross-section (CS)
of prisitne PSF membrane (M0)
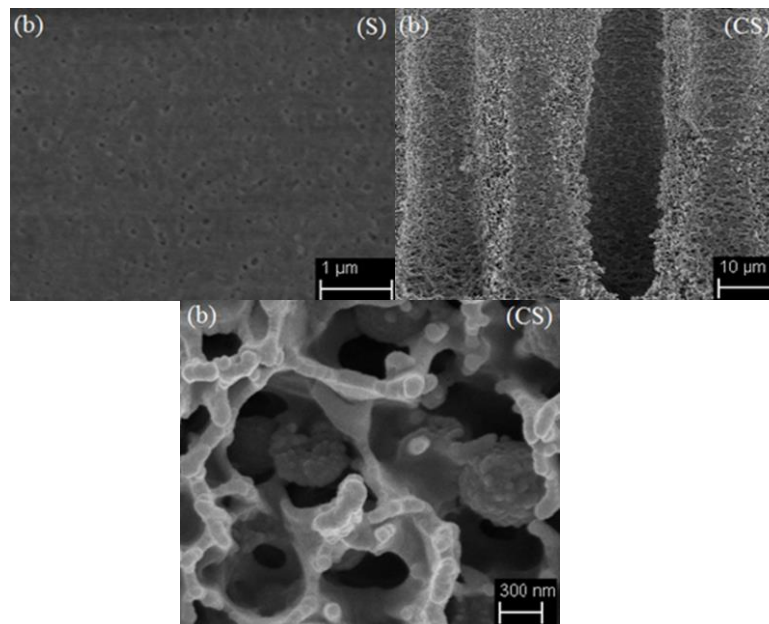
Figure 7.4b: SEM micrographas of surface (S) and cross–section (CS)
of UV cross-linked PSF membrane (M01)
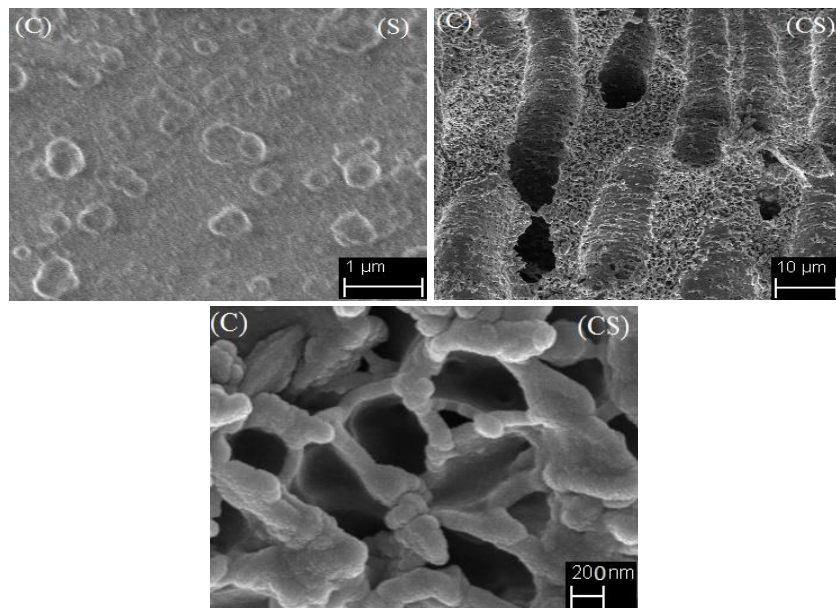
Figure 7.4c: SEM micrographas of surface (S) and cross–section (CS) of one step PDA coated (24 hr) PSF membrane (M1-24)
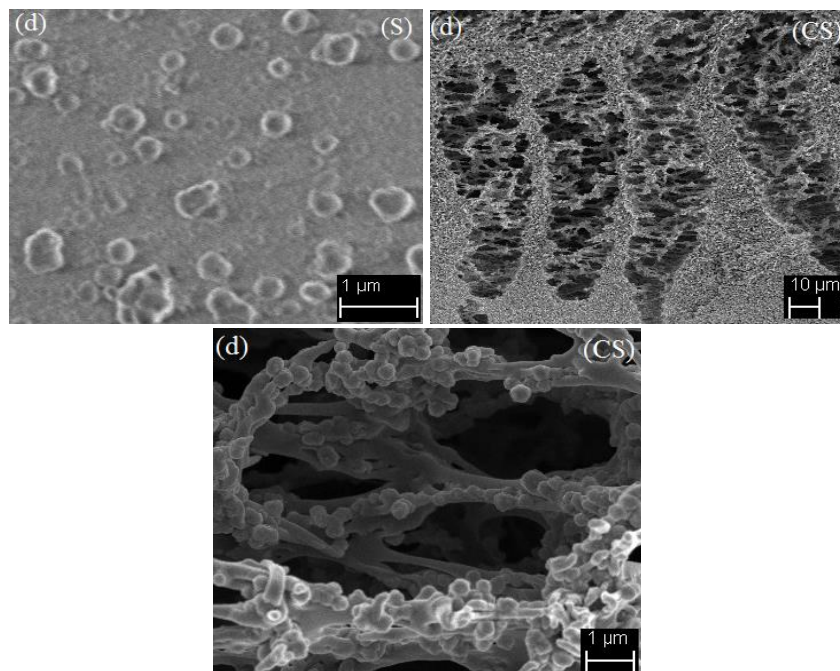
Figure 7.4d: SEM micrographas of surface (S) and cross–section (CS) of two steps PDA coated (24 hr) PSF membrane (M2-24)

With respect to morphology, though no important differences were observed for the membranes functionalized following the one-step process and the two-step process; nevertheless, slightly lower water flux was measured with the one-step coated membrane. The flux results suggest that the presence of PDA during NIPS did not change the precipitation pathway of the polymer significantly; instead, the coating of PDA achieved in the one-step method may be sufficiently thicker to reduce the size of the small pores on the surface of the asymmetric membrane. The rejection of particles having diameter 27 nm was maintained at a high level (Table 7.2). The values of contact angle indicate that the functionalization also caused a marginal increase in hydrophilicity induced by the PDA, but possibly not sufficient to cause changes in water flux.

Table 7.2: Performance evaluation of pristine, crosslinked and PDA coated membranes

membrane	water contact angle	water permeability $(L\ m^{-2}h^{-1}bar^{-1})$	rejection of 27 nm particles (%)
M0	53	338	96
M01	54	239	92
M1-6	53	16	95
M2-6	43	24	96
M1-24	45	15	89
M2-24	50	28	91

7.3.2. Specific mass adsorption of methylene blue (MB)

The PDA coating was carried out with the aim to adsorb charged molecules during depth filtration so the ultrafiltration properties of PSF membranes could be

combined with the adsorption properties of PDA. At pH 10, PDA becomes negatively charged thus should attract positively charged molecules such as the cationic dye MB. Primarily we evaluated the adsorption of MB in batch experiments. These experiments revealed that the adsorption of MB is not an equilibrium-driven process but in fact it is quantitative until saturation. Actually at liquid concentrations lower than those necessary to achieve saturation of the membrane, all MB molecules were adsorbed on the membranes and it was confirmed by the fact that the solution exhibited negligible light absorbance after being in contact with the PDA-functionalized materials. It means MB adsorbs on the surface of coated membrane until saturation is achieved.

Figure 7.5 represents the specific mass adsorbed (ratio of the mass of adsorbed dye normalized to the total mass of the membrane), at saturation, as a function of PDA coating time during membrane fabrication. The adsorption capacity was found to increase with the increase of PDA coating time and this increase was no more linear in the range of longer functionalization times. Nevertheless the membranes functionalized following the one-step method were capable of adsorbing a larger amount of dye compared to those fabricated via the two-steps approach. For the two different fabrication approaches investigated in this study, a trade-off was observed between water flux and adsorption capacity.

All the adsorption experiments were performed with an initial mass of dye in the solution and for an amount of time to allow complete saturation of each of the various membranes. The pH was fixed at 10 and temperature at 23 °C.
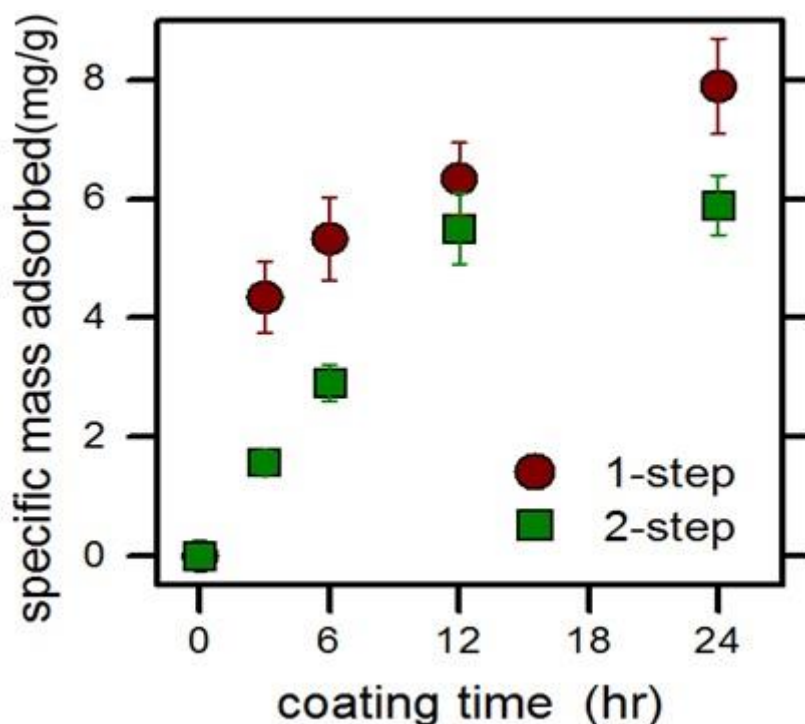
Figure 7.5: Specific mass of MB adsorbed as a function of PDA coating time, for membranes fabricated in one step (red circles) and two steps (green squares)

7.3.3. Kinetics of adsorption as function of PDA coating

The kinetics of adsorption of MB was evaluated for all the functionalized membranes and results are given in Figure 7.6. The cut–outs of membranes were immersed in 10 mL MB solution of concentration 12.5 mg/L; the light absorbance of the MB solution was monitored over time and used to calculate the mass of dye transferred from the liquid to the solid phase. The collected data reveals that both capacity and the kinetics of adsorption were higher for the membranes prepared through the one-step coating process. However the observed adsorption capacity was of high magnitude in all cases and this could be attributed to the fact that both membranes had a large number of sites available for interaction with the dye.
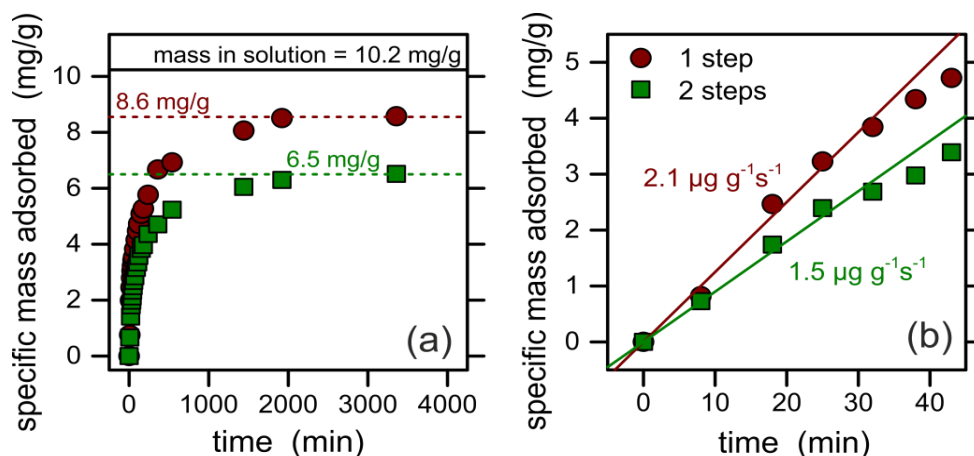
Figure 7.6: Mass of methylene blue adsorbed per unit mass of membrane as a function of time of adsorption, for membranes fabricated in one step (red circles) and two steps (green squares). (a) Complete sets of data, also showing (horizontal continuous line) the total amount of dye in solution normalized by the membrane mass and (horizontal dashed lines) the values of specific adsorbed mass at saturation for both types of membranes. (b) Enlargement of the initial part of the curves with linear fittings used to calculate the adsorption kinetics coefficients. Experiments were performed in 12.5 mg/L methylene blue, at pH 10, and at a temperature of 23°C.

In order to understand the role of PDA ionization on the adsorption of MB at saturation, the experiments were also conducted at two more pH values i.e. pH=4 and pH=7. The results are presented in Figure 7.7 and all adsorption experiments were performed in 20 mg/L methylene blue for 24 hrs at temperature 23°C. From the data collected the importance of electrostatic interactions to drive adsorption of the oppositely charged dye is quite obvious. PDA carries a lower density of charges under acidic conditions thus a lower number of sites are available for interaction with the dye molecules in solution (Figure 7.9). That is why at lower pH low adsorption of MB was observed for both the one-step and the two-steps coated membranes. Moreover, at low pH values the MB adsorption on the surface of both one and two step membranes was marginally different, possibly because of the reason that electrostatic interactions are minimal in this pH range. On the

other hand at pH 10 the one-step membrane showed higher MB adsorption as previously shown in Figures 7.6.
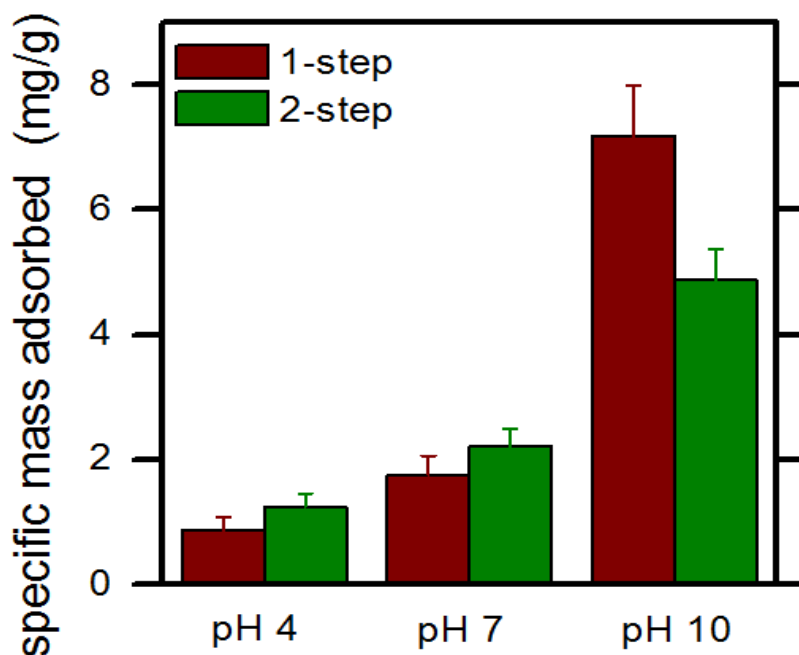
Figure 7.7: Mass of MB adsorbed per unit mass of membrane as a function of pH of solution. Data refers to membranes fabricated in one step (red bars) and two steps (green bars).

7.3.4. Cyclic stability of MB adsorption and desorption

The zwitterionic behavior of the PDA coatings was effectively exploited by subjecting the coated membranes to adsorption–desorption cycles. As mentioned previously that maximum adsorption is pH bound and a pH equal to 10 came up with the best adsorption results. Following to this finding, adsorption on functionalized membranes was performed at pH 10 for 24 hrs until the saturation was reached. While desorption steps were conducted at pH 3 for 12 hrs. PDA becomes positively charged at pH 3, due to electrostatic repulsion, most of the previously adsorbed MB dye was released. The regeneration of functionalized membranes was confirmed through repeated adsorption and desorption, the data is presented in Figure 7.8.

It is noticeable that the membranes were able to re-adsorb the same amount of dye during each of the seven adsorption cycles following desorption i.e. release of dye under the acidic conditions. Hence the functionalized membranes could be completely regenerated without loss of performance and reused by simply change of pH.
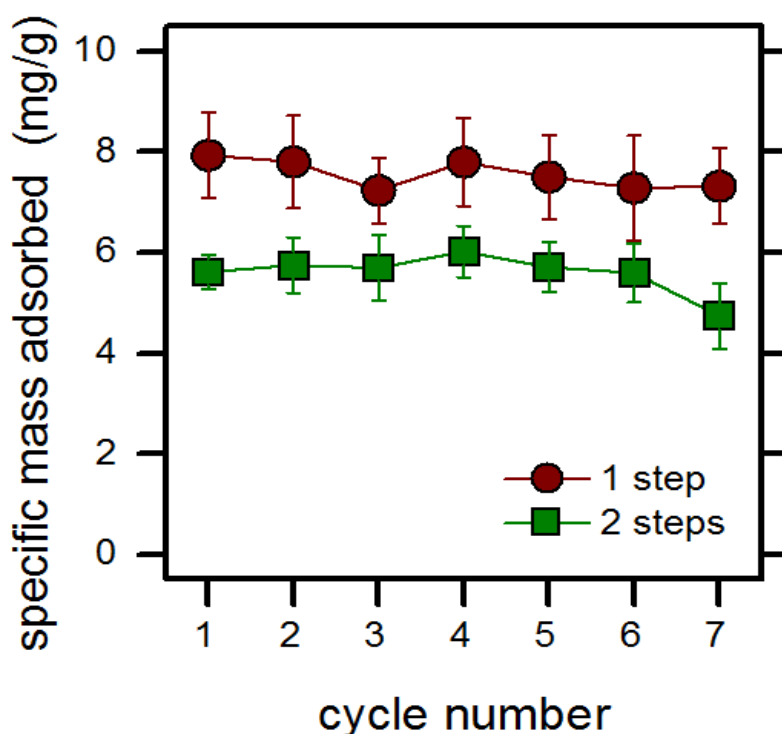
Figure 7.8: Mass of MB adsorbed per unit mass of membrane for different cycles of adsorption following the release at low pH where dye release between each adsorption cycle was performed in a dye-free solution

All experiments were performed in 20 mg/L methylene blue at a temperature of 23°. The adsorption was performed for 24 hr and the pH was set at 10 while desorption was carried out for 12 hr at pH 3. It is important to mention that adsorption at a given pH was always irreversible under unchanged conditions and no dye desorption was detected after contacting the saturated membrane with a dye-free solution of the same ionic and pH composition.
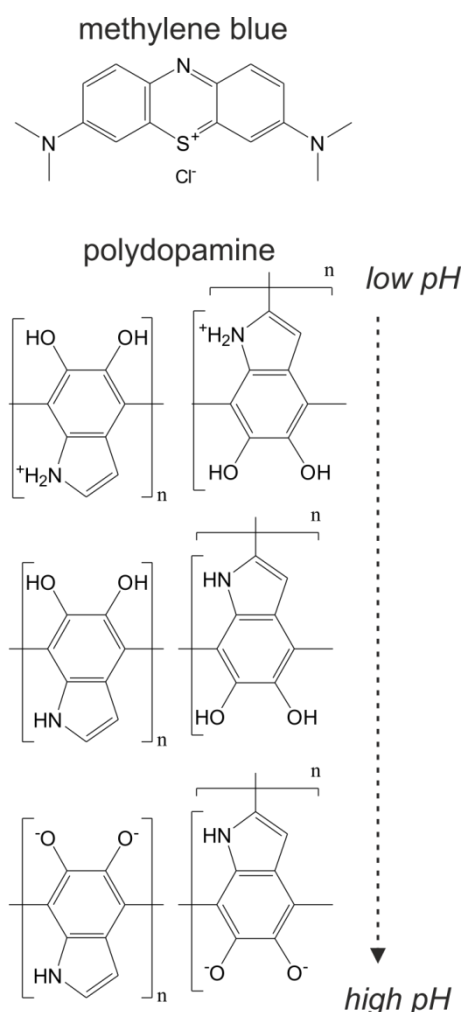
Figure 7.9: Schematic representation of the molecules of methylene blue and polydopamine under different ionization conditions as a function of pH.

7.3.5. Filtration of methylene blue

The depth filtration experiments were also performed by employing ultrafiltration conditions. For these experiments, a 0.5 g/L MB solution was filtered through the membranes functionalized with PDA and the concentration of dye in the permeate solution was monitored over time. Figure 7.10 shows the results obtained in a representative test using two-step membranes. The concentration of dye in the

permeate, presented as circles, increased with increased volume of permeate collected, following the typical breakthrough curves of depth filtration processes such as filtration of colloids or solutes through porous media. The normalized concentration in the permeate reached an asymptotic value of approximately 0.85; this results is rationalized with the expected ability of the membrane to marginally reject the dye with a rejection of roughly 15% under the test conditions. This observation was confirmed by the data collected during filtration of a tracer, which also reached the same plateau value as shown by the triangles in Figure 7.10.

Both tracer and adsorption data sets were thus fitted using an advection-dispersion model. In the case of the tracer, no adsorption was implemented in the model, which allowed calculating the dispersivity and the porosity of our system. These values were then used to model the breakthrough curve obtained during adsorption. In the later case, blocking was added, to take into account that there is a maximum value of sites available for adsorption, related to membrane saturation. The value of the kinetics adsorption coefficient and that of the specific mass adsorbed at saturation were used as fitting parameters. In these calculations, the thickness of the membranes was fixed at 100 μm. The fitting procedure yielded accurate results and the model described the experimental data well. The calculated values were 12 mg/g for the specific mass adsorbed at saturation and 0.01 1/s for the adsorption coefficient. These values are not far from the values calculated from batch experiments, suggesting that the data modeling was adequate. More importantly, both the adsorption capacity and the rate of adsorption were large: despite the use of a highly concentrated feed solution (0.5 g/L), the amount of dye in the permeate was negligible or low during the initial minutes of filtration.

Desorption of MB from the membranes carried out at pH 3 was completed after 24 hr, based on the concentration of the dye measured in the release solution. Same results were obtained for the membranes functionalized either with the one-step or the two-steps approaches. In a potential application, membranes would be operated by alternating cycles of adsorption and regeneration, ensuring that only a negligible amount of targeted contaminant reached the permeate stream. The large adsorption capacity observed for these materials would allow operating the filtration for long time before stopping the process for cleaning. Based on our results, a typical 40 m^2 spiral-wound module, operated under 2 bar of applied pressure, would allow constant operation for roughly 15 min, obtaining

approximately 300 L of permeate with a contaminant concentration always lower than 10% of the feed concentration.
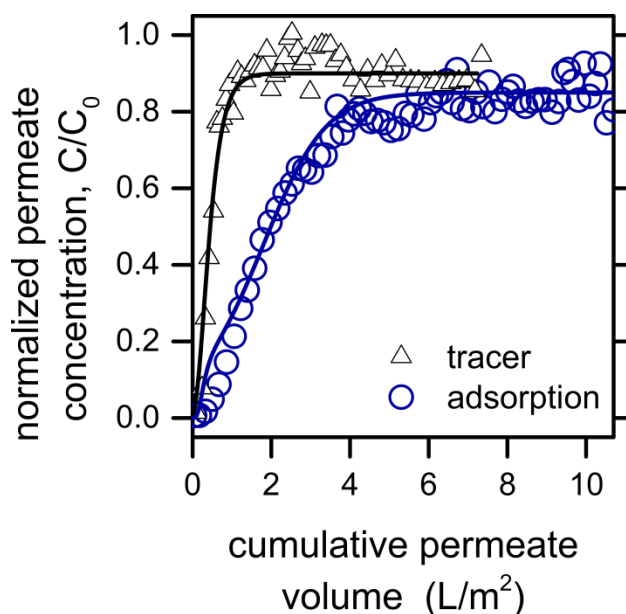
Figure 7.10 Breakthrough curves of methylene blue obtained in ultrafiltration tests for a clean membrane (blue circles) and an already saturated membrane (black triangles), the concentration in permeate was normalized by the concentration of dye in the feed and plotted against the collected volume of permeate. The data refers to a membrane functionalized following a two-steps protocol. The experimental data were fitted using advection-dispersion models, and the results are shown as continuous lines in the graph. Experiments were conducted using a feed solution of 0.5 g/L methylene blue at pH 10, filtered using an applied pressure of 10 psi at a temperature of 23 °C.

7.4. Conclusion

In this chapter, we reported the preparation and the filtration performance of polymeric membranes that combine the size–exclusion of ultrafiltration with the ability of polydopamine (PDA) to adsorb the contaminant in depth filtration process. The polysulfone based ultrafiltration membranes were prepared in the presence of an acrylic cross-linker in order to achieve chemically stable cross-

linked membranes maintaining good flux performance. Functionalization with PDA was carried out through either a two-steps method, where the UV cross-linked PSF membrane were subjected to NIPS followed by PDA coating; or in a one-step method, where UV cross-linked PSF membranes were subjected to phase separation in a water solution containing dopamine, so that phase separation and PDA functionalization occurred at the same time.

No visible differences, in terms of morphology, were observed for the membranes functionalized following the one-step process and the two-steps process; however, lower water flux was measured with the one-step coated membranes. Data suggested that the presence of PDA during NIPS did not change the precipitation pathway of the polymer significantly, but that the coating of PDA achieved in the one-step method could be sufficiently thicker to reduce the size of the smaller pores of the asymmetric membrane near its surface. Positively charged Methylene blue (MB) dye was employed as a model contaminant and dye removal was investigated both in batch and under filtration conditions. The adsorption capacity, studied at pH 10, showed an increase of MB removal with the increase of PDA coating time. The MB dye adsorbed onto the membrane until saturation was reached. Both the capacity and the kinetics of adsorption were higher for the membranes obtained via the one-step coating process thus implying a trade-off between water permeability and contaminant adsorption for the two different fabrication methods.

The results suggest that fabrication of such selective and reactive membranes may be designed depending on the application and the desired performance. In case of positively charged MB, the ionization of polydopmaine at pH=10 was found quite influential in order to drive the electrostatic adsorption. A counter argument is that a pH 10 is likely to neutralize a positively charged contaminant. Hence, a useful extended study could be application of PDA coated membranes to adsorb different positively charged contaminants.

From the current study, we are convinced that MB adsorption by a PDA coated membrane is driven electrostatically. As MB adsorbed at a given pH didn't leach out when subjected to fresh water at same pH. Moreover the membranes were completely regenerated at low pH and reused without loss of performance, as they were able to re-adsorb the same amount of dye in several adsorption cycles following dye release under acidic conditions. The membrane adsorption capacity and the rate of adsorption were evidently large during continous filtration experiments as well.

Chapter No 8

UV–induced reactive electrospinning of acrylic polysulfone fibers

In last three chapters, we reported the fabrication of UV cross-linked membranes through NIPS. The casting solution was consisted of acrylic functionalized PSF where acrylic functionality was introduced either during synthesis of methacrylated macro-monomer (c.f. 5.2.2) or through addition of acrylate cross-linker into PSF solution in DMF (c.f. 6.2.2). The developed membranes came up with excellent solvent stability and in case of di-acrylate modified membranes; reasonably high flux was obtained. In this chapter we report the development of BEDA functionalized PSF electrospun mats through sustainable UV–induced reactive electrospinning in a way that production of nano fibers and crosslinking of acrylate occur simultaneously.

8.1. Introduction

The conventional PSF membranes, developed through NIPS, are applied in ultrafiltration process as well as support layer in thin-film composite membranes (TFC) used in nano-filtration (NF), reverse osmosis (RO) and forward osmosis (FO) processes [321–323]. Nevertheless in recent years the electrospun

nanofibrous membranes (ENMs') have been successfully utilized as replacements of traditional phase separation membranes because of low resistance to mass transport and high intrinsic porosity compared to conventional asymmetric membranes obtained through phase separation [324, 325]. In order to fabricate high performance ENMs' several methodologies have been proposed such as colloidal electrospinning of composite solutions [326–331], electrospinning of polymeric blends [332, 333] and post-electrospinning modifications of the nano-fibrous mats [334–338]. Normally a post-electrospinning modification takes into account chemical reaction between a multifunctional crosslinking reagent and the polymer of membrane (nano-fibers). This post-treatment profoundly affects the different characteristics of the membrane such as mechanical properties, morphology and separation efficiency. More recently some methodologies alternate to post-electrospinning modification have been suggested in which *in-situ* functionalization of ENMs' proceeds during electrospinning, for example, *in-situ* crosslinking of a curable feed solution during the electrospinning process.

Such techniques are referred to as "reactive electrospinning". Reactive electrospinning ensures cross-linking by employing chemicals [339], UV radiations [340-344] and a combination of UV irradiation and pre [345] or post–heating [346].

It is worth mentioning that previous works on UV–induced reactive electrospinning have mainly focused on biomedical application of nanofibers, such as scaffolds and tissue engineering where a scalable production is usually not desired. Therefore, these works did not evaluate the sustainability of UV–induced electrospinning over a long span of time. Furthermore, the previously reported works have not thoroughly investigated the effect of UV irradiation on the intra fiber morphology.

In this chapter, we report the development of solvent stable polysulfone electrospun membranes via UV-induced reactive electrospinning of PSF solution containing an acrylate resin as a cross-linker. The designed system ensured two simultaneous processes, i.e. radical polymerization of the acrylic monomer and the concurrent production of polysulfone nanofibrous mats. The online UV irradiation is controlled in such a way that it irradiates only the nanofibers thus preventing the premature crosslinking of the acrylic resin and the phase separation of the polysulfone formulation. The feed solution is composed of PSF in DMF while Bisphenol-A-ethoxylate diacrylate (BEDA) was employed as a cross-linker. The acrylic double bond conversion, electrospinning parameters (flow rate,

applied voltage, needle to collector distance) and UV curing behavior were thoroughly investigated, correlated and optimized. The mats were also prepared via an offline UV curing method (post-electrospinning) and compared with the counterparts developed through online UV irradiation. The electrospun mats were fully characterized using ATR–FTIR, DSC, TGA, and FESEM, while their porosity is estimated through the difference between the density of the feed solution and that of the fibrous mats.

8.2. Experimental

8.2.1. Materials

- Polysulfone (PSF, Mn=22,000 g mol^{-1})

- N,N-Dimethyl formamide (DMF, anhydrous, 98.8%)

- Bisphenol-A-ethoxylate (2EO/phenol) diacrylate (BEDA, average Mn=512 g mol^{-1} inhibited with 1000 ppm MEHQ)

- Photo initiator (PIn) phenylbis (2,4,6-trimethylbenzoyl) phoshineoxide (BAPO)

8.2.2. Preparation of electrospinning solutions

The pristine PSF solutions in DMF were prepared in two different concentrations (15 and 18 wt. %) by gradually dissolving PSF beeds with continuous stirring at 60 ^{o}C for seven hrs followed by overnight cooling. All the feed solutions containing acrylic resin as crosslinker were prepared starting from PSF solutions at 18 wt. %, adding BEDA in three different concentrations, 5, 7 and 10 wt. % of the overall solution and the photo initiator (PIn) Irgacure 819 at 5 wt. % with respect to the acrylic monomer. All the investigated formulations are shown in Table 8.1. To ensure homogenous solution, the formulations were sonicated for 20 min in an MRC ultrasonic bath DC 80H and kept at room temperature for at least 10 min to cool down before electrospinning.

8.2.3. Electrospinning protocol

Electrospinning was performed using a Genie plus Kent scientific horizontal electrospinning setup. All the electrospinning experiments were carried out using 10 mL syringe (Becton Dickinson Company, USA) and Sterican single-use

hypodermic needles of gauge 0.60 mm by Braun, USA. To determine the optimal concentration of pristine polysulfone, the flow rate was kept at 0.01 mL/min while distance to collector and applied voltage were changed in equal proportion to the constant field strength could be maintained. Thereafter all the solutions, both pristine PSF and PSF containing acrylate, were electrospun with 0.01 mL/min flow rate, 22 cm distance between needle and collector, and 30 KV applied voltage. All the electrospinning experiments were performed at temperature of 21 ± 3 ^{o}C and relative humidity 40 ± 5 %. The electrospun mats were collected on the static rectangular aluminum collectors of size 8 cm × 12 cm. Electrospinning was run to produce fibrous mat of thickness 120 ± 10 μm. To evaporate any residual DMF, the electrospun mats were kept in a fume hood for 24 hrs prior to characterization and storage.

8.2.4. UV irradiation of electrospun fibers

The electrospun fibers, obtained from PSF formulations containing BEDA as a crosslinker, were UV irradiated either online or offline. Both these curing operations were carried out using portable UV lamp Intelli-Ray 600 by Uvitron International USA, where the power of the lamp was adjustable from 35 to 100 %. The intensity was also controlled by adjusting the distance between the lamp head and the substrate.

The online UV irradiation was conducted on the polymeric solution when it was being electrospun and before being collected. The UV irradiation was controlled to affect the convective flow only so the ohmic flow could have little or no impact of UV irradiation hence the solidification of electrospun solution at the tip of needle could be avoided. A schematic representation of UV-induced reactive electrospinning is shown in Figure 8.1. The syringe was covered with a black tape so the solution inside the syringe was never exposed to UV thus preventing premature crosslinking of the acrylic monomer. The UV lamp intensity and its vertical distance from the needle were optimized to ensure continuous electrospinning and optimum crosslinking. For the online UV irradiation, the power of lamp was always kept at 60 %, since above this threshold the solution was found to solidify at the tip of the needle causing blockage.

The offline UV irradiation (post-electrospinning) was carried out by irradiating the already electrospun mats for 1 min with 100 % power of the lamp. This procedure was chosen for economical reasons, i.e. the maximum extent of crosslinking was achieved in the minimum amount of time.
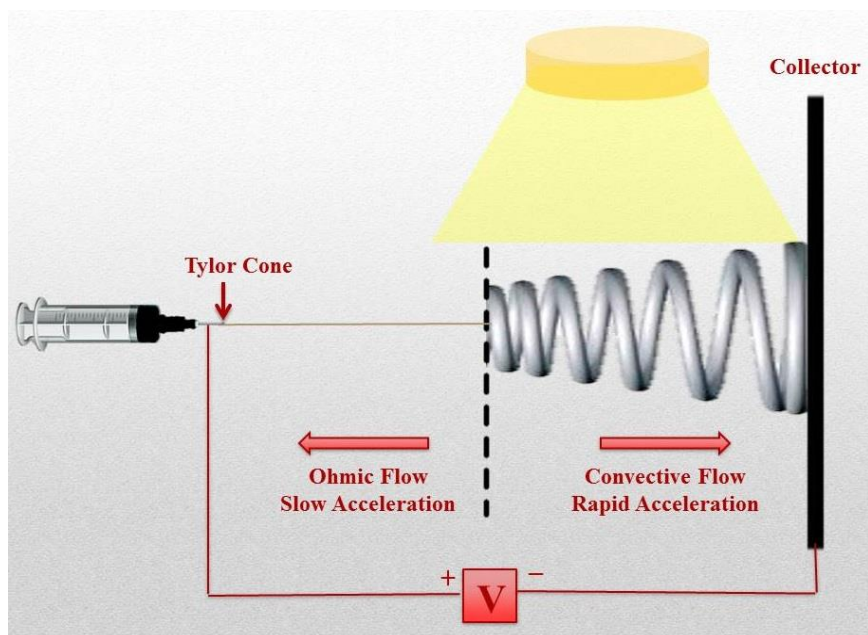
Figure 8.1: Schematic representation of the online UV-induced reactive electrospinning setup

Table 8.1: Composition of electrospinning solutions

Membrane Code	PSF wt. %	BEDA wt. %	PhI wt. % of BEDA	UV irradiation	
				Online	Offline
M00	18.0	-	-	-	-
M1F	18.0	5.0	5.0	-	✓
M1N	18.0	5.0	5.0	✓	-
M2F	18.0	7.0	5.0	-	✓
M2N	18.0	7.0	5.0	✓	-
M3F	18.0	10.0	5.0	-	✓
M3N	18.0	10.0	5.0	✓	-

8.2.5. Fourier transform infrared (FTIR) analysis

The spectrophotometer Thermo Scientific Nicolet iS10, equipped with attenuated total reflectance (ATR) accessory containing a diamond crystal internal reflection element, was used for Fourier transform infrared (FTIR) spectroscopy and attenuated total reflectance Fourier transform infrared (ATR–FTIR) spectroscopy analysis. To evaluate the double bond conversion for pure acrylic monomer, the monomer was cast onto a silicon wafer and analyzed with FTIR spectroscopy before and after UV irradiation. The analysis was carried out with a resolution of 4 cm^{-1} and 32 scans in the wavenumber range between 650 cm^{-1} and 4000 cm^{-1}. The conversion of acrylic double bonds was calculated by following the decrease of the peak area of C=C at 810 cm^{-1} normalized with the peak area of C=O at 1730 cm^{-1}. The crosslinking of electrospun mats was evaluated with ATR–FTIR analysis. The parameters during analysis and the target peaks were the same as used for the pure acrylic monomer.

8.2.6. Differential scanning calorimetry (DSC)

The glass transition temperatures of electrospun mats made of pure PSF and PSF modified with the acrylic resin were obtained through differential scanning calorimetry in a nitrogen atmosphere using TA Instrument DSC Q 200. Almost 8 mg of each fibrous mat was encased in an aluminum sample pan and heated from 0 to 260 ^{o}C at ramp temperature of 10 ^{o}C / min, followed by a cooling to 0 ^{o}C at the rate of 5 ^{o}C / min and by second heating to 260 ^{o}C at 10 ^{o}C / min.

8.2.7. Thermal gravimetric analysis (TGA)

The thermal degradation characteristics of the fibers from pure PSF and modified PSF were obtained using thermogravimetric analysis in a nitrogen atmosphere using TA instruments TGA Q500. Approximately 8 mg of each fibrous mat was heated from 20 to 600 ^{o}C and the temperature was increased by 10 ^{o}C per min.

8.2.8. Morphological analysis

For the optimization of electrospinning parameters, a qualitative morphological evaluation of the fibers was carried out using an optical microscope, OLYMPUS CX31 by Wirsam Scientific. Detailed morphology and diameter of all the fibers were analyzed through field emission scanning electron microscopy (FESEM) at an accelerating voltage 5 KV. The InLens images were obtained using a Zeiss

MERLIN FEG® scanning electron microscope equipped with state of the art GEMINI II® column ensuring the good control of current. The absence of beads was confirmed at magnification of 10K and pores on the surface of individual fiber were evidently shown at magnification of 20K. The samples were prepared by affixing a small rectangular piece of electrospun membrane on the sample stand using carbon tape. Prior to imaging all the samples were gold coated up to a thickness of 10 nm using Edward S150A sputter coater. The fibers diameters were measured directly from the images using Carl Zeiss Axio vision LE software and average value was calculated from 60 fibers in different SEM micrographs.

8.2.9. Porosity

An approximate estimation of the mats porosity was made through the difference of density between the feed solution and the fibers. The density of the solution (ρ_s) was obtained by weighing 1 mL of feed solution with careful measurement of solution volume using a calibrated Rainin micropipette. The bulk density of fibrous mats (ρ_f) was calculated by weighing a mat of size 1 cm × 1 cm. The thickness of all fibrous mats was obtained with a calibrated micrometer having resolution of 1 μm. The resultant porosity (Φ) was calculated through equation 8.1

$$\Phi\ (\%) = \left[1 - \frac{\rho_f}{\rho_s}\right] 100 \qquad\qquad \textbf{(8.1)}$$

8.2.10. Solvent resistance assessment

The solvent resistance of the crosslinked polysulfone membranes was assessed by immersing the membrane cutouts in a variety of solvents. The immersion was carried out at room temperature for at least 120 hrs. A qualitative evaluation was made based on the visual inspection of the membranes following this protocol.

The resultant membranes were categorized into three grades:

1) Stable 2) swollen 3) dissolved in a specific solvent.

8.3. Results and discussion

This study presents the fabrication and characteristics of PSF nanofibers produced by electrospinning of pristine PSF and PSF containing an acrylic crosslinker with the aim to obtain the solvent stable mats that may be used as stand-alone or support layers for liquid and gas separation. The fibers morphology and diameters resulting from electrospinning are influenced by the type of polymer, its concentration, the viscosity of solution, the type of solvent, the needle gauge, the applied voltage, the feed rate and the distance to collector [347]. Ambient parameters such as temperature and relative humidity also affect significantly the characteristics of the resultant fibers [348]. In addition to study on the effect of aforementioned parameters, we have also investigated how UV irradiation influences the fiber morphology when UV curing is performed either online (during electrospinning) or offline (post-electrospinning).

8.3.1. Effect of solution and electrospinning parameters

The pristine PSF solutions were electrospun over a wide range of electrospinning parameters in order to optimize the protocol and to minimize the formation of beads. The investigated pristine PSF solutions and different electrospinning parameters are given in Table 8.2. The feed solutions composed of 15 wt. % PSF produced beads under all the combinations of electrospinning parameters while the solution containing 18 wt. % PSF resulted into bead free fibers.

Table 8.2: Influence of concentration and electrospinning parameters on the pristine PSF fibers morphology and diameter

No.	PSF wt. %	Flow rate [ml/min]	Distance [cm]	Applied Voltage [KV]	Fiber Dia. [nm]	Resultant morphology
A	15.0	0.01	15.0	20.0	570	Beads
B	15.0	0.01	22.0	30.0	352	Beads
C	18.0	0.01	15.0	20.0	2100	No beads
D	18.0	0.01	22.0	30.0	994	No beads

Figures 8.2a and 8.2b display representative SEM micrographs of the electrospun fibers from the solutions containing 15 wt. % (solution B) and 18 wt. % (solution D) polysulfone respectively. The resultant fiber diameter increased with the increase of PSF concentration in accordance with the previous works [327, 332]. Furthermore the fiber diameter decreased with the increase of needle-to-collector distance. This observation could be explained by the well-known drawing effect.
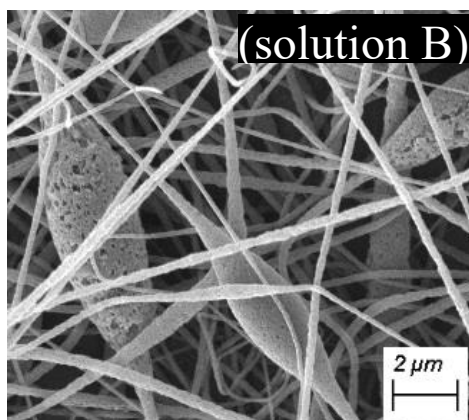
Figure 8.2a: SEM image of 15 wt. % pristine polysulfone fibers (B)
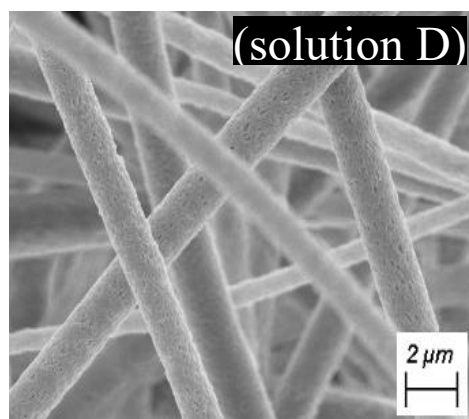
Figure 8.2b: SEM image of 18 wt. % pristine polysulfone fibers (D)

Table 8.3: Parametric analysis of solution and electrospinning parameters

Parameter	Effect on fiber morphology
Viscosity (Polymer solution)	Beads formation at low viscosity and smooth fibers at an optimum value whereas very high viscosity led to broader distribution of fibers diameters
Solution conductivity	Fiber diameter decreased with the increase of solution conductivity
Evaporation of solvents	Surface of fiber exhibited microstructre
Flow rate	Fiber diameter increased with the increase of flow rate & very high flow rate resulted into beaded morphology
Applied voltage	Initially fiber diameter decreased with the increase of applied voltage but thereafter increased
Needle to collector distance	Fiber diameter decreased with the increase of needle to collector distance
Humidity	With the increase of humidity fiber diameter increased

8.3.2. Influence of UV irradiation on PSF fibers containing BEDA

The UV irradiation conditions were optimized for the pristine BEDA monomer before investigating the effect of UV curing on the electrospun mats. The acrylic double bond conversion for the monomer was evaluated through FTIR analysis by following the decrease of the C=C peak at 810 cm^{-1} normalized with the C=O peak centered at 1730 cm^{-1} (Figure 8.3). An average conversion of 85 % was achieved after one minute of irradiation. These results were used to adjust the UV curing parameters of the PSF solutions containing the acrylate as crosslinker.

The solutions containing the acrylate BEDA were UV cured either online, during the electrospinning process, or offline, soon after electrospinning. In order to determine the degree of curing, both the online and the offline cured fibers were analyzed via ATR–FTIR spectroscopy. As an example, the spectra for the formulations containing 10 wt. % of BEDA, cured online and offline, are shown in Figure 8.4. The calculated degrees of acrylic double bond conversion in PSF fibrous mats, containing 5, 7, and 10 wt. % BEDA and irradiated online, were 85, 82, and 80% respectively. While fibrous mats, obtained from the same solutions but cured offline, exhibited acrylic double conversion degrees of 85, 85, and 82%, respectively. The comparable degrees of acrylic double bond conversion were achieved through the online and the offline processes. Nevertheless, the online irradiation process allowed the production of smooth crosslinked electrospun nanofibrous membranes in a more facile and sustainable single step operation.
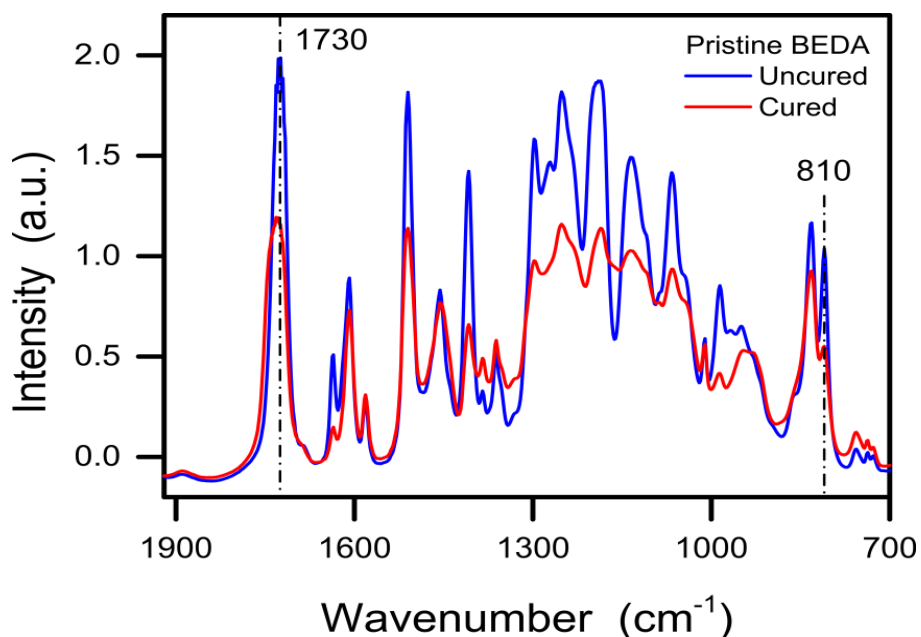
Figure 8.3: FTIR spectra of pristine BEDA before and after UV curing
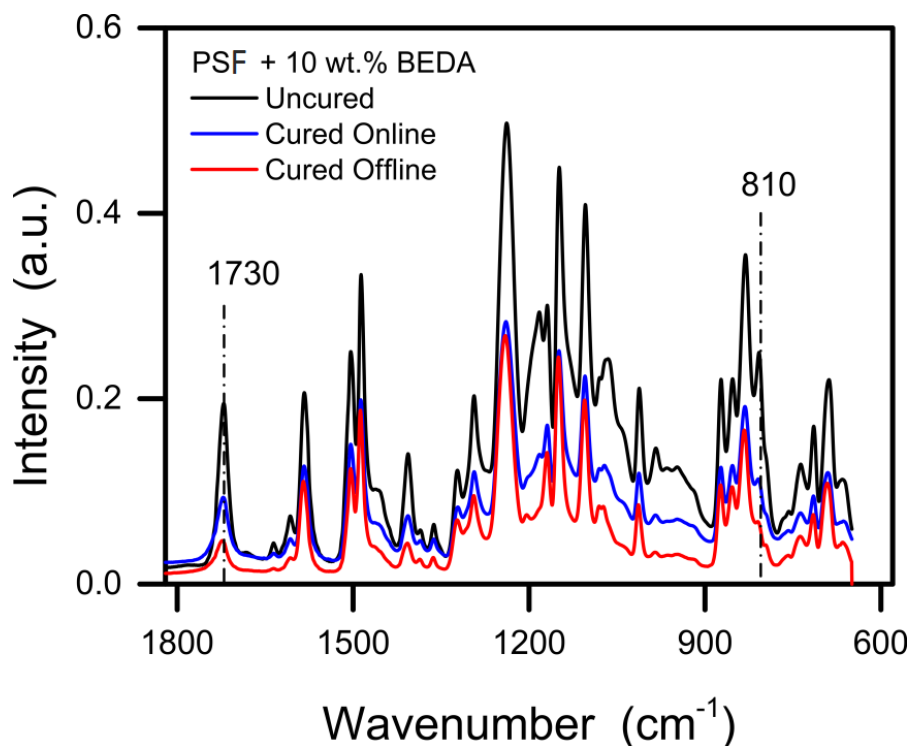
Figure 8.4: ATR–FTIR spectra of PSF electrospun fibers, containing 10 wt. % of BEDA, cured online and offline

8.3.3. Morphological analysis

Representative SEM micrographs are presented in Figure 8.5 together with the respective fiber diameter distributions. Fibers of electrospun membranes obtained from pristine PSF (solution concentration of 18 wt. %) were free of beads (Figure 8.5a) and had an average dimension of 994 nm with standard deviation of 275 nm. Moreover the fibers came up with the surface pores which could be the result of NIPS following exchange of DMF with the moisture present in the air. A similar intra-fiber structure, resulting from NIPS, was reported in a work on fabrication of porous polystyrene fibers [349].

The morphology of the PSF fibers obtained in the presence of BEDA crosslinker are shown in Figures 8.5b–e. All these fibers are free of beads with thanks to careful control of the UV–induced reactive electrospinning. With online irradiation, the fiber diameter from solution of PSF + 5 wt. % BEDA was 392±229 nm, while from PSF + 10 wt. % BEDA it was 409±253 nm. An increase

of diameter with the increase of acrylic content may be associated with the higher viscosity of the solution containing larger amount of monomer. A similar trend was observed with offline irradiated mats where the fiber diameter was 509±179 nm for mats obtained from solutions of PSF + 5 wt. % BEDA and 579±183 nm for those electrospun from PSF + 10 wt. % BEDA. In general, the size of the fibers achieved in the presence of BEDA crosslinker was lower than that obtained using pure PSF. Interestingly offline irradiated fibers' diameter were higher but had narrower diameter distribution than those resulting from irradiating the polymer solutions online. Conducting curing during fiber formation may slightly change the electrospinning conditions possibly due to the added energy flux from the UV light irradiating the samples and also could affect the rate of solvent evaporation. Overall the cross-linked mats, obtained from online and offline curing, were not so different in terms of morphological properties.

The presence of pores on the surface of fibers was found to be influenced by the weight percentage of acrylate and mode of UV curing. For instance, PSF electrospun fibers containing 10 wt. % BEDA, UV cured either online (Figure 8.5c) or offline (Figure 8.5e), were generally found to be deprived of surface pores. On contrary the fibers obtained from solution containing 5 wt. % of BEDA and cured offline retained surface pores (Figure 8.5d) while the online irradiated fibers, having similar formulation, couldn't retain those peculiar pores (Figure 8.5b). This result may be rationalized with the higher extent of DMF removal during the continuous online UV irradiation process thus no solvent was left to exchange with the ambient moisture.
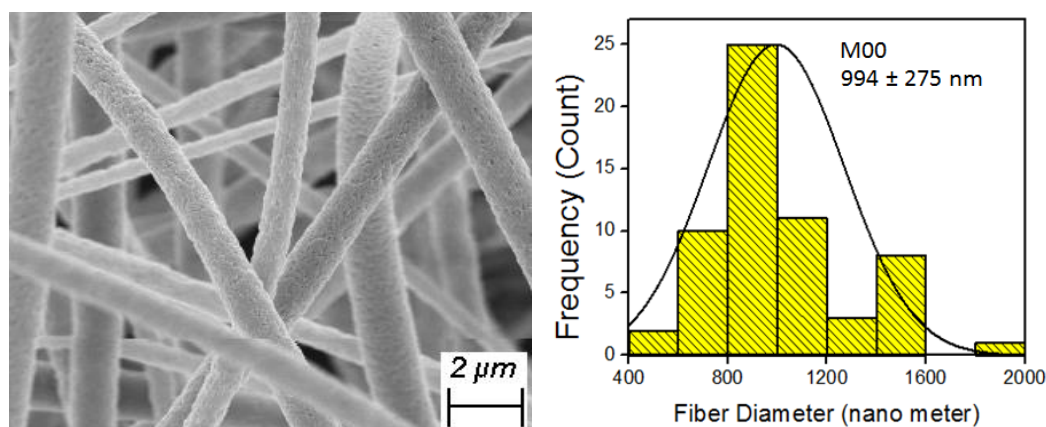
Figure 8.5a: SEM image and diameter distribution of pristine PSF fibers
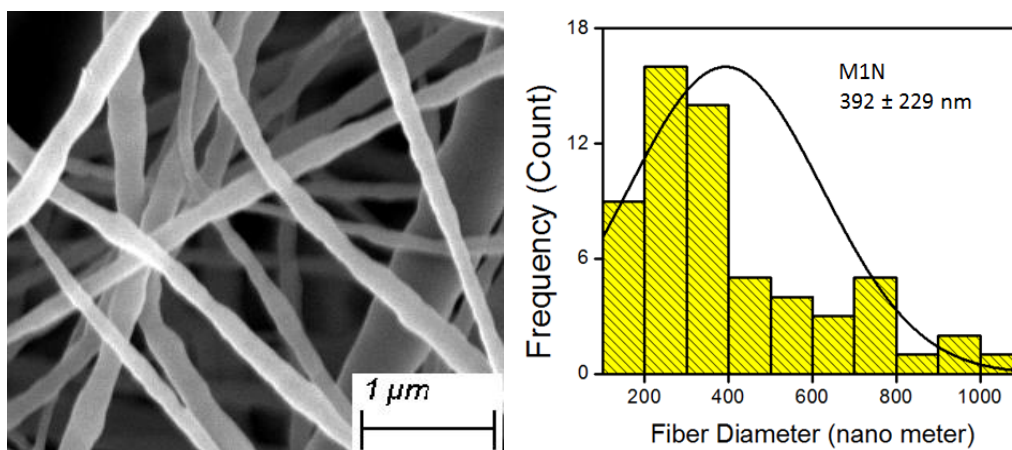
Figure 8.5b: SEM image and diameter distribution of PSF fibers containing 5 wt. % BEDA cured online
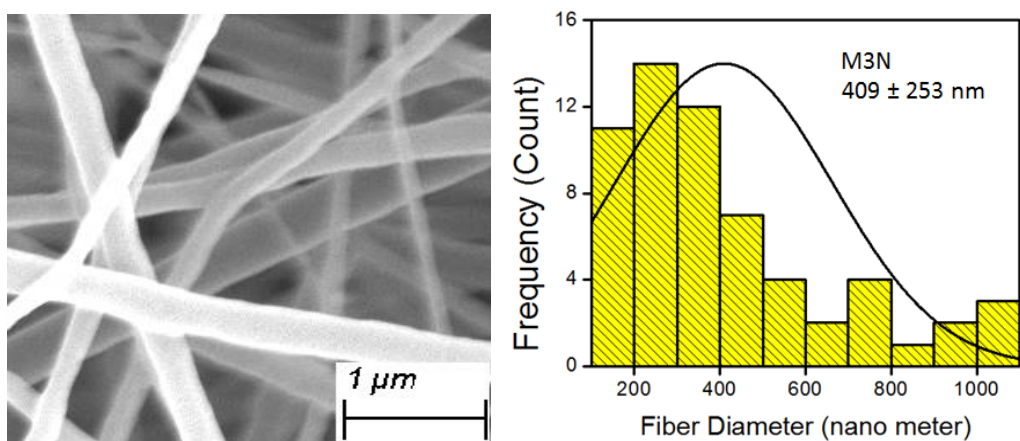
Figure 8.5c: SEM image and diameter distribution of PSF fibers containing 10 wt. % BEDA cured online
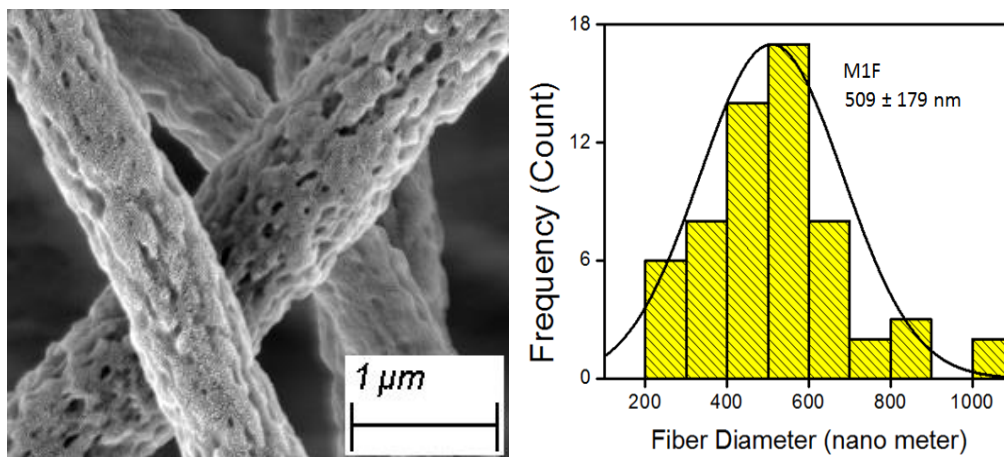
Figure 8.5d: SEM image and diameter distribution of PSF fibers containing
5 wt. % BEDA cured offline
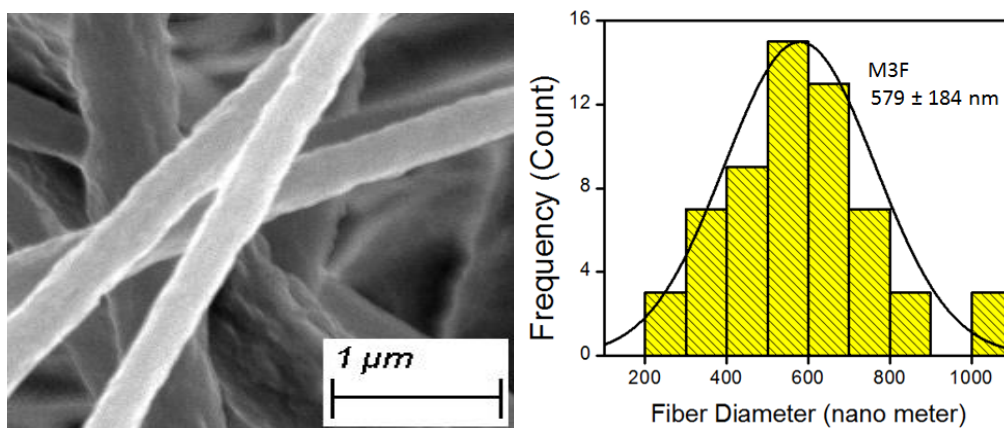
Figure 8.5e: SEM image and diameter distribution of PSF fibers containing
10 wt. % BEDA cured offline

Figure 8.6 shows the estimated macro porosity of the fibrous mats. The offline
irradiated mats had somewhat higher porosity in comparison to the mats obtained

by irradiating fibers online. Moreover the mats obtained from PSF containing 10 wt. % BEDA exhibited highest porosity.
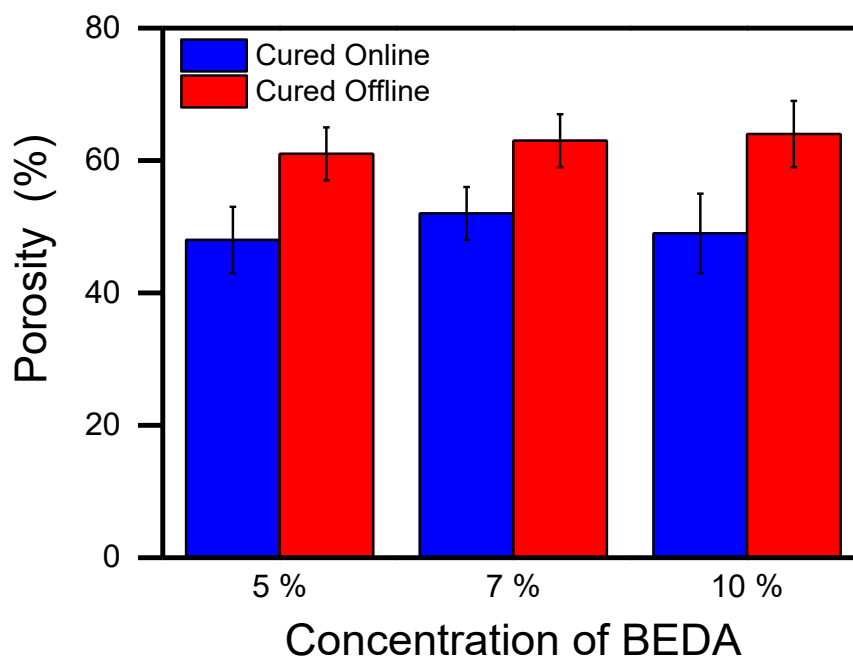
Figure 8.6: Porosity of different electrospun nanofibrous membranes

8.3.4. Thermal characterization of electrospun fibrous membranes

The DSC curves (from first heating) of online and offline UV-cured mats are shown in Figure 8.7 and compared to the pristine PSF electrospun mats. The pristine PSF fibers exhibited Tg centered around 190 $^{\circ}$C, in accordance with the reported Tg value of pristine PSF [103]. Two distinct Tg values are evident from the DSC analysis of fibers obtained from PSF solutions containing 10 wt. % of BEDA crosslinker. The first Tg, at around 90 $^{\circ}$C, is ascribed to BEDA, while the second Tg at 170 $^{\circ}$C may be attributed to the PSF. The incorporation of a low molecular weight resin (BEDA) resulted into drop of Tg of PSF from 190 to 170 $^{\circ}$C. Similar behavior was observed in our previous work where BEDA functionalized PSF membranes were developed through NIPS [103]. The thermal properties of fibers showed no significant difference between online and offline irradiation. This result is in accordance with similar acrylic double bond conversion achieved for the two methodologies.
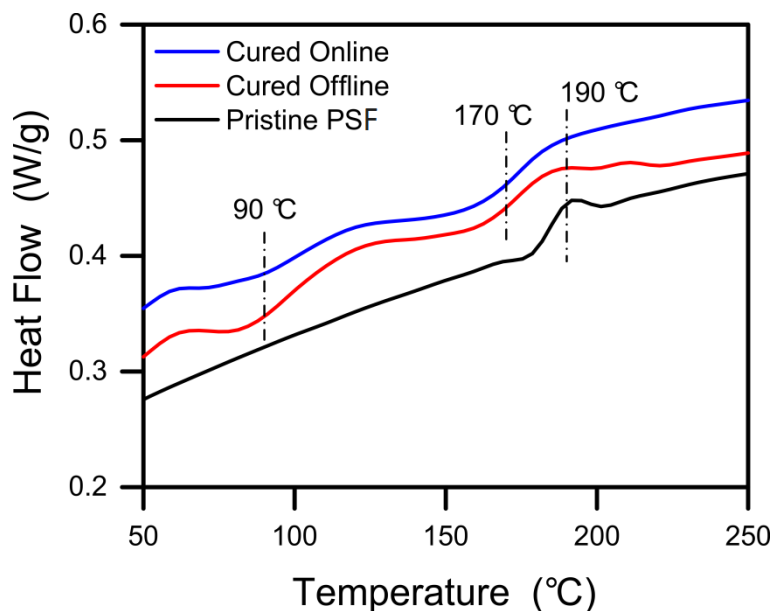
Figure 8.7: DSC curves of pristine PSF mats and of mats obtained in the presence of 10 wt. % BEDA, UV-cured online and offline

TGA analysis was performed in order to assess the thermal stability of electrospun mats. The results are shown in Figures 8.8a and 8.8b. The pristine PSF was found to undergo single step degradation at 530 ^{o}C while two-steps degradation was observed for the fibers obtained in the presence of BEDA. The first degradation step at lower temperature may be attributed to the BEDA network degradation at around 420 ^{o}C, followed by second step degradation of PSF around 510 ^{o}C. Also in this case, the thermal degradation behavior of the online and offline cured samples were similar so only the results of online cured fibers are presented here.
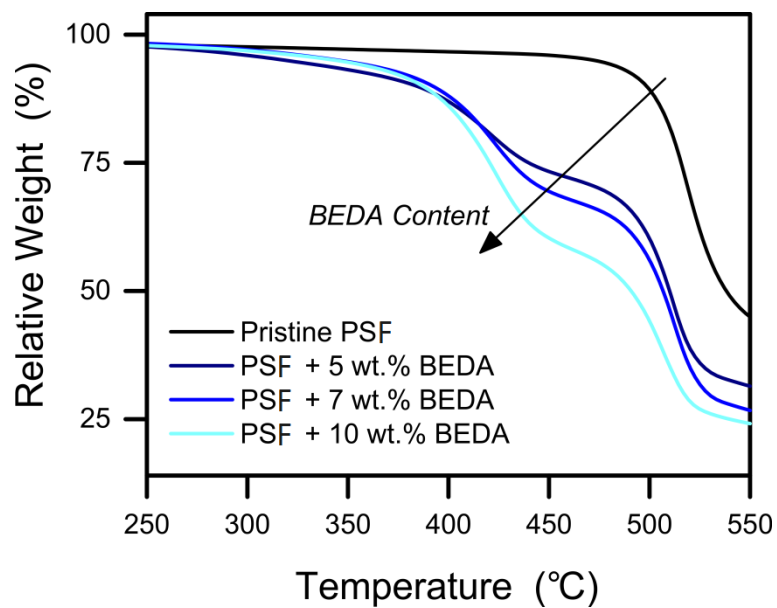
Figure 8.8a: TGA curves of pristine PSF and online cured fibers obtained in the presence of BEDA crosslinker
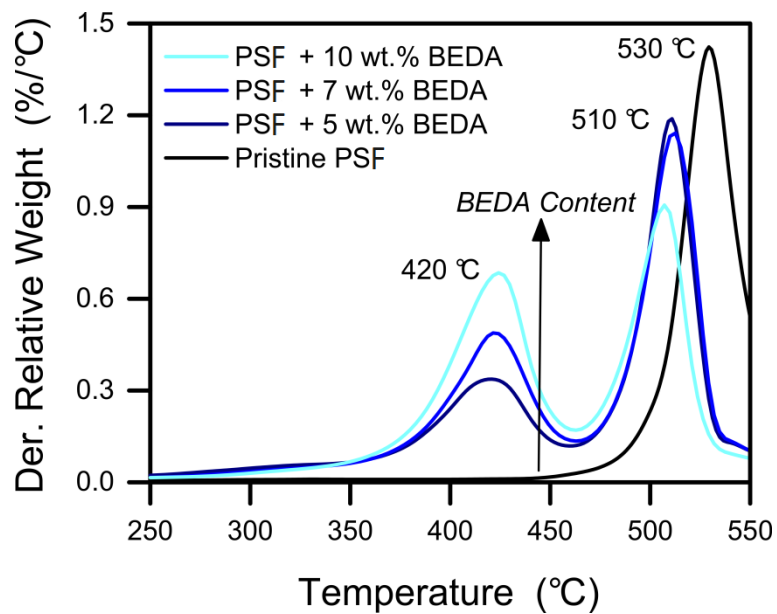
Figure 8.8b: DTGA of pristine PSF and online cured fibers obtained in the presence of BEDA crosslinker

8.3.5. Solvent stability of electrospun membranes

In order to confirm the solvent stability of the UV cured acrylic functionalized PSF electrospun nanofibrous membranes, both reference (pristine PSF) and modified membranes were immersed in different solvents at room temperature. A qualitative analysis was carried out after 120 hrs of immersion and the results are summarized in Table 8.4. Membranes made from pristine PSF solution were dissolved or swollen in all the tested solvents. By increasing the concentration of BEDA, thus the extent of crosslinking in the matrix, electrospun fibers became more chemically robust. The most resistant formulations were based on PSF containing 10 wt. % of BEDA crosslinker, which were found to be stable in THF, Acetone, Ethyl Acetate, DMSO, and Toluene. This finding is quite in accordance with our previous work on solvent stable acrylic functionalized PSF membranes developed through NIPS [103].

Table 8.4: Solvent stability of pristine and modified PSF ENMs'

Solvent	M00	M1N	M1F	M2N	M2F	M3N	M3F
THF	1	1	1	×	×	0	0
Acetone	×	0	0	0	0	0	0
Ethyl acetate	×	0	0	0	0	0	0
DMSO	1	×	×	×	×	0	0
Toluene	1	0	0	0	0	0	0

0–stable 1–dissolved ×–Swelling

8.4. Conclusion

In this work, electrospun nanofibrous membranes (ENMs') were fabricated via a sustainable reactive electrospinning method where on-line UV curing of a PSF based solution containing an acrylate crosslinker was performed. For comparison, the ENMs' were also prepared through offline UV irradiation method, in which UV curing was carried out after the formation of fibrous mats. The sustainability of online irradiation was achieved through optimization of UV curing and electrospinning parameters. The near-complete crosslinking reaction of acrylic resin in the fibers was confirmed through ATR–FTIR analysis. A thorough morphological characterization and thermal analysis of the electrospun membranes were also performed. The SEM micrographs revealed that fiber diameter decreased in the presence of the crosslinking agent BEDA compared to the pure polymer, that higher content of crosslinker produced slightly larger distribution of fiber diameters and finally that offline irradiated fibers had slightly larger diameter but overall similar to that of fibers produced via online irradiation. All the cross-linked membranes were comparable in terms of thermal properties and chemical resistance, regardless of the protocol followed for UV irradiation. Solvent stability induced by the crosslinker present in the electrospun solution was excellent in all cases. These results suggest that the a controlled online UV curing method is an effective and more convenient approach to customize fiber properties during electrospinning compared to post-fabrication strategies. Modified ENMs' may serve the purpose of solvent-stable separation membranes or support layers in gas or liquid separation processes such as ultrafiltration, reverse osmosis, perevaporation, and forward osmosis.

Chapter No. 9

General conclusion

The work reported in this thesis was focused on improving solvent stability of polysulfone (PSF) based membranes. In order to overcome the stated shortcoming of PSF based membranes we thoroughly exploited UV–induced acrylic functionalization of polysulfone in a way that cross-linked acrylic network, inter–penetrating polysulfone matrix, was developed without damaging typical pores morphology of PSF based ultrafiltration membrane. The cross-linked polysulfone membranes were prepared by employing scalable UV curing and phase separation (more precisely a non-solvent induced phase separation – NIPS) processes.

In very first approach we introduced acrylic functionality on the backbone of polysulfone structure by synthesizing a methacrylate polysulfone monomer. The precursor was synthesized by condensation polymerization and subsequent esterification. The macro-monomers of different molecular weights were fully characterized. The porous membranes were developed by dissolving the macro-monomer in DMF and thereafter fabrication of membranes through successive UV-curing and phase separation (UV-NIPS) and vice versa (NIPS-UV). The UV cross-linked membranes obtained through either of these sequences were insoluble in DMSO, Acetone and boiling water and showed a gel content value of 100%. The viscoelastic properties of the membranes evaluated through DMTA revealed that coss-linked membranes, following NIPS–UV, had Tg around 185 ^{o}C while those following UV–NIPS had about 195 ^{o}C. These values were quite in accordance with degree of crosslinking obtained via FTIR analysis. Moreover the UV–NIPS membranes exhibited comparatively better homogeneity i.e. uniform

distribution of pores. Regardless of sequence of processes, all the developed membranes had flux in the range of tight ultrafiltration. This could be attributed to low surface porosity as both surface and bulk pores determine the efficiency of filtration in case of ultrafiltration process.

In next approach we incorporated acrylic functionality as a separate addition of di-acrylate resin into PSF solution in DMF. For this purpose two structurally different di-acrylates i) Bisphenol A ethoxylate di-acrylate (BEDA) and ii) Poly (ethylene glycol) di-acrylate (PEGDA) were employed and three different concentrations of both acrylate systems were worked on. We performed a systematic investigation on the effect of the presence of acrylate resin on PSF-based membranes with the objective to obtain solvent stable cross–linked membranes without affecting their flux properties. The membranes were prepared following the method established in the first approach i.e. UV curing followed by NIPS process. All the related parameters such as wet thickness of membranes, time and intensity of UV irradiation and a controlled NIPS process were comprehensively studied, optimized and correlated. The acrylic double bond conversion of pure acrylic monomer was calculated via FTIR analysis while for cross-linked membranes containing acrylic resin we carried out ATR–FTIR analysis. The double bond conversion in modified membranes was quite in accordance with that of pristine acrylic monomers. The viscoelastic behavior of membranes was studied through dynamic mechanical thermal analysis (DMTA) and cross-linked membranes showed an evident biphasic nature that is ascribed to good interpenetration of the crosslinked acrylic network and the PSF polymeric chains. The morphological analysis was performed, through FESEM, on the surface and cross-section of pristine PSF membranes and the cross-linked PSF membranes containing either BEDA or PEGDA. The membranes modified with 10 wt. % of either of acrylic resins retained both surface and bulk porosity. While going higher in concentration the pores got closed by acrylic network. The flux value obtained for each membrane confirmed the morphological findings. For instance 30 wt. % of each acrylic resin almost closed all the pores and flux obtained was also zero. While 10 wt. % of both acrylic resins had maximum flux. The 10 % BEDA functionalized PSF was found to be best formulation in terms of both solvent stability and optimum flux (239 L m^{-2} h^{-1} bar^{-1}). As per best of our knowledge this is the highest value of flux obtained with a solvent stable membrane. Besides flux properties the rejection of 27 nm polystyrene particles was also evaluated. And almost all the developed membranes exhibited more than 90 % rejection of these particles.

The solvent stability of membranes was evaluated by immersing the membranes cut-outs in a number of solvents at room temperature for 120 hrs. Almost all the modified membranes exhibited excellent stability in DMF, Acetone, DMSO, Toluene and Ethyl Acetate. The BEDA functionalized membranes were a little better than PEGDA based membranes.

After the successful UV–induced acrylic functionalization of PSF based membranes we extended the functionalization with the aim to combine the size exclusion rejection mechanism of ultrafiltration membrane with the adsorption based contaminant removal ability of polydopamine (PDA). The 10 % BEDA functionalized PSF based membranes were coated with PDA via either a two-steps method, where the UV cross-linked PSF membrane were subjected to PDA coating just after phase separation; or a novel one-step method, where UV cross-linked PSF membranes were subjected to phase separation in a water solution containing dopamine so that phase separation and PDA functionalization occurred at the same time.

The morphology of PDA functionalized membranes did not come up with any visible difference based on methodology adopted i.e. one-step or two-steps coating. Nevertheless pure water flux was lower in case of one-step coated membranes. Data suggested that the presence of PDA during NIPS did not introduce a significant change in the precipitation pathway of the polymer but that the coating of PDA achieved in one-step method may be sufficiently thicker to reduce the size of the small pores on the surface of cross-linked membrane. Positively charged Methylene blue (MB) dye was employed as a target contaminant and dye removal was investigated both in batch and under filtration. The adsorption capacity, studied at pH 10, revealed an increase in MB removal with the increase of PDA coating time. Both the capacity and the kinetics of adsorption were higher for the membranes obtained via one-step coating process thus implying a trade-off between water permeability and contaminant adsorption for the two different fabrication methods. The results suggested that fabrication of these selective and reactive membranes may be designed depending on the application and on the desired performance. When contaminant removal is the concern, and not the productivity, fabrication does not need to comprise a cumbersome sequence of two synthesis steps but may be conducted via traditional NIPS, simply by adding dopamine and adjusting the chemistry of the non-solvent solution.

The PDA coated membranes were completely regenerated as MB got released under acidic conditions (pH=3) thereafter membranes were reused without loss of performance as they were able to re-adsorb the same amount of dye in several adsorption cycles following dye release under acidic conditions. The membranes adsorption capacity was also investigated under continuous filtration experiments. This study suggested that PDA functionalized membranes could behave as suitable ultrafiltration membranes as well as successfully filter the solutions containing positively charged contaminants.

Lastly the best formulation for solvent stable phase separation membranes i.e. BEDA functionalized PSF, was also used to produce solvent stable electropsun nanofibrous membranes (ENMs'). The ENMs' were prepared via a sustainable reactive electrospinning method where on-line UV curing of a PSF solution containing an acrylate crosslinker was performed. For the sake of comparison, the ENMs' were also prepared through offline UV irradiation method in which curing was carried out just after formation of fibrous mats. The sustainability of online irradiation was achieved through optimization of UV curing and electrospinning parameters. The near-complete crosslinking reaction of acrylic resin in the fibers was confirmed through ATR–FTIR analysis. A thorough morphological characterization and thermal analysis of electrospun membranes were performed. The SEM micrographs revealed that fiber diameter decreased in the presence of the crosslinking agent compared to the pure polymer, that higher content of crosslinker produced slightly larger distribution of fiber diameters and finally that offline irradiated fibers had slightly larger diameter but overall similar to fibers produced through online irradiation. All the cross-linked membranes were comparable in terms of thermal properties regardless of the protocol followed for UV irradiation. Solvent stability induced by the presence of the crosslinker in the electrospun solution was excellent in all the cases. These results suggest that the online UV curing method is an effective and more convenient approach to customize fiber properties during electrospinning compared to post-fabrication strategies. Modified ENMs' may serve the purpose of solvent-stable separation membranes or support layers in gas or liquid separation processes such as ultrafiltration, reverse osmosis, perevaporation and forward osmosis.

References

[1]   Menachem Elimelech. M. The global challenge for adequate and safe water. J. Water Supply Res. Technol. (2006) 55, 3–10.

[2]   Mark A. Shannon, Paul W. Bohn, Menachem Elimelech, John G. Georgiadis, Benito J. Mariñas and Anne M. Mayes. Science and technology for water purification in the coming decades. Nature (2008) 452, 301–310

[3]   Menachem Elimelech and William A. Phillip. The Future of Seawater Desalination: Energy, Technology, and the Environment, Science (2011) 333, 712–717

[4]   UNEP. Vital Water Graphics: An Overview of the State of the World's Fresh and Marine Waters, 2nd ed.; UNEP: Nairobi, Kenya, (2008)

[5]   UNESCO. World Water Assessment Program: Facts and Figures. Available at: http://www.unesco.org/water/wwap/facts_figures/. (2009)

[6]   World Health Organization. Water, Sanitation and Hygiene Links to Health (2004): Facts and Figures. Available at: http://www.who.int/water_sanitation_health/publications/facts2004/en

[7]   The United Nations World Water Development Report 3 (2009): Water in a Changing World; UNESCO Publishing: Paris

[8]   Mesfin M. Mekonnen and Arjen Y. Hoekstra. Four billion people facing severe water scarcity in Science Advances (2016) Vol. 2, no. 2, e1500323

[9]   Global   risk   report   by   world   economic   forum   (2016) http://www3.weforum.org/docs/GRR/WEF_GRR16.pdf

[10]   Rene P. Schwarzenbach, Beate I. Escher, Kathrin Fenner, Thomas B. Hofstetter, C. Annette Johnson, Urs von Gunten, Bernhard Wehrli. The challenge of micropollutants in aquatic systems. Science (2006) 313, 5790, 1072-1077

[11]   S. Alami-Younsii, A. Larbot, M. Persin, J. Sarrazin, L. Cot. Rejection of mineral salts on a gamma alumina nanofiltration membrane: application to environmental process, J. Membr. Sci. (1995)102,123–129.

[12]   N. Saffaj, H. Loukili, A. Alami-Younssi, A. Albizane, M. Bouhria, M. Persin, A. Larbot. Filtration of solution containing heavy metals and dyes by means of ultrafiltration membranes deposited on support made of Morrocan clay, Desalination (2004) 168, 301–306

[13]   Runnan Zhang, Yanan Liu, Mingrui He, Yanlei Su, Xueting Zhao, Menachem Elimelechc and Zhongyi Jiang. Antifouling membranes for sustainable water purification: strategies and mechanisms Chem. Soc. Rev. (2016) 45, 5888–5924

[14]   Vidic R. D, Brantley S. L, Vandenbossche J. M, Yoxtheimer D. and Abad, J. D. Impact of shale gas development on regional water quality. Science (2013) 340, 1235009.

[15]   Devin L. Shaffer, D. L. Laura H. Arias Chavez, Moshe Ben-Sasson, Santiago Romero-Vargas Castrillón, Ngai Yin Yip, and Menachem Elimelech. Desalination and reuse of high salinity shale gas produced water: drivers, technologies, and future directions. Environ. Sci. Technol. (2013) 47, 9569–9583

[16]   Gregory, K. B., Vidic, R. D. and Dzombak, D. A. Water management challenges associated with the production of shale gas by hydraulic fracturing. Elements (2011) 7, 181–186

[17]   Van Loosdrecht M. C. M. and Brdjanovic D. Anticipating the next century of wastewater treatment. Science (2014) 344, 1452–1453

[18]   Stanley B. Grant, Jean-Daniel Saphores, David L. Feldman, Andrew J. Hamilton, Tim D. Fletcher, Perran L. M. Cook, Michael Stewardson, Brett F. Sanders, LisaA. Levin, Richard F. Ambrose, Ana Deletic, Rebekah Brown, Sunny C. Jiang, Diego Rosso, William J. Cooper, Ivan Marusic.

Taking the "waste" out of "wastewater" for human water security and ecosystem sustainability. Science (2012) 337, 681–686

[19]   Sales, C. M. and Lee, P. K. Resource recovery from wastewater: application of meta-omics to phosphorus and carbon management. Curr. Opin. Biotechnol. (2015) 33, 260–267

[20]   Xu Wang, Perry L. McCarty, Junxin Liua, Nan-Qi Rend, Duu-Jong Leee, Han-Qing Yuf, Yi Qiang and Jiuhui Qu. Probabilistic evaluation of integrating resource recovery into wastewater treatment to improve environmental sustainability. Proc. Natl Acad. Sci. USA (2015) 112, 1630–1635

[21]   Bond, R. and Veerapaneni, S. Zero liquid discharge for inland desalination Awwa Research Foundation. (2007)
http://www.waterrf.org/PublicReportLibrary/91190.pdf

[22]   Mickley, M. Survey of high-recovery and zero liquid discharge technologies for water utilities (WateReuse Foundation) (2008)
https://www.waterboards.ca.gov/water_issues/programs/grants_loans/water_recycling/research/02_006a_01.pdf

[23]   Desalination by Reverse Osmosis; (book by Ulrich Merten) MIT Press: Cambridge, 1966.

[24]   Mohammad Soltanieh and William N. Gill. Review of Reverse Osmosis membranes and transport models In Chem. Eng. Commun, (1981) 12, 279–363.

[25]   Paul, D. R. and Morel, G. In Kirk-Othmer Encyclopedia of Chemical Technology, 3rd ed.; John Wiley: New York, (1981) pp 92–131.

[26]   Punzi, V. L. and Muldowney, G. P. An Overview of Proposed Solute Rejection Mechanisms in Reverse Osmosis Rev Chem. Eng. (1987)4,1–40.

[27]   Koros, W. J., Fleming, G. K., Jordan, S. M., Kim, T. H., Hoehn, H. H., Polymeric membrane materials for solution-diffusion based permeation separations Prog. Polym. Sci. (1988) 13, 339–401.

[28]   Parekh, B. S. Reverse Osmosis Technology: Applications for High-Purity-Water Production; (1988) New York, Marcel-Dekker

[29] Petersen, R. E.; Cadotte, J. E. Handbook of Industrial Membrane Technology; Porter, M. C., Ed.; Noyes Publications: Park Ridge, New Jersey, (1990) 307–348.

[30] Ho, W. S. W.; Sirkar, K. K. Membrane Handbook; Van Nostrand Reinhold: New York (1992)

[31] Petersen, R. J. Composite reverse osmosis and nanofiltration membranes J. Memb. Sci. (1993) 83, 81–150.

[32] Bhattacharyya, D.; Mangum, W. C.; Williams, M. E. Kirk-Othmer Encyclopedia of Chemical Technology, 4th ed.; John Wiley: New York, (1997) 303–333.

[33] Glater, J. The early history of reverse osmosis membrane development Desalination (1998) 117, 297–309.

[34] Baker, R. W. Membrane Technology and Applications, 2nd ed.; John Wiley: New York, (2004)

[35] Greenlee, L. F.; Lawler, D. F.; Freeman, B. D.; Marrot, B.; Moulin, P. Reverse osmosis desalination: Water sources, technology, and today's challenges Water Res., (2009) 43, 2317–2348.

[36] Drioli, E.; Giorno, L. Membrane Operations: Innovative Separations and Transformations; Wiley-VCH: Weinheim (2009)

[37] R.W. Bowen and F. Jenner. Theoretical description of membrane filtration of colloids and fine particles; an assessment and review, Advances in Colloid and Interface Sciences (1995) 56, 141–200

[38] J.G. Jacangelo, S.Chellam, R.R. Trussell, The membrane treatment, ASCE Civil Engineering data base (1998) 68 (9), 42–45

[39] R.R. Sharma, R. Agrawal, S. Chellam, Temperature effects on sieving characteristics of thin-film composite nanofiltration membranes: pore size distributions and transport parameters, J. Membr. Sci. (2003) 223, 69–87

[40] M.R. Wiesner, S. Chellam, The promise of membrane technology, Environmental Science and Technology (1999) 33 (17), 360A–366A

[41]   Semiat, R. Energy issues in desalination processes. Environ. Sci. Technol.
        (2008) 42, 8193–8201

[42]   Jay R. Werber, Chinedum O. Osuji and Menachem Elimelech. Materials
        for Next-Generation Desalination and Water Purification Membranes,
        Nature Reviews (Materials) (2016) 1 – 15

[43]   Geise, G. M., Park, H. B., Sagle, A. C., Freeman, B. D. & McGrath, J. E.
        Water permeability and water/salt selectivity tradeoff in polymers for
        desalination J. Membr. Sci. (2011) 369, 130–138

[44]   Baker, R. W.; Cussler, E. L.; Eykamp, W.; Koros, W. J.; Riley, R. L.;
        Strathmann, H. Membrane Separation Systems: Recent Developments and
        Future Directions; Noyes Data Corp.: Park Ridge, (1991)

[45]   Mulder, M. Basic Principles of Membrane Technology, 2ed ed., Kluwer
        Academic, (1996) Netherlands

[46]   Lonsdale, H. The growth of membrane technology. J. Memb. Sci, (1982)
        10, 81–181

[47]   Baker, R. W. Membrane Technology and Applications (John Wiley &
        Sons) (2012)

[48]   Dongming He, Heru Susanto, Mathias Ulbricht. Photo-irradiation for
        preparation, modification and stimulation of polymeric membranes,
        Progress in Polymer Science (2009) 34, 62–98

[49]   Belfort, G., Rotem, Y.; Katzenelson, E. Virus concentration using hollow
        fiber membranes. Water Res. (1975) 9 (1), 79-85.

[50]   Yang, S. Y.; Park, J.; Yoon, J.; Ree, M.; Jang, S. K.; Kim, J. K. Virus
        filtration membranes prepared from nanoporous block copolymers with
        good dimensional stability under high pressures and excellent solvent
        resistance. Advanced Functional Materials (2008) 18 (9), 1371-1377.

[51]   Urase, T.; Yamamoto, K.; Ohgaki, S. Effect of pore structure of
        membranes and module configuration on virus retention. J. Membr. Sci.
        (1996) 115 (1), 21-29.

[52] Wickramasinghe, S. R.; Stump, E. D.; Grzenia, D. L.; Husson, S. M.; Pellegrino, J. Understanding virus filtration membrane performance. J. Membr. Sci. (2010) 365 (1-2), 160-169.

[53] Yang, S. Y.; Ryu, I.; Kim, H. Y.; Kim, J. K.; Jang, S. K.; Russell, T. P. Nanoporous membranes with ultrahigh selectivity and flux for the filtration of viruses. Advanced Materials (2006) 18 (6), 709-712.

[54] Fane, A. G.; Fell, C. J. D.; Waters, A. G. Ultrafiltration of protein solutions through partially permeable membranes−the effect of adsorption and solution environment. J. Membr. Sci. (1983) 16 (0), 211-224.

[55] Görisch, H. Drop dialysis: Time course of salt and protein exchange. Analytical Biochemistry (1988) 173 (2), 393-398.

[56] Zeman, L. J.; Zydney, A. L. Microfiltration and ultrafiltration: Principles and applications; Marcel Dekker CRC Press (1996)

[57] Elsaied, H. E.; Sato, M.; Naganuma, T. Viable cytophaga-like bacterium in the 0.2 μm-filtrate seawater. Systematic and Applied Microbiology (2001) 24 (4), 618-622.

[58] Hagen, K. Removal of particles, bacteria and parasites with ultrafiltration for drinking water treatment. Desalination (1998) 119 (1‑3), 85-91.

[59] Hahn, M. W. Broad diversity of viable bacteria in 'sterile' (0.2 μm) filtered water. Research in Microbiology (2004) 155 (8), 688-691.

[60] Jackson, E. A. Hillmyer, M. A. Nanoporous membranes derived from block copolymers: From drug delivery to water filtration. ACS Nano (2010) 4 (7), 3548-3553.

[61] Lee, S.-A. Choo, K.-H. Lee, C.-H. Lee, H.-I. Hyeon, T. Choi, W; Kwon, H.-H. Use of ultrafiltration membranes for the separation of tio2 photocatalysts in drinking water treatment. Industrial & Engineering Chemistry Research (2001) 40 (7), 1712-1719.

[62] Mavrov, V. Chmiel, H. Kluth, J. Meier, J. Heinrich, F. Ames, P. Backes, K. Usner, P. Comparative study of different mf and uf membranes for drinking water production. Desalination (1998) 117 (1‑3), 189-196.

[63] Rotzetter, A. C. C.; Kellenberger, C. R.; Schumacher, C. M.; Mora, C.; Grass, R. N.; Loepfe, M.; Luechinger, N. A.; Stark, W. J. Combining phosphate and bacteria removal on chemically active filter membranes allows prolonged storage of drinking water. Advanced Materials (2013) 25 (42), 6057-6063.

[64] Shirey, J. J.; Bissonnette, G. K. Detection and identification of groundwater bacteria capable of escaping entrapment on 0.45-micron-pore-size membrane filters. Applied and Environmental Microbiology (1991) 57 (8), 2251-2254

[65] Van Der Bruggen, B.; Vandecasteele, C.; Van Gestel, T.; Doyen, W.; Leysen, R. A review of pressure-driven membrane processes in wastewater treatment and drinking water production. Environmental Progress (2003) 22 (1), 46-56.

[66] Wang, Y.; Hammes, F.; Boon, N.; Egli, T. Quantification of the filterability of fresh water bacteria through 0.45, 0.22, and 0.1 μm pore size filters and shape dependent enrichment of filterable bacterial communities. Environmental Science & Technology (2007) 41 (20), 7080-7086.

[67] Jiao, K.; Graham, C. L.; Wolff, J.; Iyer, R. G.; Kohli, P. Modulating molecular and nanoparticle transport in flexible polydimethylsiloxane membranes. J. Membr. Sci. (2012) 401–402 (0), 25-32.

[68] P. M. Bungay, H. K. Lonsdale, and M. N. de Pinho, "Transport Principles - Porous Membranes," in Synthetic Membranes: Science, Engineering and Applications, Eds. Dordrecht: Springer Netherlands, (1986) pp. 109–153.

[69] Renkin EM. Filtration, diffusion and molecular sieving through porous cellulose membranes. J. Gen. Physiol. (1954) 20; 38(2):225-243.

[70] Jochen A. Kerres, Development of ionomer membranes for fuel cells. J. Membr. Sci. (2001) 185 (1), 3-27.

[71] Kreuer, K. D. On the development of proton conducting polymer membranes for hydrogen and methanol fuel cells. J. Membr. Sci. (2001) 185 (1), 29-39.

[72]   Nguyen, T. V.; White, R. E. A water and heat management model for proton exchange membrane fuel cells. Journal of the Electrochemical Society (1993) 140 (8), 2178-2186.

[73]   Gerba, C. P. Applied and theoretical aspects of virus adsorption to surfaces. In Advances in applied microbiology, Allen, I. L., Ed.; Academic Press, (1984) Vol. Volume 30, pp 133-168

[74]   Wegmann, M.; Michen, B.; Graule, T. Nanostructured surface modification of microporous ceramics for efficient virus filtration. Journal of the European Ceramic Society (2008) 28 (8), 1603-1612.

[75]   Farrah, S. R.; Preston, D. R.; Toranzos, G. A.; Girard, M.; Erdos, G. A.; Vasuhdivan, V. Use of modified diatomaceous earth for removal and recovery of viruses in water. Applied and Environmental Microbiology (1991) 57 (9), 2502-2506.

[76]   Wegmann, M.; Michen, B.; Luxbacher, T.; Fritsch, J.; Graule, T. Modification of ceramic microfilters with colloidal zirconia to promote the adsorption of viruses from water. Water Res. (2008) 42, 1726-1734.

[77]   Farrah, S. R.; Shah, D. O.; Ingram, L. O. Effects of chaotropic and antichaotropic agents on elution of poliovirus adsorbed on membrane filters. Proceedings of the National Academy of Sciences (1981) 78 (2), 1229-1232.

[78]   Sobsey, M. D.; Jones, B. L. Concentration of poliovirus from tap water using positively charged microporous filters. Applied and Environmental Microbiology (1979) 37 (3), 588-595.

[79]   Logan, K. B.; Rees, G. E.; Seeley, N. D.; Primrose, S. B. Rapid concentration of bacteriophages from large volumes of freshwater: Evaluation of positively charged, microporous filters. Journal of Virological Methods (1980) 1 (2), 87-97.

[80]   Klein, E. Affinity membranes: A 10-year review. Journal of Membrane Science (2000) 179 (1‑2), 1-27.

[81]   Roper, D. K.; Lightfoot, E. N. Separation of biomolecules using adsorptive membranes. Journal of Chromatography A (1995) 702 (1‑2), 3-26.

[82]   Ma, Z.; Kotaki, M.; Ramakrishna, S. Electrospun cellulose nanofiber as affinity membrane. J. Membr. Sci. (2005) 265, 115-123.

[83]   Ma, Z.; Kotaki, M.; Ramakrishna, S. Surface modified nonwoven polysulphone (psu) fiber mesh by electrospinning: A novel affinity membrane. J. Membr. Sci. (2006) 272 (1‑2), 179-187.

[84]   Chang, L. T.; Farrah, S. R.; Bitton, G. Positively charged filters for virus recovery from wastewater treatment plant effluents. Applied and Environmental Microbiology (1981) 42 (5), 921-924.

[85]   Ren, J.; Wang, R. Preparation of polymeric membranes. In Membrane and desalination technologies, Wang, L.; Chen, J.; Hung, Y.-T.; Shammas, N., Eds.; Humana Press, (2011) 13, 47-100.

[86]   Peinemann, K.-V.; Pereira Nunes, S. Polymer membranen. In Membranen; Wiley-VCH Verlag GmbH & Co. KGaA, (2006), 1-21

[87]   Boom, R. M.; Wienk, I. M.; van den Boomgaard, T.; Smolders, C. A. Microstructures in phase inversion membranes. Part 2. The role of a polymeric additive. J. Membr. Sci. (1992) 73 (2‑3), 277-292.

[88]   Chae Park, H.; Po Kim, Y.; Yong Kim, H.; Soo Kang, Y. Membrane formation by water vapor induced phase inversion. Journal of Membrane Science (1999) 156 (2), 169-178

[89]   Kesting, R. E. The four tiers of structure in integrally skinned phase inversion membranes and their relevance to the various separation regimes. Journal of App. Poly. Sci. (1990) 41 (11-12), 2739-2752

[90]   Kimmerle, K.; Strathmann, H. Analysis of the structure-determining process of phase inversion membranes. Desalination (1990) 79, 283-302

[91]   Pinnau, I.; Koros, W. J. Structures and gas separation properties of asymmetric polysulfone membranes made by dry, wet, and dry/wet phase inversion. Journal of App. Poly. Sci. (1991) 43 (8), 1491-1502.

[92]   Strathmann, H.; Kock, K. The formation mechanism of phase inversion membranes. Desalination (1977) 21 (3), 241-255.

[93]   Tsay, C. S.; McHugh, A. J. Mass transfer modeling of asymmetric membrane formation by phase inversion. Journal of Polymer Science Part B: Polymer Physics (1990) 28 (8), 1327-1365.

[94]   Tsay, C. S.; McHugh, A. J. Mass transfer dynamics of the evaporation step inmembrane formation by phase inversion. J. Membr. Sci. (1991) 64 (1‑2), 81-92.

[95]   Wienk, I. M.; Boom, R. M.; Beerlage, M. A. M.; Bulte, A. M. W.; Smolders, C. A.; Strathmann, H. Recent advances in the formation of phase inversion membranes made from amorphous or semi-crystalline polymers. J. Membr. Sci. (1996) 113 (2), 361-371.

[96]   Young, T.-H.; Chen, L.-W. Pore formation mechanism of membranes from phase inversion process. Desalination (1995) 103 (3), 233-247.

[97]   Zeman L, Fraser T. Formation of air-cast cellulose acetate membranes. Part I. Study of macrovoid formation. J. Membr. Sci. (1993) 84, 93–106

[98]   Pekny MR, Zartman J, Krantz WB, Greenberg AR, Todd P. Flow visualization during macrovoid pore formation in dry-cast cellulose acetate membranes. J. Membr. Sci. (2003) 211, 71–90

[99]   Matsuyama H, Teramoto M, Nakatani R, Maki T. Membrane formation via phase separation induced by penetration on nonsolvent from vapor phase. I. Phase diagram and mass transfer process. J. Appl. Polym. Sci. (1999), 74, 159–170

[100]   Yip Y, McHugh AJ. Modeling and simulation of nonsolvent vaporinduced phase separation. J. Membr. Sci. (2006) 271, 163–176

[101]   Khare VP, Greenberg AR, Krantz WB. Vapor-induced phase separation—effect of the humid air exposure step on membrane morphology.PartI. Insight from mathematical modeling. J. Membr. Sci. (2005), 258, 140–156

[102]   Sangermano, M. Farrukh, M. Mian, Tiraferri, A. Dizman, C and Yagci, Y. Synthesis, preparation and characterization of UV-cured methacrylated polysulfone-based membranes. Mat. Tod. Comm. (2015) 5, 64-69

[103] Farrukh, Mehmood Mian, Bosch, Paula, Giagnorio, Mattia, Tiraferri, Alberto and Sangermano, Marco Solvent-stable UV-cured acrylic polysulfone membranes. Poly. Inter. (2017) 66, 64-69

[104] Boom, R. M.; van den Boomgaard, T.; Smolders, C. a. Mass transfer and thermodynamics during immersion precipitation for a two-polymer system: Evaluation with the system PES–pvp–nmp–water. J. Membr. Sci. (1994) 90 (3), 231-249.

[105] Lin, D.-J.; Chang, H.-H.; Chen, T.-C.; Lee, Y.-C.; Cheng, L.-P. Formation of porous poly(vinylidene fluoride) membranes with symmetric or asymmetric morphology by immersion precipitation in the water/tep/pvdf system. European Polymer Journal (2006) 42 (7), 1581-1594.

[106] Radovanovic, P.; Thiel, S. W.; Hwang, S.-T. Formation of asymmetric polysulfone membranes by immersion precipitation. Part i. Modelling mass transport during gelation. J. Membr. Sci. (1992) 65 (3), 213-229

[107] Radovanovic, P.; Thiel, S. W.; Hwang, S.-T. Formation of asymmetric polysulfone membranes by immersion precipitation. Part ii. The effects of casting solution and gelation bath compositions on membrane structure and skin formation. J. Membr. Sci. (1992) 65 (3), 231-246

[108] Reuvers, A. J.; Smolders, C. A. Formation of membranes by means of immersion precipitation : Part ii. The mechanism of formation of membranes prepared from the system cellulose acetate-acetone-water. J. Membr. Sci. (1987) 34 (1), 67-86

[109] Reuvers, A. J.; van den Berg, J. W. A.; Smolders, C. A. Formation of membranes by means of immersion precipitation : Part i. A model to describe mass transfer during immersion precipitation. J. Membr. Sci. (1987) 34 (1), 45-65

[110] Wijmans, J. G.; Baaij, J. P. B.; Smolders, C. A. The mechanism of formation of microporous or skinned membranes produced by immersion precipitation. J. Membr. Sci. (1983) 14 (3), 263-274.

[111] Yong, S. K.; Hyo, J. K.; Un, Y. K. Asymmetric membrane formation via immersion precipitation method. I. Kinetic effect. J. Membr. Sci. (1991) 60 (2‑3), 219-232

[112] Pinnau, I. Recent advances in the formation of ultrathin polymeric membranes for gas separations. Polym. Adv. Technol. (1994) 5, 733–744

[113] Van de Witte P, Dijkstra PJ, van den Berg JWA, Feijen J. Phase separation processes in polymer solutions in relation to membrane formation. J. Membr. Sci. (1996) 117, 1–31

[114] Stropnik C, Kaiser V. Polymeric membranes preparation by wet phase separation: mechanisms and elementary processes. Desalination (2002) 145, 1–10

[115] Ziabicki, A. Fundamentals of Fiber Formation; John Wiley: New York, (1976)

[116] Craig, J. P.; Knudsen, J. P.; Holland, V. F. Characterization of Acrylic Fiber Structure Text. Res. J. (1962) 32, 435–448

[117] Knudsen, J. P. The Influence of Coagulation Variables on the Structure and Physical Properties of an Acrylic Fiber. Text. Res. J. (1963) 33,13–20

[118] Paul, D. R. Diffusion during the coagulation step of wet-spinning J. Appl. Polym. Sci. (1968) 12, 383–402

[119] Koros, W. J.; Pinnau, I. In Polymeric Gas Separation Membranes; Paul, D. R.; Yampolskii, Y., Eds.; CRC Press: Boca Raton, (1994)

[120] Broens, L.; Koenhen, D. M.; Smolders, C. A. On the mechanism of formation of asymmetric ultra- and hyper-filtration membranes. Desalination (1977) 22, 205–219

[121] Koenhen, D. M.; Mulder, M. H. V.; Smolders, C. A. Phase separation phenomena during the formation of asymmetric membranes. J. Appl. Polym. Sci. (1977) 21, 199–215

[122] Smolders, C. A. In Ultrafiltration and Applications; Cooper, I., Ed.; Plenum Press: New York, (1980)

[123] Burghardt, W. R.; Yilmaz, L.; McHugh, A. J. Glass transition, crystallization and thermoreversible gelation in ternary PPO solutions; relationship to asymmetric membrane formation Polymer (1987) 28, 2085–2092.

[124]   Cohen, C.; Tanny, G. B.; Prager, S. Gas Separation Membranes. Polymeric and Inorganic. J. Polym. Sci: Polym. Phys. (1979) 17, 477–489

[125]   Bokhorst, H.; Altena, F. W.; Smolders, C. A. Formation of asymmetric cellulose acetate membranes. Desalination (1981) 38, 349–360.

[126]   Mulder, M. H. V.; Hendrikman, J. O.; Wijmans, J. G.; Smolders, C. A. A rationale for the preparation of asymmetric pervaporation membranes. J. Appl. Polym. Sci. (1985) 30, 2805–2820.

[127]   Wijmans, J. G.; Kant, J.; Mulder, M. H. V.; Smolders, C. A. Phase separation phenomena in solutions of polysulfone in mixtures of a solvent and a nonsolvent: relationship with membrane formation. Polymer (1985) 26, 1539–1545.

[128]   Kimmerle, K. Quantitative Betrachtung des Phase inversions prozesses bei der Herstellung von Membranen, Ph.D. Thesis; University of Stuttgart: Germany, (1988)

[129]   Gaides, G. E.; McHugh, A. J. Gelation in an amorphous polymer: a discussion of its relation to membrane formation. Polymer (1989) 30, 2118–2123.

[130]   Matsuyama, H.; Berghmans, S.; Lloyd, D. R. Formation of hydrophilic microporous membranes via thermally induced phase separation. J. Memb. Sci. (1998) 142, 213–224.

[131]   Bierenbaum, H. S.; Isaacson, R. B.; Lantos, P. R. (Celanese Corporation, New York, NY). U.S. Patent 3,426,754, February 11, 1969

[132]   Taskier, H. T. (Celanese Corporation, New York, NY). U.S. Patent 3,853,601, December 10, 1974.

[133]   Gore, R. W. (W. L. Gore & Associates, Inc., Newark, DE). U.S. Patent 3,953,566, April 27, 1976.

[134]   Tabatabaei, S. H.; Carreau, P. J.; Ajji, A. Microporous membranes obtained from polypropylene blend films by stretching J. Memb. Sci. (2008) 325, 772–782

[135] Sadeghi, F.; Ajji, A.; Carreau, P. Analysis of row nucleated lamellar morphology of polypropylene obtained from the cast film process: Effect of melt rheology and process conditions J. Polym. Eng. Sci. 2007, 47, 1170–1178.

[136] Nogales, A.; Hsiao, B. S.; Somani, R. H.; Srinivas, S.; Tsou, A. H.; Balta-Calleja, F. J.; Ezquerra, T. A. Shear-induced crystallization of isotactic polypropylene with different molecular weight distributions: in situ small- and wide-angle X-ray scattering studies. Polymer 2001, 42, 5247–5256.

[137] Sadeghi, F.; Tabatabaei, S. H.; Ajji, A.; Carreau, P. J. Effect of PVDF characteristics on extruded film morphology and porous membranes feasibility by stretching. J. Polym. Sci. Part B: Polym Phys 2009, 47, 1219–1229.

[138] Mazzei, R.; Bernaola, O. A.; Saint Martin, G.; De Rey, B. M. Submicroscopic kinetics of track formation in ssntd. Nuclear Instruments and Methods in Physics Research Section B: Beam Interactions with Materials and Atoms 1985, 9 (2), 163-168

[139] Fleischer, R. L.; Price, P. B.; Symes, E. M. Novel filter for biological materials. Science 1964, 143 (3603), 249-250.

[140] Apel, P. Track etching technique in membrane technology. Radiation Measurements 2001, 34 (1‑6), 559-566.

[141] Ferain, E.; Legras, R. Track-etch templates designed for micro- and nanofabrication Nuclear Instruments and Methods in Physics Research Section B: Beam Interactions with Materials and Atoms 2003, 208 (0), 115-122.

[142] Apel, P. Y.; Blonskaya, I. V.; Didyk, A. Y.; Dmitriev, S. N.; Orelovitch, O. L.; Root, D.; Samoilova, L. I.; Vutsadakis, V. A. Surfactant-enhanced control of track-etch poremorphology. Nuclear Instruments and Methods in Physics Research Section B: Beam Interactions with Materials and Atoms 2001, 179 (1), 55-62.

[143] Lee, D.; Nolte, A. J.; Kunz, A. L.; Rubner, M. F.; Cohen, R. E. Ph-induced hysteretic gating of track-etched polycarbonate membranes: Swelling/deswelling behavior of polyelectrolyte multilayers in confined

geometry. Journal of the American Chemical Society 2006, 128 (26), 8521-8529.

[144] Hillmyer, M. Nanoporous materials from block copolymer precursors. Advances in Polymer Science, (2005) 190, 137-181.

[145] Park, M.; Harrison, C.; Chaikin, P. M.; Register, R. A.; Adamson, D. H. Block copolymer lithography: Periodic arrays of ~1011 holes in 1 square centimeter. Science 1997, 276 (5317), 1401-1404.

[146] Urbas, A.; Sharp, R.; Fink, Y.; Thomas, E. L.; Xenidou, M.; Fetters, L. J. Tunable block copolymer/homopolymer photonic crystals. Advanced Materials 2000, 12 (11), 812-814.

[147] Bates, F. S.; Schulz, M. F.; Khandpur, A. K.; Förster, S.; Rosedale, J. H.; Almdal, K.; Mortensen, K. Fluctuations, conformational asymmetry and block copolymer phase behaviour. Faraday Discussions 1994, 98, 7-18.

[148] Ruzette, Anne-Valérie; Leibler, Ludwik. Block copolymers in tomorrow's plastics. Nature Materials (2005) 4, 19 – 31

[149] Wulff, G. Molecular imprinting in crosslinked materials with the aid of molecular templates – a way towards artificial antibodies. Angewandte Chemie International Edition in English 1995, 34 (17), 1812-1832.

[150] Thomas, A.; Goettmann, F.; Antonietti, M. Hard templates for soft materials: Creating nanostructured organic materials. Chemistry of Materials 2008, 20 (3), 738-755.

[151] Liu, H. Y.; Liu, L. L.; Yang, C. L.; Li, Z. H.; Xiao, Q. Z.; Lei, G. T.; Ding, Y. H. A hard-template process to prepare three-dimensionally macroporous polymer electrolyte for lithium-ion batteries. Electrochimica Acta 2014, 121 (0), 328-336.

[152] Wilke, A.; Weber, J. Hierarchical nanoporous melamine resin sponges with tunable porosity-porosity analysis and CO_2 sorption properties. Journal of Materials Chemistry 2011, 21 (14), 5226-5229.

[153] Rossinyol, E.; Arbiol, J.; Peiró, F.; Cornet, A.; Morante, J. R.; Tian, B.; Bo, T.; Zhao, D. Nanostructured metal oxides synthesized by hard

template method for gas sensing applications. Sensors and Actuators B: Chemical 2005, 109 (1), 57-63.

[154] Johnson, S. A.; Ollivier, P. J.; Mallouk, T. E. Ordered mesoporous polymers of tunable pore size from colloidal silica templates. Science 1999, 283 (5404), 963-965.

[155] Joo, J. B.; Kim, P.; Kim, W.; Kim, J.; Yi, J. Preparation of mesoporous carbon templated by silica particles for use as a catalyst support in polymer electrolyte membrane fuel cells. Catalysis Today 2006, 111 (3), 171-175.

[156] Park, S. H.; Xia, Y. Macroporous membranes with highly ordered and three-dimensionally interconnected spherical pores. Advanced Materials 1998, 10 (13), 1045-1048.

[157] Velev, O. D.; Lenhoff, A. M. Colloidal crystals as templates for porous materials. Current Opinion in Colloid & Interface Science 2000, 5 (1‑2), 56-63.

[158] http://www.htiwater.com/technology/forward_osmosis/index.html

[159] Wang, Y.; Hammes, F.; Düggelin, M.; Egli, T. Influence of size, shape, and flexibility on bacterial passage through micropore membrane filters. Environmental Science & Technology 2008, 42 (17), 6749-6754

[160] Fu, X.; Matsuyama, H.; Teramoto, M.; Nagai, H. Preparation of hydrophilic poly(vinyl-butyral) hollow fiber membrane via thermally induced phase separation. Separation and Purification Technology 2005, 45 (3), 200-207.

[161] Li, D.; Krantz, W. B.; Greenberg, A. R.; Sani, R. L. Membrane formation viathermally induced phase separation (tips): Model development and validation. Journal of Membrane Science 2006, 279 (1‑2), 50-60.

[162] Lin, Y. K.; Chen, G.; Yang, J.; Wang, X. L. Formation of isotactic polypropylene membranes with bicontinuous structure and good strength via thermally induced phase separation method. Desalination 2009, 236 (1‑3), 8-15.

[163] Lloyd, D. R.; Kinzer, K. E.; Tseng, H. S. Microporous membrane formation via thermally induced phase separation. I. Solid-liquid phase separation. J. Membr. Sci. 1990, 52 (3), 239-261.

[164] Matsuyama, H.; Berghmans, S.; Lloyd, D. R. Formation of anisotropic membranes via thermally induced phase separation. Polymer 1999, 40 (9), 2289-2301.

[165] Matsuyama, H.; Okafuji, H.; Maki, T.; Teramoto, M.; Kubota, N. Preparation of polyethylene hollow fiber membrane via thermally induced phase separation. J. of Membr. Sci. 2003, 223 (1‑2), 119-126.

[166] Gore, R. W. Porous products and process therefor U.S. Patent 4,187,390. 1980.

[167] Fisher, H. M.; Leone, D. E.; Lowery, J. J. Microporous membranes having increased pore densities and process for making the same U.S. Patent 5,013,439. 1991.

[168] Gan, Q.; Field, R. W.; Bird, M. R.; England, R.; Howell, J. A.; McKechnie, M. T.; O'Shaughnessy, C. L. Beer Clarification by Cross-Flow Microfiltration: Fouling Mechanisms and Flux Enhancement Chem Eng Res Des 1997, 75, 3–8.

[169] Czekaj, P.; Lopez, F.; Guell, C. Membrane fouling during microfiltration of fermented beverages J. Memb. Sci. 2000, 166, 199–212.

[170] Haller, C. M.; Rölleke, S.; Vybiral, D.; Witte, A.; Velimirov, B. Investigation of 0.2 μ m filterable bacteria from the western mediterranean sea using a molecular approach: Dominance of potential starvation forms. FEMS Microbiology Ecology 2000, 31 (2), 153-161.

[171] Waterhouse, S.; Hall, G. M. The validation of sterilising grade microfiltration membranes with pseudomonas diminuta a review. J. of Memb. Sci. 1995, 104 (1‑2), 1-9.

[172] ASTMF838. Standard test method for determining bacterial retention of membrane filters utilised for liquid filtration. Annual Book of ASTM standards, Am. Soc. Testing Mater. 1992, 1061-1069

[173] Guigui, C.; Rouch, J.; Durand-Bourlier, L.; Bonnelye, V.; Aptel, P. Impact of coagulation conditions on the in-line coagulation/uf process for drinking water production. Desalination 2002, 147 (1), 95-100.

[174] Park, P.-k.; Lee, C.-h.; Choi, S.-J.; Choo, K.-H.; Kim, S.-H.; Yoon, C.-H. Effect of the removal of doms on the performance of a coagulation-uf membrane system for drinking water production. Desalination 2002, 145 (1), 237-245.

[175] Combe, C.; Molis, E.; Lucas, P.; Riley, R.; Clark, M. M. The effect of CA membrane properties on adsorptive fouling by humic acid. J Memb Sci 1999, 154, 73–87.

[176] Ulbricht, M. Advanced functional polymer membranes. Polymer 2006, 47, 2217–2262.

[177] Loeb, S.; Sourirajan, S. High flow porous membranes for separating water from saline solutions. Patent Application Country: Application. Patent Application Country: Application: US; Patent Country: US; Priority Application Country: US Patent 3133132, 1964.

[178] Loeb, S.; Sourirajan, S.; Weaver, D. E. High flow porous membranes for separating water from saline solutions Patent Application Country: Application: US; Patent Country: US; Priority Application Country: US Patent 3133137, 1964.

[179] Xia, S.; Nan, J.; Liu, R.; Li, G. Study of drinking water treatment by ultrafiltration of surface water and its application to china. Desalination 2004, 170 (1), 41-47.

[180] Madaeni, S. S.; Fane, A. G.; Grohmann, G. S. Virus removal from water and wastewater using membranes. Journal of Membrane Science 1995, 102 (0), 65-75.

[181] Beuvier, E.; Berthaud, K.; Cegarra, S.; Dasen, A.; Pochet, S.; Buchin, S.; Duboz, G. Ripening and quality of Swiss-type cheese made from raw, pasteurized or microfiltered milk. Int Dairy J 1997, 7, 311–323

[182] Zydney, A. L. Protein separations using membrane filtration: new opportunities for whey fractionation. Int Dairy J 1998, 8, 243–250

[183] Maubois, J. L.; Mocquot, G. Application of Membrane Ultrafiltration to Preparation of Various Types of Cheese. J Dairy Sci 1975, 58, 1001–1007

[184] Guell, C.; Davis, R. H. Membrane fouling during microfiltration of protein mixtures. J. Memb. Sci. 1996, 119, 269–284

[185] Reinard, T.; Jacobsen, H.-J. An inexpensive small volume equilibrium dialysis system for protein-ligand binding assays. Analytical Biochemistry 1989, 176 (1), 157-160

[186] Akthakul, A.; Salinaro, R. F.; Mayes, A. M. Antifouling polymer membranes with subnanometer size selectivity. Macromolecules 2004, 37 (20), 7663-7668.

[187] Gullinkala, T.; Escobar, I. A green membrane functionalization method to decrease natural organic matter fouling. J. of Memb. Sci. 2010, 360 (1‑2), 155-164

[188] Sun, M.; Su, Y.; Mu, C.; Jiang, Z. Improved antifouling property of PES ultrafiltration membranes using additive of silica-pvp nanocomposite. Industrial & Engineering Chemistry Research 2009, 49 (2), 790-796

[189] Peter-Varbanets, M.; Margot, J.; Traber, J.; Pronk, W. Mechanisms of membrane fouling during ultra-low pressure ultrafiltration. J. of Memb. Sci. 2011, 377 (1‑2), 42-53.

[190] Howe, K. J.; Clark, M. M. Fouling of microfiltration and ultrafiltration membranes by natural waters. Environmental Science & Technology 2002, 36 (16), 3571-3576

[191] Reddy, A. V. R.; Patel, H. R. Chemically treated polyethersulfone /polyacrylonitrile blend ultrafiltration membranes for better fouling resistance. Desalination 2008, 221 (1‑3), 318-323

[192] Kochan, J.; Wintgens, T.; Hochstrat, R.; Melin, T. Impact of wetting agents on the filtration performance of polymeric ultrafiltration membranes. Desalination 2009, 241 (1‑3), 34-42

[193] Kull, K. R.; Steen, M. L.; Fisher, E. R. Surface modification with nitrogen-containing plasmas to produce hydrophilic, low-fouling membranes. J. of Memb. Sci. 2005, 246 (2), 203-215

[194] Leo, E.; Cameroni, R.; Forni, F. Dynamic dialysis for the drug release evaluation from doxorubicin-gelatin nanoparticle conjugates. International Journal of Pharmaceutics 1999, 180 (1), 23-30.

[195] Amoozgar, Z.; Rickett, T.; Park, J.; Tuchek, C.; Shi, R.; Yeo, Y. Semi-interpenetrating network of polyethylene glycol and photocrosslinkable chitosan as an in-situ-forming nerve adhesive. Acta Biomaterialia 2012, 8 (5), 1849-1858.

[196] Pelton, R.; Ren, P.; Liu, J.; Mijolovic, D. Polyvinylamine-graft-tempo adsorbs onto, oxidizes, and covalently bonds to wet cellulose. Biomacromolecules 2011, 12 (4), 942-948

[197] Kamps, M. P.; Sefton, B. M. Acid and base hydrolysis of phosphoproteins bound to immobilon facilitates analysis of phosphoamino acids in gel-fractionated proteins. Analytical Biochemistry 1989, 176 (1), 22-27.

[198] LeGendre, N.; Matsudaira, P. Direct protein microsequencing from immobilon-p transfer membrane. BioTechniques 1988, 6 (2), 154-159

[199] Szewczyk, B.; Summers, D. F. Preparative elution of proteins blotted to immobilon membranes. Analytical Biochemistry 1988, 168 (1), 48-53

[200] Momtaz, M.; Dewez, J.-L.; Marchand-Brynaert, J. Chemical reactivity assay and surface characterization of a poly (vinylidene fluoride) microfiltration membrane (＂durapore dvpp＂). J. of Memb. Sci. 2005, 250 (1), 29-37

[201] Andreou, V. G.; Clonis, Y. D. A portable fiber-optic PESticide biosensor based on immobilized cholinesterase and sol‑gel entrapped bromcresol purple for in-field use. Biosensors & Bioelectronics 2002, 17 (1-2), 61-69.

[202] Alguacil, F. J.; Coedo, A. G.; Dorado, M. T. Transport of chromium (vi) through a cyanex 923‑xylene flat-sheet supported liquid membrane. Hydrometallurgy 2000, 57 (1), 51-56

[203] Smuleac, V.; Butterfield, D. A. and Bhattacharyya, D. Permeability and Separation Characteristics of Polypeptide-Functionalized Polycarbonate Track-Etched Membranes. Chem. Mater. 2004, 16, 2762-2771

[204] Mulder, M. Basic principles of membrane technology second edition; Kluwer Academic Pub1996.

[205] Reid, C. E.; Breton, E. J. Water and ion flow across cellulosic membranes. Journal of Applied Polymer Science 1959, 1 (2), 133-143.

[206] Ramakrishna, S.; Ma, Z.; Matsuura, T. Polymer membranes in biotechnology: Preparation, functionalization and application; World Scientific2011.

[207] Livingston, A.; Peeva, L.; Silva, P. Organic solvent nanofiltration. Membrane Technology in the Chemical Industry 2006, 2nd Edition

[208] Wong, H.t.; Pink, C. J.; Ferreira, F. C.; Livingston, A. G. Recovery and reuse of ionic liquids and palladium catalyst for suzuki reactions using organic solvent nanofiltration. Green Chemistry 2006, 8 (4), 373-379.

[209] See Toh, Y.; Loh, X.; Li, K.; Bismarck, A.; Livingston, A. In search of a standard method for the characterisation of organic solvent nanofiltration membranes. J. of Memb. Sci. (2007) 291 (1), 120-125.

[210] See Toh, Y. H.; Lim, F. W.; Livingston, A. G. Polymeric membranes for nanofiltration in polar aprotic solvents. J. of Memb. Sci. (2007) 301 (1‑2), 3-10.

[211] Decker C. Photoinitiated crosslinking polymerization. Prog Polym Sci (1996) 21, 593–650

[212] Andrzejewska E. Photopolymerization kinetics of multifunctional monomers. Prog Polym Sci (2001) 26, 605–665.

[213] Dyer DJ. Photoinitiated synthesis of grafted polymers. Adv Polym Sci (2006) 197, 47–65

[214] Endruweit A, Johnson MS, Long AC. Curing of composite components by ultraviolet radiation: a review. Polym Compos (2006) 27, 119–128.

[215] Nakayama Y, Matsuda T. Preparation and characteristics of photocrosslinkable hydrophilic polymer having cinnamate moiety. J. Polym. Sci A: Polym Chem (1992) 30, 2451–2457.

[216] Burgoyne WF, Langsam M, Ford ME, Casey JP. Membranes formed from unsaturated polyimides. US Patent 4,931,182; 1990.

[217] Langsam M, Burgoyne WF, Casey JP, Ford ME. Membranes formed from unsaturated polyimides. US Patent 4,952,220; 1990.

[218] Ulbricht M, Hicke HG. Photomodification of ultrafiltration membranes. 1. Photochemical modification of polyacrylonitrile ultrafiltration membranes with aryl azides. Angew. Makromol. Chem. 1993)210:69–95.

[219] Ulbricht M, Hicke HG. Photomodification of ultrafiltration membranes. 2. Ultrafiltration properties of polyacrylonitrile membranes photochemically modified with aryl azides. Angew. Makromol. Chem. (1993) 210, 97–117

[220] Ludwigs S, Schmidt K, Stafford CM, Amis EJ, Fasolka MJ, Karim A, et al. Combinatorial mapping of the phase behaviour of ABC triblock terpolymers in thin film: experiments. Macromolecules (2005) 38, 1850–1858

[221] Ismail AF, LornaW. Penetrant-induced plasticization phenomenon in glassy polymers for gas separation membrane. Sep Purif Technol (2002) 27, 173–194

[222] Castilho LR, Deckwer WD, Anspach FB. Influence of matrix activation and polymer coating on the purification of human IgG with protein A affinity membranes. J Membr Sci (2000) 172, 269–277.

[223] Borcherding H, Hicke HG, Jorcke D, Ulbricht M. Affinity membranes as a tool for life science applications. Ann NY Acad Sci (2003) 984, 470–479.

[224] Li Q, He R, Jensen JO, Bjerrum NJ. Approaches and recent development of polymer electrolyte membranes for fuel cells operating above 100 °C. Chem. Mater. (2003) 15, 4896–4915

[225]   Chu LY, Niitsuma T, Yamaguchi T, Nakao S. Thermoresponsive transport through porous membranes with grafted PNIPAMgates. AIChE. J. (2003) 49, 896–909

[226]   Adhikari B, Majumdar S. Polymers in sensor applications. Prog. Polym. Sci. (2004) 29, 699–766

[227]   Lanza RP, Langer R, Vacanti J, editors. Principles of tissue engineering. 2nd ed. San Diego, CA: Academic Press; 2000.

[228]   Drioli E, Giorno L. Biocatalytic membrane reactors. London: Taylor and Francis Ltd.; 1999.

[229]   Wang PC, DeVoe DL, Lee CS. Integration of polymeric membranes with microfluidic networks for bioanalytical applications. Electrophoresis (2001) 22, 3857–3867

[230]   Braslavsky ES. Glossary of terms used in photochemistry, 3rd ed. (IUPAC Recommendation 2006). Pure Appl. Chem. (2007) 79, 293–465

[231]   Van Gerven T, Mul G, Moulijn J, Stankiewicz A. A review of intensification of photocatalytic processes. Chem Eng Process (2007) 46, 781–789.

[232]   Moad CL, Winzor DJ. Quantitative characterization of radiation degradation polymers by evaluation of scission and cross-linking yields. Prog. Polym. Sci. (1998) 23, 759–813.

[233]   Malesic J, Kolar J, Strlic M, Kocar D, Fromageot D, Lemaire J, et al. Photo-induced degradation of cellulose. Polym. Degrad. Stab. (2005) 89, 64–69.

[234]   Tang L,Wu Q, Qu B. The effects of chemical structure and synthesis method on photodegradation of polypropylene. J. Appl. Polym. Sci. (2007) 95, 270–279.

[235]   Norman K, Kingshott P, Kaeselev B, Ghanbari-Siahkali A. Photodegradation of poly(ether sulphone). Part 1. A time-offlight secondary ion mass spectrometry study. Surf. Interf. Sci. (2004) 36, 1533–1541.

[236] Kotzyba-Hibert F, Kapfer I, Goeldner M. Recent trends in photoaffinity labeling. Angew. Chem. Int. Ed. (1995) 34, 1296–1312.

[237] Arica Y, Hasirci VN. Immobilization of glucose oxidase in poly(2-hydroxyethyl methacrylate) membranes. Biomaterials (1987) 8, 489–495.

[238] Arica MY, Denizli A, Salih B, Piskin E, Hasirci V. Catalase adsorption onto Cibacron Blue F3GA and Fe(III)-derivatized poly(hydroxyethyl methacrylate) membranes and application to a continuous system. J. Membr. Sci. (1997) 129, 65–76.

[239] Edelmann K, Reiche A, Sandner B, Marstalerz J, Müller H.Copolymers from oligosiloxane methacrylates as a plasticizer-free membrane matrix for ion-selective sensors. Polymer (2005) 46, 407–417.

[240] Elmer AM, Jannasch P. Polymer electrolyte membranes by in situ polymerization of poly(ethylene carbonate-co-ethylene oxide) macromonomers in blends with poly(vinylidene fluoride-cohexafluoropropylene). J Polym Sci B: Polym Phys (2007) 45, 79–90.

[241] Song S, Singh AK, Shepodd TJ, Kirby BJ. Microchip dialysis of proteins using *in-situ* photopatterned nanoporous polymer membranes. Anal Chem (2004) 76, 2367–2373.

[242] Song S, Singh AK, Kirby BJ. Electrophoretic concentration of proteins at laser-patterned nanoporous membranes in microchips. Anal Chem (2004) 76, 4589–4592.

[243] Nakayama H, Kaetsu I, Uchida K, Sakata S, Tougou K, Hara T, et al. Radiation curing of intelligent coating for controlled release and permeation. Radiat Phys. Chem. (2002) 63, 521–523.

[244] PeppasNA, Kim B. Stimuli-sensitive protein delivery systems. J Drug Deliv. Sci. Technol. (2006) 16, 11–18.

[245] Morishita M, Goto T, Takayama K, Peppas NA. Oral insulin delivery systems based on complexation polymer hydrogels. J. Drug. Deliv. Sci. Technol. (2006) 16, 19–24.

[246]   Spizzirri UG, Peppas NA. Structural analysis and diffusional behavior of molecularly imprinted polymer networks for cholesterol recognition. Chem. Mater. (2005) 17. 6719–6727.

[247]   Hilt JZ, Byrne ME, Peppas NA. Microfabrication of intelligent biomimetic networks for recognition of d-glucose. Chem. Mater. (2006) 18, 5869–5875.

[248]   Liu Y, Lee JY, Hong L. In situ preparation of poly(ethylene oxide)-SiO2 composite polymer electrolytes. J. Power Sources (2004) 129, 303–311.

[249]   Hayes RA. Polyimide gas separation membranes. US Patent 4,717,393; 1988.

[250]   Kita H, Inada T, Tanaka K, Okamoto K. Effect of photocrosslinking on permeability and permselectivity of gases through benzophenone containing polyimide. J. Membr. Sci. (1994) 87, 139–147

[251]   Liu Y, Ding M, Xu J. Gas permeabilities and permselectivity of photochemically crosslinked polyimides. J. Appl. Polym. Sci. (1995) 58, 485–489

[252]   Liu Y, Pan C, Ding M, Xu J. Effect of crosslinking distribution on gas permeability and permselectivity of crosslinkedpolyimides. Eur. Polym. J. (1999) 35, 1739–1741

[253]   Scaiano JC,Netto-Ferreira JC, Becknell AF, Small RD. The mechanism of photocure of inherently photosensitive polyimides containing a benzophenone group. Polym. Eng. Sci. (1989) 29, 942–944.

[254]   Lin AA, Sastri VR, Tesoro G, Reiser A, Eachus R. On the cross-linking mechanism of benzophenone-containing polyimides. Macromolecules (1988) 21, 1165–1169.

[255]   Meier IK, Langsam M. Photochemically induced oxidative surface modification of polyimide films. J Polym Sci A: Polym Chem (1993) 31, 83–89

[256]   Meier IK, Langsam M, Klotz HC. Selectivity enhancement via photooxidative surface modification of polyimide air separation membranes. J. Membr. Sci. (1994) 94, 195–212.

[257] Matsui S, Ishiguro T, Higuchi A, Nakagawa T. Effect of ultraviolet light irradiation on gas permeability in polyimide membranes 1. Irradiation with low pressure mercury lamp on photosensitive and nonphotosensitive membranes. J Polym Sci B: Polym Phys (1997) 32, 2259–2269.

[258] Matsui S, Nakagawa T. Effect of ultraviolet light irradiation on gas permeability in polyimide membranes. II. Irradiation of membranes with high-pressuremercury lamp. J. Appl. Polym. Sci. (1998) 67, 49–60.

[259] Matsui S, Sato H, Nakagawa T. Effects of low molecular weight photosensitizer and UV irradiation on gas permeability and selectivity of polyimide membrane. J. Membr. Sci. (1998) 141, 31–43.

[260] Wright CT, Paul DR. Gas sorption and transport in UV-irradiated polyarylate copolymers based on tetramethyl bisphenol-A and dihydroxybenzophenon. J. Membr. Sci. (1997) 124, 161–174

[261] McCaig MS, Paul DR. Effect of UV crosslinking and physical aging on the gas permeability of thin glassy polyarylate films. Polymer (1999) 40, 7209–7225

[262] Wright CT, Paul DR. Gas sorption and transport in UV-irradiated poly(2,6-dimethyl-1,4-phenylene oxide) films. J. Appl. Polym. Sci. (1998) 67, 875–883

[263] Tanihara N, Tanaka K, Kita H, Okamoto K. Pervaporation of organic liquid mixtures through membranes of polyimides containing methyl-substituted phenylenediamine moieties. J. Membr. Sci. (1994) 95, 161–169

[264] Ishikawa J, Fujiyama S, Inoue K, Omi T, Tamai S. Highly sulfonated poly(aryl ether ketone) block coplymers having a cross-linking structure. J. Membr. Sci. (2007) 298, 48–55.

[265]. Wycisk R, Pintauro PN, Wang W, O'Connor S. Polyphosphazene membranes. I. Solid-state photocrosslinking of poly[(4- ethylphenoxy)-(phenoxy)phosphazene]. J. Appl. Polym. Sci. (1996) 59, 1607–1617

[266] Dudley C. N; Schöberl B; Sturgill G. K; Becham H. W; Rezac M. E; Influence of crosslinking technique on the physical and transport

properties of ethynyl-terminated monomer/polyetherimide asymmetric membranes. J. Membr. Sci. (2001) 191, 1–11

[267] Trushinski BJ, Dickson JM, Childs RF, McCarry BE. Photochemically modified thin-film composite membranes. I. Acid and ester membranes. J Appl. Polym. Sci. (1993) 48, 187–198

[268] Trushinski BJ, Dickson JM, Childs RF, McCarry BE, Gagnon DR. Photochemically modified thin-film compositemembranes. II. Bromoethyl ester, dioxolan, and hydroxyethyl estermembranes. J. Appl. Polym. Sci. (1994) 54, 1233–1242

[269] Darkow R, Yoshikawa M, Kitao T, Tomaschewski G. Photomodification of a poly(acrylonitrile-co-butadiene-co-styrene) containing diaryltetrazolyl groups. J. Polym. Sci. A: Polym Chem (1994) 32, 1657–1664

[270] Bora U, Sharma P, Kannan K, Nahar P. Photoreactive cellulose membrane—a novel matrix for covalent immobilization of biomolecules. J Biotechnol (2006) 126, 220–229

[271] Kumar S. Nahar P. Sunlight-induced covalent immobilization of proteins. Talanta (2007) 71, 1438–1440.

[272] Rajam S, Ho C. Graft coupling of PEO to mixed cellulose esters microfiltration membranes by UV irradiation. J. Membr. Sci. (2006) 281, 211–218

[273] Susanto H, Ulbricht M. Photografted thin polymer hydrogel layers on PES ultrafiltration membranes: characterization, stability, and influence on separation performance. Langmuir (2007) 23, 7818–7830

[274] Ulbricht M, Oechel A, Lehmann C, Tomaschewski G, Hicke HG. Gas-phase photoinduced graft polymerization of acrylic acid onto polyacrylonitrile ultrafiltration membranes. J Appl Polym Sci (1995) 55, 1707–1723.

[275] Ulbricht M, Yang H. Porous polypropylene membranes with different carboxyl polymer brush layers for reversible protein binding via surface-initiated graft copolymerization. Chem. Mater. (2005) 17, 2622–2631

[276] Ulbricht M, Schwarz HH. Novel high performance photo-graft composite membranes for separation of organic liquids by pervaporation. J. Membr. Sci. (1997) 136, 25–33.

[277] Hicke HG, Ulbricht M, Becker M, Radosta S, Heyer AG. Novel enzyme-membrane reactor for polysaccharide synthesis. J. Membr. Sci. (1999) 161, 239–245.

[278] Becker M, Provart N, Lehmann I, Ulbricht M, Hicke HG. Polymerization of glucans by enzymatically active membranes. Biotechnol Prog (2002) 18, 964–968.

[279] Crivello JV, Belfort G, Yamagishi H. Low fouling ultrafiltration and microfiltration aryl polysulfone, US Patent 5,468,390; 1995.

[280] Yamagishi H, Crivello JV, Belfort G. Development of a novel photochemical technique for modifying poly(arylsulfone) ultrafiltration membranes. J. Membr. Sci. (1995) 105, 237–247

[281] Ulbricht M, Riedel M, Marx U. Novel photochemical surface functionalization of polysulfone ultrafiltration membranes for covalent immobilization of biomolecules. J. Membr. Sci. (1996) 120, 239–259.

[282] Yamagishi H, Crivello JV, Belfort G. Evaluation of photochemically modified poly(arylsulfone) ultrafiltration membranes. J. Membr. Sci. (1995) 105, 249–259

[283] Pieracci J, Crivello JV, Belfort G. UV-assisted graft polymerization of N-vinyl-2-pyrrolidinone onto poly(ether sulfone) ultrafiltration membranes using selective UV wavelengths. Chem. Mater. (2002) 14, 256–265

[284] Taniguchi M, Pieracci J, Samsonoff WA, Belfort G. UV-assisted graft polymerization of synthetic membranes: mechanistic studies. Chem. Mater. (2003) 15, 3805–3812

[285] Kaeselev B, Pieracci J, Belfort G. Photoinduced grafting of ultrafiltration membranes: comparison of poly(ether sulfone) and poly(sulfone). J. Membr. Sci. (2001) 194, 245–261.

[286] P. Vandezande, L.E.M. Gevers, I.F.J. Vankelecom. Solvent resistant nanofiltration: separating on a molecular level. Chem. Soc. Rev. (2008) 37, 365–405.

[287] K. Vanherck, G. Koecklberghs, I.F.J. Vankelecom. Crosslinking polyimides for membrane applications: A review. Prog. Polym. Sci. (2013) 38, 874-896.

[288] K. Vanherck, A. Cano-Odena, G. Koecklberghs, T. Dedroag, I.J.F. Vankelecom. A simplified diamine crosslinking method for PI nanofiltration membranes. J. Membr. Sci. (2010) 353, 135-143.

[289] Li, A. Oshima, T. Miura, M. Washio. Preparation of the crosslinked polyethersulfone films by high-temperature electron-beam irradiation. Polym. Degr. Stab. (2006) 91, 2867–2873.

[290] Struzynska-Piron, J. Loccufier, L. Vanmale, I-F.J. Vankelecom. Parameter Study on the Preparation of UV\rDepth-Cured Chemically Resistant\rPolysulfone-Based Membranes Macromol. Chem. Phys. (2014) 215, 614-623.

[291] Struzynska-Piron, M.R. Biland, J. Loccufier, L. Vankelecom. Influence of UV curing on morphology and performance of polysulfone membranes containing acrylates. J. Memb. Sci. (2014) 462, 17-22.

[292] Jouanneau, R. Mercier, L. Gonon, G. Gebel. Synthesis of sulfonated polybenzimidazoles from functionalized monomers: preparation of ionic conducting membranes Macromolecules (2007) 40, 983-990.

[293] H. R. Kricheldorf, L. Vakhtangishvili, D. Fritsch. Synthesis and functionalization of poly(ether sulfone)s based on 1,1,1-tris(4-hydroxyphenyl)ethane. J. Polym. Sci. Polym. Chem. (2002) 40, 2967-2978.

[294] T. Koch, H. Ritter. Functionalized polysulfones from 4,4-bis(4-hydroxyphenyl)pentanoic acid, 2,2-isopropylidenediphenol and bis(4-chlorophenyl) sulfone: synthesis, behaviour and polymer analogous amidation of the carboxylic groups Macromol. Chem. Phys. (1994) 195, 1709-1719.

[295] C. G. Herbert, H. Ghassemi, A. S. Hay. Introduction of amino, aliphatic, and aliphatic carboxylic acid side groups onto poly(arylene ether sulfone)s via transimidization reactions J. Polym. Sci. Pol. Chem. (1997) 35, 1095-1104.

[296] M. D. Guiver, G. P. Robertson, S. Foley. Chemical Modification of Polysulfones II: An Efficient Method for Introducing Primary Amine Groups onto the Aromatic Chain. Macromolecules (1995) 28, 7612-7621.

[297] H. Toiserkani, G. Yilmaz, Y. Yagci, L. Torun. Functionalization of Polysulfones by Click Chemistry. Macromol. Chem. Phys. (2010) 211, 2389-2395.

[298] C. Dizman, D. O. Demirkol, S. Ates, L. Torun, S. Sakarya, S. Timur, Y. Yagci. Photochemically prepared polysulfone poly(ethylene glycol) amphiphilic networks and their biomolecule adsorption properties. Colloids Surf. B (2011) 88, 265-270.

[299] M. Karadag, G. Yilmaz, H. Toiserkani, D. O. Demirkol, S. Sakarya, L. Torun, S. Timur, Y. Yagci. Polysulfone/Pyrene Membranes: A New Microwell Assay Platform for Bio applications Macromol. Biosci. (2011) 11, 1235-1243.

[300] G. Yilmaz, H. Toiserkani, D. O. Demirkol, S. Sakarya, S. Timur, L. Torun, Y. Yagci. Polysulfone based amphiphilic graft copolymers by click chemistry as bioinert membranes. Mater. Sci. Eng. (2011) 31C,1091-1097.

[301] S. Ates, C. Dizman, B. Aydogan, B. Kiskan, L. Torun, Y. Yagci. Synthesis, characterization and thermally activated curing of polysulfones with benzoxazine end groups. Polymer (2011) 52, 1504-1509.

[302] G. Yilmaz, H. Toiserkani, D. O. Demirkol, S. Sakarya, S. Timur, Y. Yagci, L. Torun. Modification of polysulfones by click chemistry: Amphiphilic graft copolymers and their protein adsorption and cell adhesion properties. J. Polym. Sci. Pol. Chem. (2011) 49, 110-117.

[303] B. Van der Bruggen. Chemical modification of polyethersulfone nanofiltration membranes: A review, J. Appl. Polym. Sci. (2009) 114, 630-642.

[304]   Breitbach, E. Hinke, E. Staude, Angew. Heterogeneous functionalizing of polysulfone membranes. Makromol. Chem. (1991) 184, 183-196.

[305]   C. Dizman, S. Ates, T. Uyar, M. A. Tasdelen, L. Torun, Y. Yagci. Polysulfone/Clay Nanocomposites by in situ Photoinduced Crosslinking Polymerization Macromol. Mater. Eng. (2011) 296, 1101-1106.

[306]   Sangermano, I. Roppolo, V. H. A. Camara, C. Dizman, S. Ates, L. Torun, Y. Yagci. Polysulfone/Metal Nanocomposites by Simultaneous Photoinduced Crosslinking and Redox Reaction. Macromol. Mater. Eng. (2011) 296, 820-825.

[307]   Dizman C, Ates S, Torun L, Yagci Y. Beilstein. Synthesis, characterization and photoinduced curing of polysulfones with (meth) acrylate functionalities. J. Organ. Chem. (2010) 56.

[308]   Viswanathan, R.; Johnson, B. C.; McGrath, J. E. Synthesis, kinetic observations and characteristics of polyarylene ether sulphones prepared via a potassium carbonate DMAC process. Polymer (1984) 25, 1827-1833.

[309]   V. S.T. Sim, Q. She, T. H. Chong, C. Y. Tang, A. G. Fane, W. B. Krantz. Strategic Co-Location in a Hybrid Process Involving Desalination and Pressure Retarded Osmosis (PRO). Membranes, (2013) 3, 98–125.

[310]   Chakrabarty B., Ghoshal A.K. , Purkait M.K. Preparation, characterization and performance studies of polysulfone membranes using PVP as an additive. J. Membr. Sci. (2008) 315, 36-47.

[311]   Sangermano M., Vitale A., Razza N., Favetto A., Paleari M., Ariano P. Multilayer UV-cured organic capacitors. Polymer (2015) 56, 131-134.

[312]   Mrówczynski, R.; Bunge, A. Polydopamine an organocatalyst rather than an innocent polymer, J:. Chem. Europ. J. (2014) 20, 8647–8653.

[313]   Liebscher, J. Mrowczynski, R. Scheidt, H.A. Filip, C; Hadade, N.D Turcu, R; Bende, A. Beck, S. Structure of polydopamine. A never ending story?, Langmuir, (2013) 29, 10539–10548.

[314]   Lee, H. Dellatore, S.M. Miller, W.M. Messersmith, P.B. Mussel inspired surface chemistry for multifunctional coatings. Science (2007) 318, 426–430.

[315] Jiang, J. Zhu, L. Zhu, L. Zhu, B. Xu, Y. surface characteristics of a self-polymerized dopamine coating deposited on hydrophobic polymer films, Langmuir, (2011) 27, 14180–14187.

[316] Yu, B. Liu, Y. Liu, S. Zhou, F. Pdop layer exhibiting zwitterionicity: a simple electrochemical interface for governing ion permeability, Chem. Commun., (2010) 46, 5900–5902.

[317] McCloskey, B. D. Park, H.B. Ju, H. Rowe, B.W. Miller, D.J. Chun, B.J. Kin, K. Freeman, B.D. Influence of polydopamine deposition conditions on pure water flux and foulant adhesion resistance of reverse osmosis, ultrafiltration and microfiltration membranes. Polymer, (2010) 51, 3472–3485.

[318] Miller, D.J. Araujo, P.A. Correia, P.B. Ramsey, M.M. Kruithof, J.C. Van Loosdrecht, M.C.M Freeman, B.D. Paul, D.R. Whiteley, M. Vrouwenvelder, J.S. Short-term adhesion and long-term biofouling testing of polydopamine and poly(ethylene glycol) surface modifications of membranes and feed spacers for biofouling control, Water Res., (2012) 46, 3737–3753.

[319] Choi, Y.S. Kang, H. Kim, D.G. Cha, S.H. Lee, J.C. Mussel-inspired dopamine-and plant-based cardanol-containing polymer coatings for multifunctional filtration membrane, ACS Appl. Mat. Int., (2014) 6, 21297–21307.

[320] Wei, Q. Zhang, F. Li, J. Li, B. a Zhao, C. Oxidant induced dopamine polymerization for multifunctional coatings Polym. Chem. (2010) 1, 1430–1433.

[321] Yang Zhang, Min Guo, Guoyuan Pan, Hao Yan, Jian Xu and Yuanteng Shi. Preparation and properties of novel pH-stable TFC membrane based on organic-inorganic hybrid composite materials for nanofiltration J. Membr. Sci. (2015) 476, 500–507

[322] Byeong-Heon Jeong, Eric M.V. Hoek, Yushan Yan, Arun Subramani, Xiaofei Huang and Gil Hurwitz. Interfacial polymerization of thin film nanocomposites: A new concept for reverse osmosis membranes. J. Membr. Sci. (2007) 294, 1 – 7.

[323] Alberto Tiraferri, Ngai Yin Yip, William A. Phillip, Jessica D. Schiffman and Menachem Elimelech. Relating performance of thin-film composite forward osmosis membranes to support layer formation and structure. J. Membr. Sci. (2011) 367, 340–352

[324] Yoon, K. Kim, K. Wang, X. Fang, D. Hsiao and B. S. Chu. High flux ultrafiltration membranes based on electrospun nanofibrous PAN scaffolds and chitosan coating. Polymer (2006) 47, 2434–2441

[325] Subramanian, S and Seeram, R. New directions in nanofiltration applications - Are nanofibers the right materials as membranes in Desalination. Desalination 2013, 308, 198–208

[326] M. Obaid. Gehan M.K. Tolba, Moaaed Motlak, Olfat A. Fadali, Khalil Abdelrazek Khalil, Abdulhakim A. Almajid, Bongsoo Kim and Nasser A.M. Barakat. Effective polysulfone-amorphous SiO_2 NPs electrospun nanofiber membrane for high flux oil/water separation. Chem. Eng. J. (2015) 279, 631–638

[327] M. Obaid, Zafar Khan Ghouri, Olfat A. Fadali, Khalil Abdelrazek Khalil, Abdulhakim A. Almajid and Nasser A. M. Barakat, Amorphous SiO_2 NP-Incorporated PVDF Electrospun Nanofiber Membrane for High Flux Forward Osmosis Desalination. ACS Appl. Mater. & Interfaces (2016) 8, 4561-4574.

[328] Ming Hang Tai, Peng Gao, Benny Yong Liang Tan, Darren D. Sun and James O. Leckie, Highly efficient and Flexible Electrospun Carbon − Silica Nanofibrous Membrane for Ultrafast Gravity-Driven Oil − Water Separation. ACS Appl. Mater. Interfaces (2014) 6, 9393-9401.

[329] Shuai Jiang, Beatriz Chiyin Ma, Jonas Reinholz, Qifeng Li, Junwei Wang, Kai A. I. Zhang, Katharina Landfester and Daniel Crespy. Efficient Nanofibrous Membranes for Antibacterial Wound dressing and UV Protection. ACS Appl. Mater. Interfaces (2016) 8, 29915-29922.

[330] M. Obaid, Nasser A.M. Barakat, O.A. Fadali, Moaaed Motlak, Abdulhakim A. Almajid and Khalil Abdelrazek Khalil Effective and reusable oil/water separation membranes based on modified polysulfone electrospun nanofiber mats. Chem. Eng. J. (2015) 259, 449–456.

[331] Jiajia Xue, Yuzhao Niu, Min Gong, Rui Shi, Dafu Chen, Liqun Zhang and Yuri Lvov, Electrospun microfiber membranes Embedded with Drug-Loaded Clay nano tubes for sustained antimicrobial protection. ACS Nano (2015) 9(2), 1600–1612.

[332] Alexis Wagner, Vida Poursorkhabi, Amar K. Mohanty and Manjusri Misra, Analysis of Porous Electrospun Fibers from Poly(L-lactic acid)/Poly(3-hydroxybutyrate-co-3-hydroxyvalerate) Blends. ACS Sustainable Chem. Eng. (2014) 2, 1976-1982.

[333] Andreia F. de Faria, Francois Perreault, Evyatar Shaulsky, Laura H. Arias Chavez and Menachem Elimelech, Antimicrobial Electrospun Biopolymer Nanofi ber Mats Functionalized with Graphene Oxide − Silver Nanocomposites. ACS Appl. Mater. Interfaces (2015) 7, 12751-12759.

[334] Hee Joong Kim, Min-Young Lim, Kyung Hwa Jung, Dong-Gyun Kima and Jong-Chan Lee, High performance reverse osmosis nanocomposite membranes containing the mixture of carbon nanotubes and graphene oxides. J. Mater. Chem. A (2015) 3, 6798-6809.

[335] Jianqiang Wang, Pan Zhang, Bin Liang, Yuxuan Liu, Tao Xu, Lifang Wang, Bing Cao and Kai Pan, Graphene Oxide as an Effective Barrier on a Porous Nanofibrous Membrane for Water Treatment. ACS Appl. Mater. Interfaces (2016) 8, 6211-6218.

[336] H. j. Cho, S.K. Madhurakkat, J. h. Lee, J. Lee, K. M. Lee, C.S. Shin and H. Shin, Effective immobilization of BMP-2 mediated by polydopamine coating on biodegradable nanofibers for enhanced in vivo bone formation ACS Appl. Mater. Interfaces (2014) 6, 11225-11235.

[337] X. Wang, S. Yuan, D. Shi, Y. Yang, T. Jiang, S. Yan, H. Shi, S. Luan and J. Yin, Integrated antifouling and bactericidal polymer membranes through bioinspired polydopamine/poly(N-vinyl pyrrolidone). Appl. Surf. Sci. (2016) 375, 9-18.

[338] Qiuxia Fu, Xueqin Wang, Yang Si, Lifang Liu, Jianyong Yu, and Bin Ding, Scalable Fabrication of Electrospun Nanofibrous Membranes Functionalized with Citric Acid for High-Performance Protein Adsorption. ACS Appl. Mater. Interfaces (2016) 8(18), 11819-11829.

[339] Christina Tang, Carl D. Saquing, Jonathon R. Harding and Saad A. Khan, In situ Cross-Linking of electrospun Poly(vinyl alcohol) Nanofibers. ACS Macromolecules (2010) 43, 630-637.

[340] Hong -Wei He, Le Wang, Xu Yan, Li-Hua Zhang, Miao Yu, Gui-Feng Yu, Rui-Hua Dong, Lin-Hua Xia, Seeram Ramakrishna and Yun-Ze Long, Solvent-free electrospinning of UV curable polymer microfibers. RSC Adv. (2016) 6, 29423-29427.

[341] Wei-Han Lin and Wei-Bor Tsai, In situ UV – crosslinking gelatin electrospun fibers for tissue engineering applications. Biofabrication (2013) 5(035008), 1.

[342] Heyun Wang, Yakai Feng, Wencheng Zhang, Minglin Sun. Zichen Fang, Wenjie Yuan and Massuri Khan, Fabrication of PU/PEGMA crosslinked hybrid scaffolds by in situ UV photopolymerization favoring human endothelial cells growth for vascular tissue engineering. J Mater Sci: Mater Med (2012) 23, 1499-1510.

[343] Seong Han Kim, Sae-Hoon Kim, Sujith Nair and Eric Moore, Reactive Electrospinning of Cross-Linked Poly(2-hydroxyethyl methacrylate) Nanofibers and Elastic Properties of Individual Hydrogel Nanofibers in Aqueous Solutions. ACS Macromolecules (2005) 38, 3719-3723.

[344] Pankaj Gupta, Scott R. Trenor, Timothy E. Long and Garth L. Wilkes, In Situ Photo-Cross-Linking of Cinnamate Functionalized Poly(methyl methacrylate-co-2-hydroxyethyl acrylate) Fibers during Electrospinning. ACS Macromolecules (2004) 37, 9211-9218.

[345] Xiaoming Xu, Jian-Feng Zhang and Yuwei Fan, Fabrication of Cross-Linked polyethyleneimine Microfibers by Reactive Electrospinning with In Situ Photo-Cross-Linking by UV Radiation. ACS Biomacromolecules (2010) 11, 2283-2289.

[346] Emre Bastürk, Burcu Oktay and Memet Vezir Kahraman, Dual-crosslinked thiol-ene/sol gel hybrid electrospun nanowires: preparation and characterization. J Polym. Res. (2015) 22(7), 1-7.

[347]   Shin, Y. Hohman, M. Brenner and M. Rutledge, G, Electrospinning: A whipping fluid jet generates submicron polymer fibers. Appl. Phys. Lett. (2001) 78(8), 1149-1151.

[348]   Megelski, S. Stephens, J. S. Chase, D. B. Rabolt and J. F. Microand, Micro and nanostructured surface morphology on electrospun polymer fibers. ACS Macromolecules (2002) 35(22), 8456-8466.

[349]   Jinyou Lin, Bin Ding, Jianmao Yang, Jianyong Yu and Gang Sunf, Subtle regulation of the micro- and nanostructures of electrospun polystyrene fibers and their application in oil absorption. Nanoscale (2012) 4, 176-182.

List of Journal and Conference Papers

- Synthesis, preparation and characterization of UV–cured methacrylated polysulfone-based membranes, *Materials Today Communication* (**2015**) 5, 64–69 M. Sangermano, M. Mian Farrukh, A. Tiraferri, C. Dizman, Y. Yagci

- Versatility of light induced polymerization reaction. Oral presentation at European symposium of photopolymer Science (**11–14 Sep 2016** Leipzig Germany) Marco Sangermano, Mian Farrukh, Alberto Tiraferri

- Solvent–stable UV–cured acrylic Polysulfone membranes, *Polymer International* (**2017**) 66, 64–69 Mehmood Mian Farrukh, Paula Bosch, Mattia Giagnorio, Alberto Tiraferri, Marco Sangermano

- Ultrafiltration membranes functionalized with polydopamine with enhanced contaminant removal by adsorption, *Macromolecular Materials and Engineering* (**2017**) 392, 1600481 Luigi. C. Capozzi, Mehmood M. Farrukh, Mattia Giagnorio, Alberto Tiraferri, Marta Cerruti, Marco Sangermano

- Promising chemical stable membranes developed through combined effect of radical polymerization and non–solvent induced phase separation of acrylic functionalized polysulfone – Oral Presentation at 253rd Annual meeting of American Chemical Society (**2–6 April 2017**, San Francisco USA) Mian Farrukh Mehmood, Paula Bosch, Mattia Giagnorio,Alberto Tiraferri, Marco Sangermano

- Solvent stable electrospun membranes developed through ultraviolet induced reactive electrospinning – Oral Presentation at 253rd Annual meeting of American Chemical Society (**2–6 April 2017**, San Francisco USA Mian Farrukh Mehmood, Marco Sangermano, Njabu Gule, Peter E. Mallon

- Online UV curing of electrospun polysulfone fibers containing acrylate as cross-linker. *Macromolecular Chemistry and Physics* (**2017**) 218, 5, 1700125 Mian Farrukh Mehmood, Marco Sangermano, Prudence Nonjabulo Gule, Alberto Tiraferri, Peter E. Mallon